DISCLAIMER NOTICE

THIS DOCUMENT IS BEST QUALITY PRACTICABLE. THE COPY FURNISHED TO DTIC CONTAINED A SIGNIFICANT NUMBER OF PAGES WHICH DO NOT REPRODUCE LEGIBLY.

Technical Summary

AD-A206 712

Weather Radar Studies

31 March 1988

Lincoln Laboratory
MASSACHUSETTS INSTITUTE OF TECHNOLOGY
LEXINGTON, MASSACHUSETTS

Prepared for the Federal Aviation Administration

TECHNICAL REPORT STANDARD TITLE PAGE

1. Report No.	2. Government Accession No.	3. Recipient's Catalog No.
DOT/FAA/PS-88/2		

4. Title and Subtitle	5. Report Date
Weather Radar Studies	31 March 1988
	6. Performing Organization Code

7. Author(s)	8. Performing Organization Report No.
David M. Bernella	

9. Performing Organization Name and Address	10. Work Unit No. (TRAIS)
Massachusetts Institute of Technology Lincoln Laboratory P.O. Box 73 Lexington, MA 02173-0073	11. Contract or Grant No. DT-FA01-80-Y-10546

12. Sponsoring Agency Name and Address	13. Type of Report and Period Covered
Department of Transportation Federal Aviation Administration Systems Research and Development Service Washington, DC 20591	Technical Summary 1 October 1986 — 31 March 1988
	14. Sponsoring Agency Code

15. Supplementary Notes

The work reported in this document was performed at Lincoln Laboratory, a center for research operated by Massachusetts Institute of Technology, under Air Force Contract F19628-85-C-0002.

16. Abstract

The FAA-funded FL-2 Doppler weather radar activities are reported here for the period 1 October 1986 through 31 March 1988.

The activities in this reporting period included: final data-gathering operations in Huntsville, AL; dismantling, moving, and re-erecting the radar and associated mesonet stations in Denver, CO; and gathering wind-shear-event data during the 1987 summer experimental period. In parallel with the radar operation and data-collection activities, a large data-analysis effort has been under way in support of automatic wind-shear detection algorithm development and system performance evaluation.

A proof-of-concept demonstration of the Terminal Doppler Weather Radar test bed will be held at Stapleton International Airport in Denver, CO during July and August 1988. Work leading to, and the final preparations for, the demonstration is also reported herein.

The report is divided into five sections. Section I is an introduction; Section II discusses the radar test bed; Section III discusses the experimental operations; Section IV describes algorithm development and performance; and Section V describes the NEXRAD/TDWR interactions and Group 43 support activities.

17. Key Words		18. Distribution Statement
weather radar	Central Weather Processor	Document is available to the public through the National Technical Information Service, Springfield, VA 22161.
low-altitude wind shear	turbulence	
NEXRAD	Doppler radar	
TDWR	ethernet	

19. Security Classif. (of this report)	20. Security Classif. (of this page)	21. No. of Pages	22. Price
Unclassified	Unclassified	146	

FORM DOT F 1700.7 (8-69)

ABSTRACT

The FAA-funded FL-2 Doppler weather radar activities are reported here for the period 1 October 1986 through 31 March 1988.

The activities in this reporting period included: final data-gathering operations in Huntsville, AL; dismantling, moving, and re-erecting the radar and associated mesonet stations in Denver, CO; and gathering wind-shear-event data during the 1987 summer experimental period. In parallel with the radar operation and data-collection activities, a large data-analysis effort has been under way in support of automatic wind-shear detection algorithm development and system performance evaluation.

A proof-of-concept demonstration of the Terminal Doppler Weather Radar test bed will be held at Stapleton International Airport in Denver, CO during July and August 1988. Work leading to, and the final preparations for, the demonstration is also reported herein.

The report is divided into five sections. Section I is an introduction; Section II discusses the radar test bed; Section III discusses the experimental operations; Section IV describes algorithm development and performance; and Section V describes the NEXRAD/TDWR interactions and Group 43 support activities.

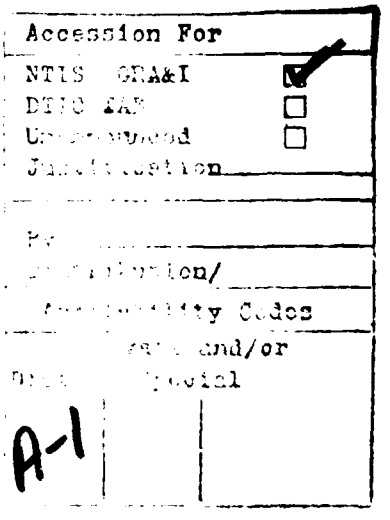

TABLE OF CONTENTS

LIST OF ILLUSTRATIONS

LIST OF TABLES

WEATHER RADAR STUDIES

I. INTRODUCTION

The principal areas of emphasis for the weather radar program over the period 1 October 1986 through 31 March 1988 are listed below.

(a) Continued checkout and upgrading of the transportable Doppler weather radar test bed being utilized in a series of experimental programs during the period 1986 to 1988.

(b) Wind-shear data-gathering operations at the test-bed sites near Huntsville, AL and Denver, CO.

(c) Moving of the FL-2 test bed from Huntsville to Denver for the 1987 to 1988 summer storms season.

(d) Reduction and analysis of data from the Huntsville and Denver radar experiments in support of the Terminal Doppler Weather Radar (TDWR) programs.

(e) Development and refinement of automated TDWR algorithms.

(f) Various analyses in support of the TDWR program.

(g) Refinements to certain Central Weather Processor (CWP) products to be generated by the NEXRAD system, and support to the Federal Meteorological Handbook committee.

(h) Development of scoring techniques and algorithms for evaluation of the TDWR test bed.

(i) Planning for operational evaluations of the TDWR products in the 1987 to 1988 time frame in conjunction with the National Center for Atmospheric Research (NCAR), the National Severe Storms Laboratory (NSSL), the FAA Technical Center (FAATC), and the University of North Dakota (UND).

II. TEST-BED DEVELOPMENT

A. RADOME

The antenna radome is an inflatable, Teflon impregnated, Dacron bag 55 ft in diameter manufactured by the Birdair Corporation of Buffalo, NY. Inflation is maintained by a dual blower pressure system linked to an external anemometer. When wind velocity exceeds 55 mph, the system increases internal radome pressure from 3 in of water to 7 in.

The radome was first put in service at the Memphis, TN field site in August 1984. It was moved to Huntsville, AL in December 1985 and then to the Denver, CO site in March 1987.

During this reporting period, the radome and blower system have operated without incident. There are no plans for any extraordinary activity involving this equipment during the next reporting period.

B. ANTENNA

The FL-2 antenna consisting of a 33-ft parabolic reflector, employing a horizontally polarized, focus-mounted feedhorn, was designed, built, tested, and installed by H&W Industries, Inc. of Cohasset, MA. The RF feedhorn structure was designed and fabricated at Lincoln Laboratory, and installed by H&W Industries.

The antenna is maneuvered by a Scientific-Atlanta pedestal which was modified by the Lincoln Laboratory Control Systems Group to meet the NEXRAD Technical Requirements (NTR) of $15°/s^2$ acceleration in both axes, 30°/s peak azimuth velocity, and 15°/s peak elevation velocity. The mount was further modified by installing a forced flow lubrication system for the azimuth gearbox.

The antenna and pedestal were installed and used at both Memphis and Huntsville before being moved to Denver for the 1987-1988 operations. The antenna has continued to perform without incident other than routine bolt tightening. During the late autumn of 1987, both rotary joints and much of the waveguide were replaced in order to reduce the reflected power level. The rotary joints were worn due to slight misalignment, and were rebuilt to be held as spares. The replaced sections of waveguide suffered from some arcing. No work on the antenna is planned for the next reporting period, other than routine preventive maintenance.

The synchro/digital converter (SDC) that was delivered with the pedestal was capable of angle output each 10 ms and had a built-in delay of 20 ms, thus causing significant position errors to be present when the antenna was moving at maximum velocity. In August 1987, a replacement SDC was installed which converts at a rate that insures very accurate positioning at rates up to 70°/s. A series of tests was conducted to show that antenna position response to commands is accurate, predictable, and repeatable.

During the next reporting period, several tests and changes will be performed on the pedestal drive system. The source of a small 10-Hz oscillation in the antenna structure will be sought, and corrected when found. System gains will be adjusted to prevent the power amplifiers from saturating when maximum rate commands are given.

C. TRANSMITTER/RECEIVER

The test bed uses a regular production ASR-8 transmitter (on loan from the US Navy) with a Lincoln-developed instantaneous automatic gain control (AGC) receiver.

1. Transmitter

The klystron final amplifier was replaced twice during this reporting period. Both failures were caused by arcing which followed the fracture of a Lucite rod supporting the heater connections to the tube.

There have been three cases of waveguide pressure window destruction caused by arcing in the waveguide. All failures occurred prior to the systematic waveguide upgrading described in Section II-B.

The 60-Hz filament and core bias power supplies were replaced with a PRF synchronous filament supply and a dc switching bias supply, respectively. This was done to eliminate the 60-, 120-, and 180-Hz spectral lines that were contaminating the transmitted signal. The only visible spurious line now present in the transmitter output is a small 360-Hz component that is generated in either the high-voltage power supply or the focus coil supply.

2. Receiver

A TPQ 35 radar operated by the US Marine Corps is located not far from the Denver site. Although it has been inoperative since before our arrival in the area, their current plans call for radiating during the spring and summer of 1988 on an assigned RF not far from that of FL-2. In anticipation of that activity, a tunable preselector filter from an FPS-18 radar system was installed in the FL-2 waveguide just ahead of the RF amplifier. Introducing the additional filter causes a loss in radar sensitivity of about 0.9 dB. This filter will be removed if it becomes definite that the Marine Corps radar will not be active this summer.

During the move to Denver, the A/D converters were sent to Lincoln Laboratory for testing and evaluation. Measurements indicated that there had been no appreciable loss in performance since the original installation in 1984. More recently, one of the units developed a large dc offset and was returned to the manufacturer for repair.

Sensitivity Time Control (STC), although available in hardware, has never been utilized during data gathering. Recent analysis showed that close-in clutter signals were saturating the radar front end. When the STC correction was re-inserted later in the processing chain, the resulting amplitude changed the actual values to the point where they were even higher than they were

originally. This effect will be compensated for by constructing an STC clutter map and flagging those resolution cells that are saturated. The clutter map will be implemented early in the next reporting period.

During the summer of 1987, receiver gain was raised 6 dB so that receiver noise is now large compared with A/D quantization noise. Prior to the change, extremely small signals (especially, very low reflectivity clear-air returns) were not detectable.

At about the same time, it was discovered that the 16-bit logic hardware in the signal processor cannot accommodate the full receiver dynamic range supplied by the AGC system. Since it was felt that A/D saturation is preferable to signal processor overflow, the AGC system was changed to lower the maximum permitted attenuation in the receiver. The result is that the A/D converters now limit (instead of folding over) when the received signal is greater than 96 dB above noise. In the near future, a new floating-point signal processor will be implemented which will obviate that limitation. At that time, the AGC system will be reconfigured to its former design.

The signal processor contains a lookup table of coefficients which is used to restore full magnitude to signals that have been attenuated by the AGC system. Until very recently there was no analysis software to permit evaluation of coefficient accuracy, so no attempt had been made to make use of the complex multiplication capabilities that are present. We have now determined that the existing real coefficients still leave transients at the AGC crossover points on the order of 0.1 dB magnitude and 2° phase shift. During the next reporting period, the coefficients will be changed to complex numbers and software will be generated to check them periodically against hardware drift due to time and temperature changes.

D. SIGNAL PROCESSOR

1. Overview

The FL-2 test-bed Signal Processor (SP) is a Lincoln Laboratory-built special-purpose digital processor which collects and processes digitized pulse returns from the radar. The basic computational tasks are AGC normalization, low-velocity clutter suppression, and autocorrelation. The parameters for these computations are downloaded to the SP from a host computer. The results of the computations are then sent to the Data Acquisition and Analysis (DAA) processor for use in the next processing step of the weather-analysis algorithms.

Two signal-processor systems have been built. One is in use with the FL-2 weather radar test bed at the current test site near Denver, CO, and the other is in use at Lincoln Laboratory as a hardware and software development tool. The block diagram of the SP in Figure II-1 illustrates its internal architecture and its relationship to the surrounding elements of the FL-2 system.

Each of the functions of the SP is controlled by parameters sent to it by the Concurrent host computer. One of the two major computational tasks is the low-velocity clutter suppression. This is realized by a 39-point FIR filter with a notch width of 1 to 3 m/s. The filters produce more than 50 dB suppression of stationary clutter.

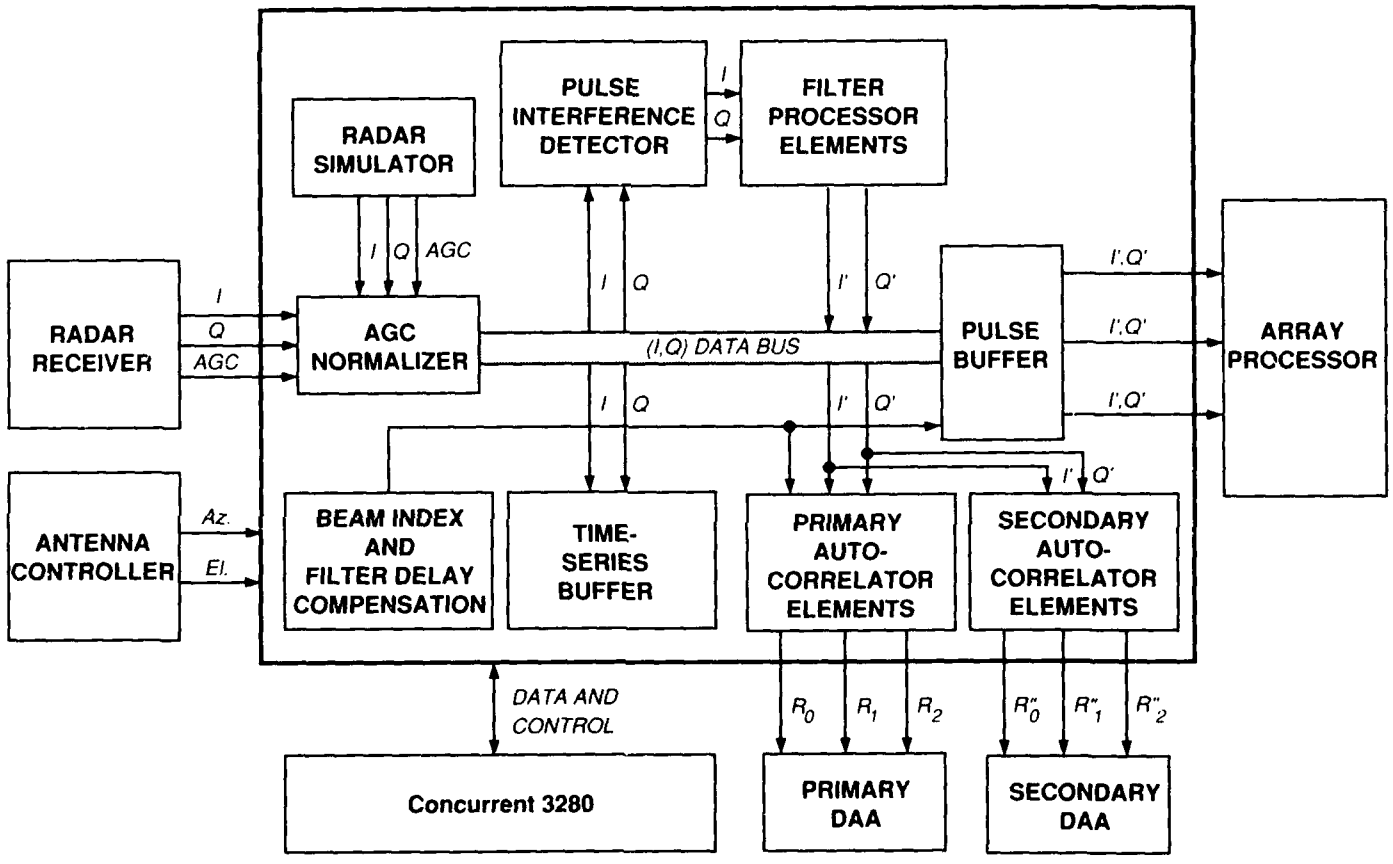

Figure II-1. FL-2 Signal Processor subsystem diagram.

109733-1

The other principal computational task is the autocorrelation function which generates three lag products (0,1,2) estimators. These are formed by integrating the complex filter pulse returns in each range gate over the radar antenna beam width

$$R_0 \propto \sum^{N} s_i \cdot s_i^*$$

$$R_1 \propto \sum^{N} s_i \cdot s_{i-1}^*$$

$$R_2 \propto \sum^{N} s_i \cdot s_{i-2}^* \quad .$$

The number (N) of pulses integrated depends on the scan rate and the pulse repetition frequency (PRF).

The SP has been upgraded so that each integration is performed between integer degree positions of the antenna. Hence, the system can repeatably visit and collect data from fixed, indexed positions in space. Another upgrade to the SP attaches the current antenna position to each set of pulse-return data. A special filter delay compensation memory was added to the SP so that the antenna position values can be delayed by a number of pulses appropriate to the length of the selected filter. This permits all pulse and lag product data to be correctly tagged with their spatial position. In addition, each radial in each tilt of each scan is now tagged with a sequential integer number so that missing radials can be more easily detected.

Other components of the SP include a pulse interference discriminator which zeros pulses that encounter interference from nearby radars, a radar signal simulator with a buffer memory which can be loaded with known signal patterns from the host computer, a single gate output port for diagnostics, and a time-series buffer for recording a limited set of per-pulse data samples at real-time rates.

Another set of recent upgrades to the SP enables it to feed output data to an expanded DAA environment. A dual-DAA configuration is fed lag product outputs from a pair of duplexed autocorrelators. The second set of autocorrelators was included as part of the original SP design in order to provide second trip data processing. That capability of the SP was never utilized, leaving the autocorrelators available for other purposes. The SP parameters are now adjusted to divide the radial data range gates for the two DAAs between the two autocorrelators. This configuration will permit us to gather full rate data this summer.

A new DAA design, which performs its own computation of the lag products in three separate array processors, is fed filtered data via a new set of three pulse data buffers. The SP parameters are adjusted for the new DAA so as to divide the pulse data range gates among the three pulse buffers. Other new information analogous to the quantities described above, i.e., the antenna position and a sequential pulse tag number, is also sent to the new DAA. Figure II-1 illustrates the paths from the SP to both the dual DAAs and to the array processors in the new DAA.

2. Status

The test-bed SP was moved from Huntsville and installed in the new Denver site in April 1987. It was tested during May, with no significant problems, and was in satisfactory operational use throughout the 1987 summer experiments.

During and after this period the development SP in Lexington was upgraded to provide several new capabilities and data paths in preparation for the summer 1988 experiments. As the various modified components of the SP were debugged and checked out, they were exchanged with the corresponding ones at the field site. All the changes, except for one time-series buffer modification to a spare board, have now been completed.

The upgrades support both the dual and the new DAA configurations in the indexed beam mode of operation. Both the Lexington and site systems are now being continually tested for further verification of correct SP operations in the all-new modes.

One new autocorrelator board was constructed in order to provide adequate support for the dual-DAA configuration. Three SP pulse buffer boards (one spare) and eight associated VMEbus interface boards (two spares) were constructed and successfully tested with the new array processors in Lexington. The boards will be tested on-site when the array processors are installed there.

A full complement of spare boards is now available to support the summer 1988 activities with the test-bed SP. Preparations have included an upgrade of all the boards, with the exception of the one time-series buffer, to the same revision level.

Future work on the SP includes improving the dynamic range and performance of the AGC normalizer and the small Doppler clutter filters. An investigation of candidate integrated-circuit manufacturers has led to identification of 32-bit floating-point multiplier-ALU packages with sufficient processing power to permit reduction of the number of filter processor banks from eight to four. Some of the packages are being procured for further evaluation and testing in Lexington.

E. DATA ACQUISITION AND ANALYSIS PROCESSOR

1. Overview

The current Data Analysis and Acquisition (DAA) processor is a Lincoln Laboratory-built programmable multiprocessor computer. It transforms three autocorrelator outputs from the Signal Processor (SP) into the compressed, factors data format used by the Concurrent host computer. The DAA also acquires antenna and time status information, as well as aircraft beacon messages, and merges the information into the flow of factors data messages to the host computer. In the dual-DAA configuration that is now in use, antenna position information is acquired with the data from the SP.

Three of the current DAA processor systems are in operation. Two are in use with the FL-2 weather radar test bed in Denver, CO, while the other one is in the development and support

system at Lincoln Laboratory. The latter is coupled with a Signal Processor and two Concurrent computers to simulate the test-bed configuration and to run the real-time system software. Until late in 1987, the second of the two DAAs now at the test-bed site was used in Lexington as a hardware component test and diagnostic tool.

Figure II-2 is a block diagram of the internal structure of the DAA. Three processing element (PE) boards are used for the factors and message computations. They communicate with each other via a shared multiported memory (MPM), and with the host computer via a monitor (MON) processor board. The two DAAs on-site are configured identically except for a multiplexor (MUX) board connection to the first PE.

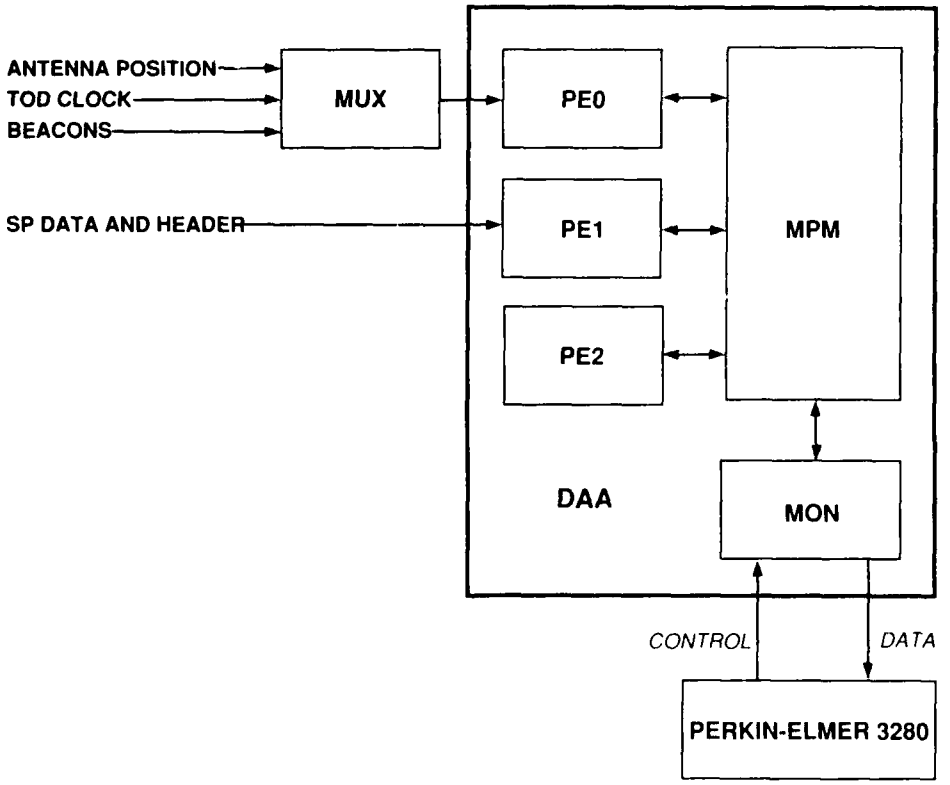

109733-2

Figure II-2. Data Acquisition and Analysis (DAA) computer.

The MUX provides beacon, time, and antenna-position information to the DAA. The MUX antenna information is no longer used by the application software; instead, the second PE in the primary DAA obtains more accurate values from the SP along with the lag product radial data. The PEs in both the primary and secondary DAAs also obtain the number (N) of pulses integrated in each radial and an identifying sequential-number stamp value for each radial in each tilt of a radar scan.

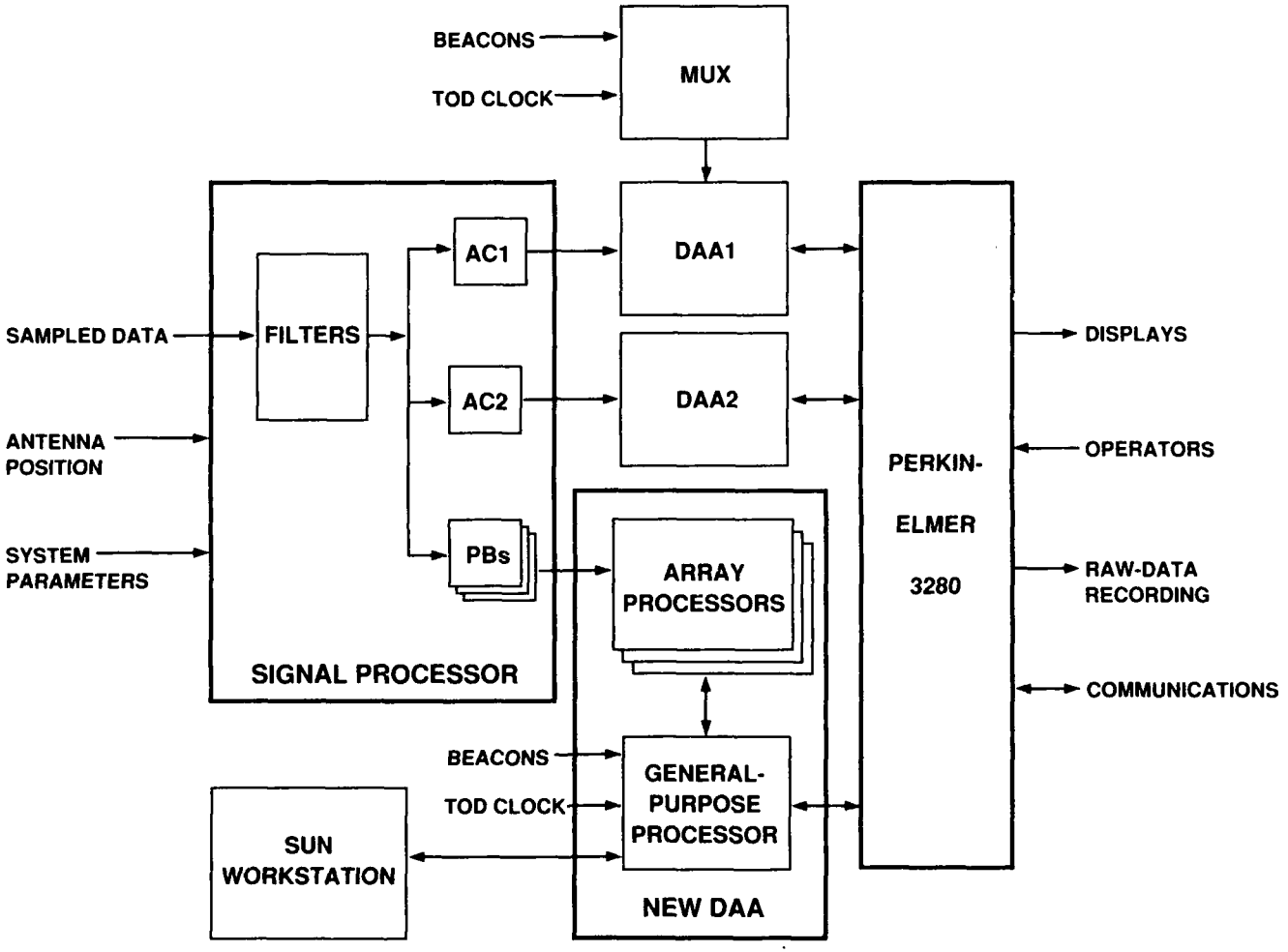

Figure II-3. FL-2 DAA subsystem configuration.

109733-3

More than 40 pulses of data are needed to fill the filter and autocorrelator internal buffer memories in the SP with new data at the beginning of each tilt, and, depending upon the tilt parameters, N can frequently be less than 20. Hence, the DAAs discard the first two radials of each tilt.

Development of a new DAA processor was initiated in early 1987. The new DAA will also contain multiple processors, but it is based on commercially available board components in an industry standard VMEbus backplane chassis configuration. It is intended to offer more functional capability, higher throughput performance, and a greater dynamic range for the data.

Figure II-3 is a block diagram of the configuration of the new DAA and its relation to the signal processor, the current DAAs, and the host computers. High-performance array processors perform the computation intensive data-processing algorithms, and general-purpose processors manage and reformat the data.

Three primary vendors have been chosen for the initial set of components: Mercury Computer for their 20-MFLOP ZIP array processors, Force Computer for their 20-MHz 68020 CPU-21A general-purpose processors, and Technical Systems Consultants for their Unix-like Uniflex multiprocessor real-time software operating system.

Two new DAA processor systems have been procured. Each will be connected as illustrated and operated in parallel with the existing DAA systems, one at Denver and the other at Lexington. That will permit complete testing and gradual phasing in of the new capabilities.

Software development and support for the current DAAs are provided on the Concurrent host computers. These activities frequently interfere with real-time algorithm operations and with development efforts. The new DAA uses a host Sun Unix workstation for development work, hence DAA support and real-time host development activities proceed independently of each other. Application software that is developed on the Sun workstation for the new DAA is written in high-level C-like languages in order to simplify program development.

In the current DAA configuration, the lag (autocorrelator) values are generated by the SP and sent to the DAA. In the new DAA configuration, the lags are generated by the ZIP array processors. As described earlier, radar-data pulse-return buffers have been built into the SP. They bypass the existing autocorrelators and transmit the sampled and filtered data directly to the array processors. Both the pulse buffers and the array processors are designed to handle wider dynamic range data than now required by the current system in order to be compatible with future upgrades of the SP filters. All the new features installed in the current dual-DAA configuration, including the indexed beam mode, will be available with the new DAA.

2. Status

The test-bed DAA was moved to the Denver site in April 1987 with the other system equipment. Both before and after the move there were numerous reliability problems associated with DAA operations. A concentrated effort was made to solve these problems during the following two months, with the result that a number of improvements were made in both performance and reliability. The efforts were completed by the end of May 1987.

One effort made use of a new software package in the DAA which used three, rather than two, processing elements. The configuration improved the throughput of the DAA from five to more than fifteen radials of factors data per second. By reducing the number of range gates in each radial from the nominal 800 to 400, the antenna scan rate could be increased to as much as 30°/s. These limits were used as the system's operating parameters during the summer 1987 experiments at the test bed.

A concentrated debugging effort has also resulted in greatly improved reliability; the only system failures during the summer resulted from three PE board component failures. A new online spare board procedure minimized the system downtime from these failures, and a full complement of spare boards was available for this period.

After the end of the 1987 summer experiments, additional effort was made to increase the throughput of the DAA. A dual-DAA configuration that divides the computational load for each radial between two DAAs was tested and debugged in Lexington in the fall of 1987, using the two DAAs there. One of them was then moved to the test-bed site to generate the same dual configuration.

The software was also changed to handle a new indexed beam mode of operation, the primary impacts being from the variable number of pulses in a radial of data and from the different source for antenna position information. System tests of this configuration at site have been under way since January 1988, with no significant problems being found. The performance level being achieved is 30 radials/s with a total of 800 range gates per radial. Adequate spare DAA boards of all types are currently available at the test bed to support two DAAs, with the exception of the MPMs. Two MPMs are currently under construction.

During the same period, the two new DAA systems were delivered and installed for test and checkout in Lexington. The principal components of the application software for the array processors and for the host processors have been coded and are now being tested.

The array processor application code has successfully demonstrated the ability to read the data from the SP and compute the lag products in a 32-bit floating-point format. The remaining task is to integrate this software with the code which sends the results to the Force processors and demonstrate that all of these operations can be carried on simultaneously while maintaining the desired performance level. Identical copies of the software will be operated simultaneously in parallel on the three ZIP array processors.

The major effort with the Force processors has been directed toward overcoming reliability problems with the multiprocessor hardware and with the operating system software. These problems are being investigated with both the hardware and the software vendors. We have successfully tested an application software package which avoids reliability problems by using a high-overhead message-polling technique, but it has less than half the required throughput performance. Additional work is still needed with this package in order to integrate it with the three array processors and with the Concurrent computer.

F. CONCURRENT COMPUTER SYSTEMS

The FL-2 Weather Radar has historically used two computers manufactured by Concurrent Computer Corporation (formerly Perkin-Elmer): a Model 3212 and a Model 3260MPS. The 3212 was used for real-time control of the radar system, radar antenna movement, the signal processor, and the DAA. It was also the host for the DAA software. The 3260 was the main minicomputer for the test bed, and provided high-speed data recording, display computation and management, system control, and detection algorithm execution.

During this reporting period, the 3260MPS used at the Huntsville site was replaced by a Concurrent Model 3280MPS. The changeover took place during site erection in Denver in May 1987, and the 3280 was used throughout the 1987 data-collection season. Computation capability increased as expected (by approximately a factor of 4), and the system was capable of twenty-five 400-gate radials per second throughput, including recording, display, microburst detection, gust-front detection, and PRF determination.

In October 1987, the functions served by the 3212 were merged onto the 3280. With the substantial differential in computing power between the 3280 and the 3212, combined with the relatively high maintenance costs related to 3212 operation (both in service agreements and configuration control of shared software), it was deemed that the 3212 was superfluous to test-bed operations. Additionally, executing both radar control and data acquisition and processing software in a single operating system environment enhances system cohesiveness. The 3212 will be removed from the site and shipped to Lincoln by the end of April 1988.

There were a number of initial problems with the 3280MPS system, largely due to the fact that the FL-2 3280MPS was Serial Number 2. Most problems were solved before the start of official operations, though some auxiliary processing unit (APU) difficulties persisted throughout the reporting period. The problems were intermittent in nature, and may have been exacerbated by poor voltage regulation in the site electrical supply. Concurrent personnel were commendably prompt and attentive when dealing with the problems; no significant data-collection opportunities were lost.

In September 1987, two additional 6250-bpi/125-ips tape drives were installed. Motivation for the additional drives was to (1) provide redundancy for data-collection operations, and (2) allow multiple translation and other data-analysis programs to be executed during periods when data were not being collected.

Figure II-4 shows the FL-2 test-bed 3280MPS computer system configuration as of the end of this reporting period.

G. ANTENNA/RADAR CONTROL SOFTWARE

1. Overview

Since the last reporting period, the antenna/radar control software was merged with the real-time control software to run on a single Concurrent 3280 system. Figure II-5 shows the new test-bed configuration. The antenna/radar control software responsibilities are as follows:

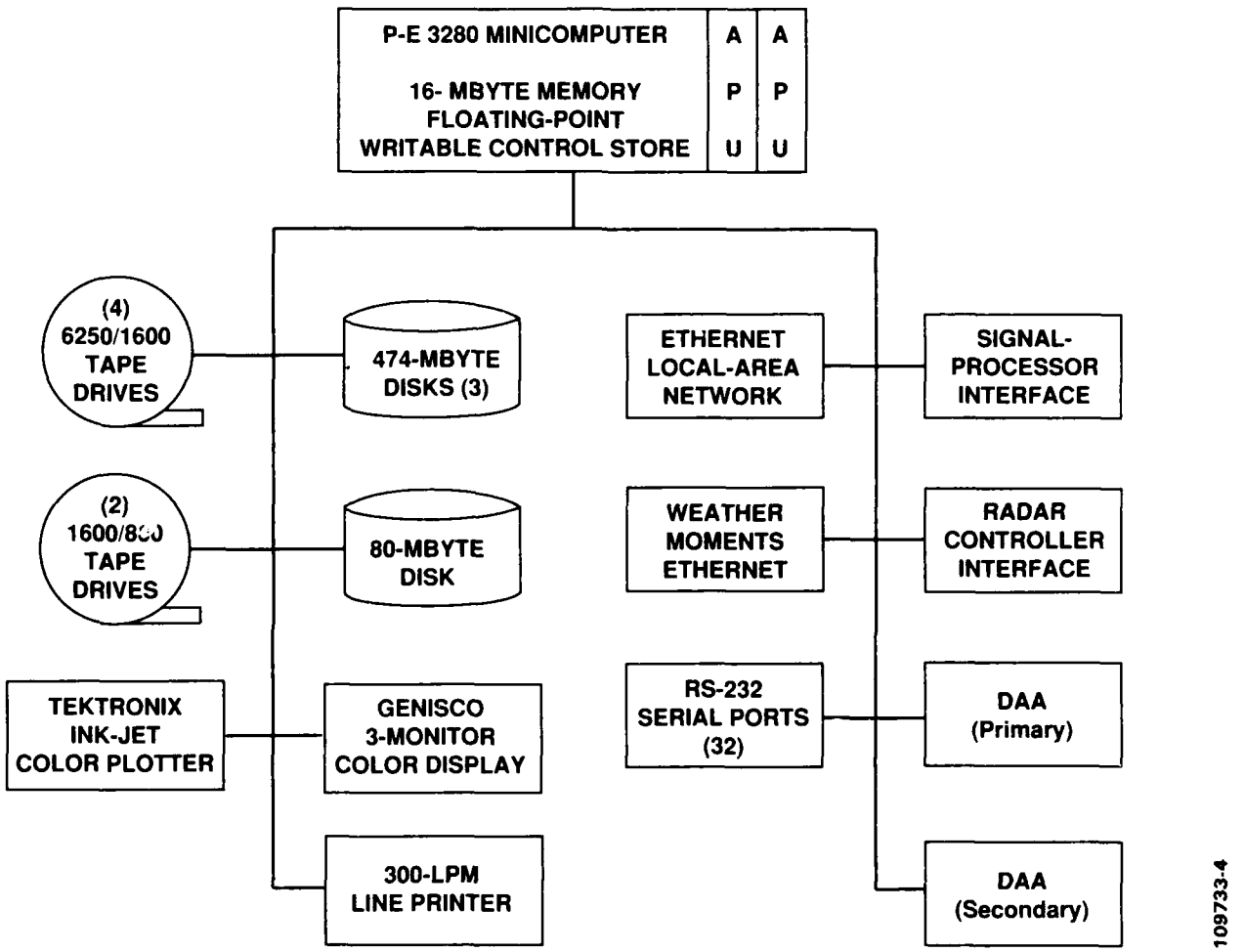

Figure II-4. FL-2 test-bed computer system configuration.

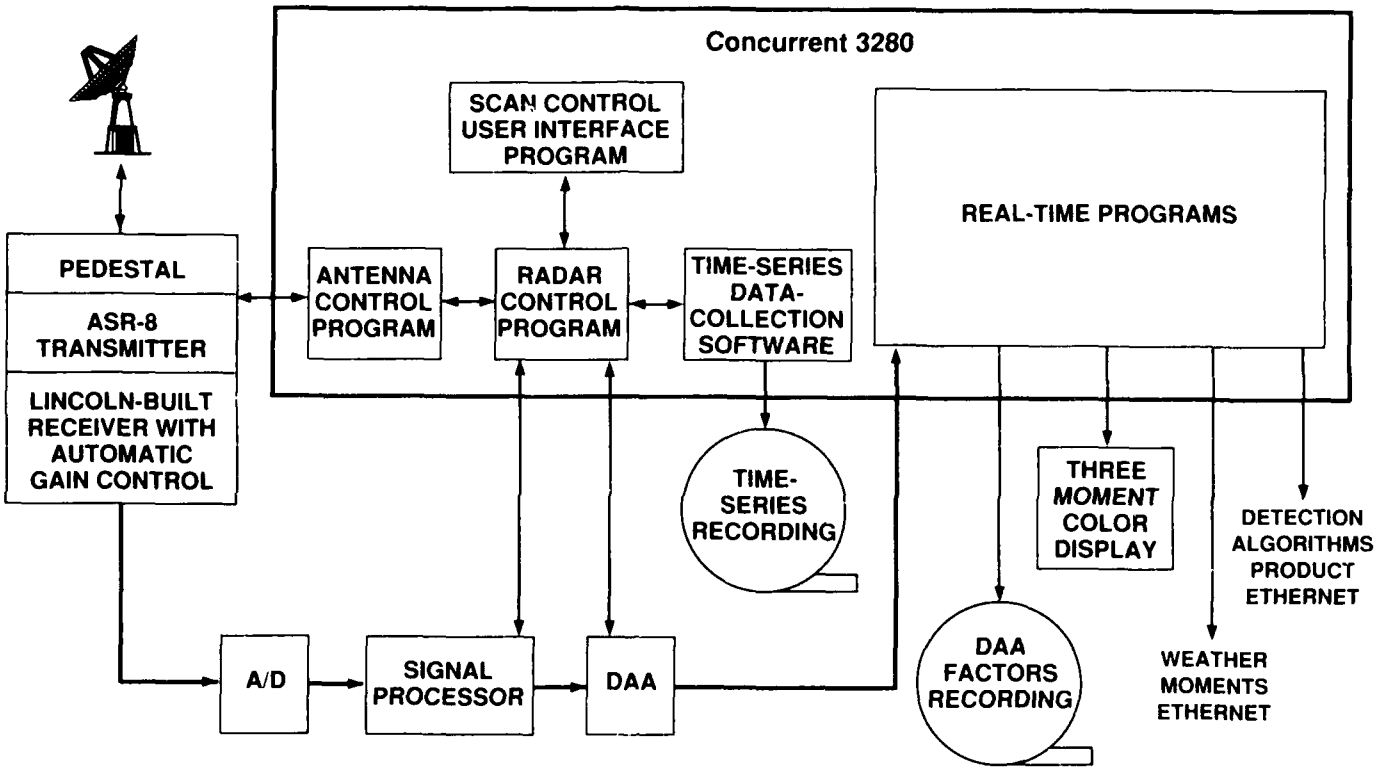

Figure II-5. FL-2 test-bed block diagram.

(a) Provide users with an interactive scan control utility with which a number of scans (PPI, RHI, and POINT) can be defined and commanded.

(b) Translate user scan definitions into sequences of commands to be distributed among the various hardware devices associated with the radar system including the antenna pedestal, the signal processor, the DAA data processor(s), and additional application software packages.

(c) Provide users with access to various application programs for specific functions during real-time operations including the following:

- Real-time aircraft beacon tracking in which scans are dynamically defined to include selected aircraft positions.
- Time-series recording of either filtered or unfiltered I and Q radar measurements.
- Antenna simulation for software development and testing in the laboratory.

(d) Real-time scan monitoring capability providing users with current scan and antenna position information.

A number of modifications were made to the antenna/radar controller software in preparation for the weather radar demonstration in Denver during the summer of 1988. The modifications ranged from minor performance improvements in existing software to complete design and development of new and improved software packages.

2. Scan Control

A new scan control utility was designed and developed to replace the existing interactive scan edit utility. The new software was designed to offer users more scan control flexibility than the existing software. The first working version of the new scan control program was delivered to the site at Denver in November 1987. Operator comments and requests since then have been received and acted upon to further improve the software. The new scan editor is run on the same machine as the radar controller, thereby eliminating the intermachine RS-232 communication link used by the old scan editor. The following features are available in the new scan editor.

(a) The scan editor low-level routines that maintain the various windows displayed on the users screen were improved to run as event driven packages independent of I/O. The previous editor was driven by I/O and did not support event driven processing. As a result of these changes, the scan editor is capable of updating internal data and control information immediately upon receiving messages from other tasks running in the system.

(b) Scan definitions are now stored on disk in readable ASCII files. The previous editor stored scans on disk in unreadable binary form, making editing a difficult task.

(c) The new scan editor maintains a set of internal registers that can be updated in real time by any other task in the system. The registers provide a mechanism to dynamically update scan control characteristics without user intervention. For example, the PRF of the radar used during operations may either be entered explicitly by the user or read from a register that is automatically updated by the range obscuration software also running in the system. The register control software permits any scan control parameter supported by the scan editor to be substituted with a register value. The previous scan editor provided no automatic scan parameter substitution.

(d) A real-time monitor menu has been added to the scan editor. The monitor displays current antenna activity, i.e., the current scan, the current tilt, the elapsed time of the current scan, the scan number, the current position of the antenna (azimuth and elevation), and the status of the requested scan queue.

(e) The scan scheduler menu from which scan control commands are entered was upgraded to make up to 32 scans immediately accessible. The program also allows up to 15 scans to be scheduled for execution. A user may choose to repeat a specific scan schedule once or indefinitely.

(f) The number of scan control parameters available to the scan editor users was increased to provide users with as much flexibility as necessary for operations during the summer demonstration in 1988. The scan parameters are entered in any of three display menus: one for global scan characteristics, and two for tilt characteristics.

(g) A subtasking feature was added to the new scan editor that the old scan editor was unable to support. The new scan editor is capable of starting or stopping a number of tasks whose status is automatically monitored by the scan editor. Thus, if one of the tasks changes state (halts or is canceled), the scan editor will be immediately informed and a status message will be delivered to a user display. Currently, the programs that run as subtasks of the scan editor are the radar controller program, a radar controller simulator program, the time-series buffer recording software, aircraft beacon tracking software, and a simulated antenna controller task for lab simulations in Lincoln Laboratory.

(h) The number of tilts permitted in a scan has been limited to 25. Before the summer of 1988, the new scan editor will be adjusted to support up to 96 tilts per scan.

3. Antenna Controller

In this reporting period, significant changes were made to the antenna control program. Before the antenna program was transported to the new 3280 system, it consumed 60 percent of available CPU time on the 3212 leaving little time for other functions. To alleviate the problem, the program cycle time was reduced from about 70 to 10 Hz. That reduced the CPU utilization

to less than 10 percent of available time with no degradation in performance. The following changes were also implemented to insure precise control of the antenna at the reduced update rate.

(a) The antenna control program cycle times were programmed to vary between a maximum of 100 ms and the optimal delay necessary for proper antenna positioning to a tolerance of 0.3° (i.e., when the antenna approaches the end of a tilt sweep, the cycle time of the antenna control program is reduced in order to update antenna positioning with finer precision).

(b) Antenna velocity is determined by antenna tachometers instead of by numerical differentiation of position.

(c) Servo response delay times are now compensated for when formulating pedestal control commands.

During performance tests of the new antenna control program modifications, it was discovered that the azimuth servo response was excessively underdamped. The oscillatory response observed may have contributed to the azimuth coupling failures experienced over the past year. The problem may be in the azimuth torque bias unit, although further work will be required to pinpoint and correct it.

Work has begun to rewrite and document the antenna control program to make it easier to understand and maintain. Accordingly, we expect to complete the following changes during the next reporting period:

(a) The program will be written in Fortran 77 instead of the current version of RATFOR. Fortran 77 was chosen to maintain consistency with the rest of the real-time system software.

(b) All computations related to antenna positioning will be performed in floating-point arithmetic instead of the current integer implementation. The original design intent of integer computations was to minimize execution delays associated with floating-point arithmetic. The impact of floating-point arithmetic is not expected to degrade performance, but it will improve software clarity.

(c) The new program will make use of modular structure, i.e., subroutines and functions will be introduced.

(d) Inline documentation will be included in the code to assist in future software modifications.

(e) Changes of the antenna fixed angle will be made outside the data-collection area while the antenna begins to accelerate in the sweep direction.

4. Radar Controller

The modifications made to the radar controller software matched the upgrades in the new scan editor program. The communication scheme developed between the scan editor program and

the radar controller program affected the front end of the radar program where scan definitions were received from the editor and scan control information was extracted.

(a) The following features which were not previously supported have been added to the new radar controller program:

- Control of the DAA output: factors, moments, or resampled Cartesian data.
- Control of clutter map application.
- Control of scan strategy: executing all tilts in one direction, alternating scan direction each tilt, or permitting a user complete control over the direction of the antenna during each tilt.
- Control of the beam indexing feature supported in the signal processor hardware.
- Antenna rotation rate between 0 and 30.0°/s in either direction along azimuth (clockwise or counterclockwise) and between 0 and 15.0°/s in either direction along elevation (up or down).
- A noise thresholding factor was added to increase or decrease the DAA sensitivity to noise during data thresholding. The DAA threshold can be raised from 0 to 20 dB in order to reduce unwanted low-level signal noise.
- The automatic clutter filter selection algorithm was upgraded to recognize 13 new 39-point clutter filters available in the FL-2 signal processor. The new filters were designed for optimal clutter rejection at four different PRF values: 700, 900, 1050, and 1200 Hz with a minimal clutter suppression of 50 dB. The four previous clutter filters were designed for a nominal PRF of 1200 only. This full set of clutter filters will be operational during the summer demonstration in 1988 in Denver.
- The control of the FL-2 Coherent Oscillator (COHO) switching, and Sensitivity Timing Control (STC) were made available to the scan editor and are supported by the new radar controller software.
- The control of the FL-2 Pulse Interference Detector (PID) was made available to the scan editor and is supported by the new radar controller software. Modifications to signal processor hardware are expected before the summer of 1988 to actually control the PID through software.
- The control of the radar simulator was made available to the scan editor to implement a number of front-to-end system diagnostic tests. The scan editor user can channel up to 1024 range gates of simulated I, Q, and AGC scaling values from the radar simulator into the signal processor.
- Time-series data collection can be enabled through the scan editor. A user must specify a desired starting and stopping range (in kilometers) to collect

either filtered or unfiltered time-series data. Preliminary tests indicate that with no weather detection algorithms running on the 3280 system, at least 80 range gates per pulse can be successfully recorded with the time-series software.

(b) All communication to and from the radar controller program was implemented through task messages supported by the operating system. The RS-232 communication link used by the previous software is no longer used.

(c) The substitution of all tilt parameters maintained in registers (except the fixed angle, stopping angle, and antenna rotation rate) is now performed at the start of each tilt. This feature allows new register values generated by detection algorithms to be applied as soon as possible, i.e., in the next tilt. Before the change, register values were substituted only at the start of each scan.

(d) Modifications were made to the radar controller program to support up to three DAA devices in a number of modes of operation:

- No DAA at all (for diagnostic tests only).
- A single existing DAA processing up to 800 range gates at 15 radials/s.
- An existing DAA processing up to 800 range gates at 15 radials/s running in parallel with a new DAA device.
- Two existing DAA devices processing up to 400 range gates each for a combined data throughput capacity of 800 range gates and 30 radials/s.
- Two existing DAA devices processing up to 400 range gates each for a combined data throughput capacity of 800 range gates at 30 radials/s running in parallel with a new DAA device.
- A single new DAA device processing up to 800 ranges gates at 30 radials/s.

5. Diagnostics and Calibration

Antenna noise power has previously been reported erroneously. The actual mean value for receiver noise was 0.60 counts, with a standard deviation of 0.02, a minimum value of 0.56 counts, and a maximum value of 0.63 counts. The error was caused by a misnomer in the daily calibration records which concealed a discrepancy between the computer output and the recorded entries.

In order to maintain correct calibration of critical system characteristics, a number of offline diagnostic software packages have been developed. Daily calibration tests performed on the radar system produce measurements that are recorded and analyzed at Lincoln Laboratory to insure proper system performance. New software packages combined with existing calibration software tools provide sufficient information to maintain satisfactory radar measurements. Some of the system analysis results derived from the improved calibration software output are listed below.

(a) In an effort to avoid future interpretation problems, the calibration program was updated so that the displayed information includes the mean and standard deviation of each digital channel along with the average power of the two channels. The measured values are also logged to a running calibration file used only for record keeping and not for actual real-time operations.

(b) Logging daily calibration measurements was useful for tracking and analysis. The log of system noise calibrations (measured in digital units) revealed an increase in system noise beginning late in the summer of 1986. The main value of the noise in the system increased from 0.60 to 1.22 counts.

(c) A new set of AGC values were installed on-site. The new numbers were designed to eliminate a persistent saturation problem in the AGC normalizer hardware at the front end of the radar system. Incoming signals that exceeded the dynamic range of the AGC unit were causing unpredictable received data magnitudes. Testing and verification of the new AGC values were done in July by injecting an RF ramp into the front end of the radar channel with and without the new AGC numbers in place. The resultant I and Q quantities coming out of the signal processor normalizer were recorded with time-series data-collection software. Figures II-6 and II-7 contain a plot of the signal power $[10 \log_{10}(I^2 + Q^2)]$ of the decreasing input ramp with the old and new AGC values in place. Figure II-6 illustrates the signal degradation caused by AGC saturation. Figure II-7 verifies that the new AGC numbers provide satisfactory limiting of excessive input signals.

(d) Injecting simulated data from the radar simulator into the signal processor has resulted in the discovery of a number of defects in the signal processor hardware. The causes of the defects were investigated and resolved.

(e) Implementing a software simulation of the antenna control program has enabled complete front-to-end system tests to be performed at the site and in Lincoln Laboratory to verify identical system behavior.

H. MAIN MINICOMPUTER SOFTWARE

The FL-2 real-time system (RTS) operates in the Concurrent Computer Corporation Model 3280MPS computer. Figure II-5 is a block diagram showing the primary elements of the central computer subsystem. Its functions are:

(1) Acquisition of preprocessed radar sample data from the DAA.

(2) Recording of DAA data on magnetic tape.

(3) Converting the DAA data to weather moments (reflectivity, velocity, and spectral width) for each radar sample gate.

(4) Resampling the computed moments from polar to rectangular coordinates for output to separate color displays for each moment.

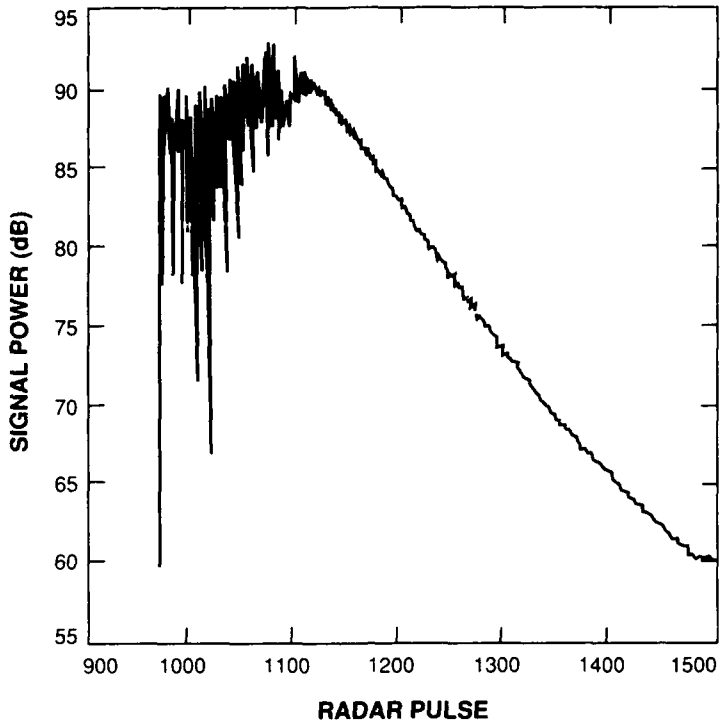

109733-6

Figure II-6. Signal degradation with previous AGC normalizing factors.

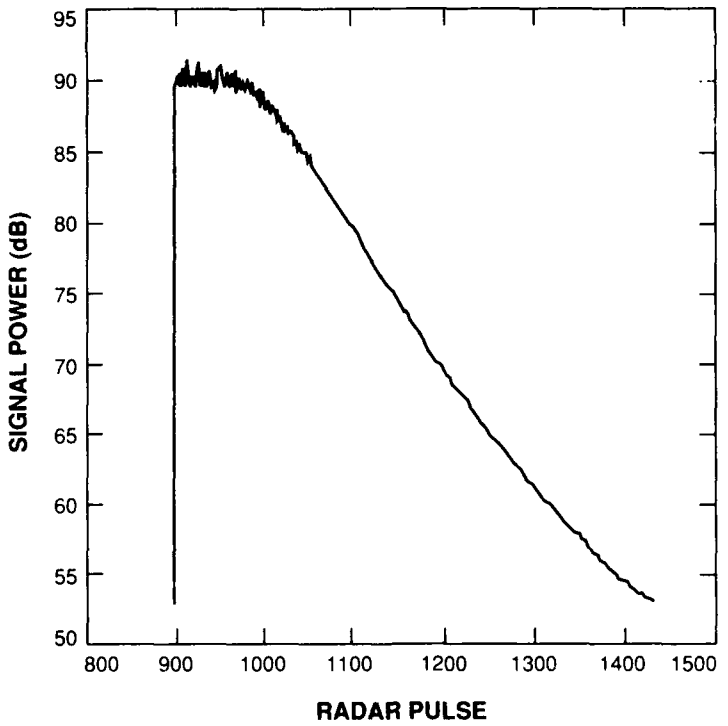

109733-7

Figure II-7. Signal improvement with new AGC normalizing factors.

(5) Transmission of resampled moment images and other weather products to remote computer systems and workstations.

(6) Providing a real-time data base and hosting environment for algorithms for automated detection of hazardous weather phenomena.

(7) Providing manual and semiautomated operator control over antenna scan patterns, data recording, and display of weather moments data.

1. Data Acquisition and Recording

This portion of the RTS is responsible for reading radar sample data from the DAA via a direct memory access (DMA) link, and for recording these data on 6250-bpi/125-ips magnetic tape drives. While the basic functionality of this portion of the system did not change during the reporting period, a number of features were implemented early in the period to reduce operator workload in anticipation of increased data-recording rates in 1987 and 1988:

(a) Improved ability to manage tape drive use within the context of the RTS, including rewind, unload, and forward/back file capabilities.

(b) Ability to switch automatically from one drive to another when approaching the end of a tape reel.

(c) Improved ability for operators to acquire information concerning the current tape utilization status.

This portion of the system is limited neither by available CPU time nor by I/O time, and hence is easily capable of the maximum 30 radial/s data-collection rate anticipated for 1988.

2. Data Distribution

This portion of the RTS is central to the operation of all tasks in the system except the data acquisition and recording operation. It is a two-stage process, beginning with the data as recorded on tape, and ending with whatever task (e.g., resampler, or weather detection algorithm) might request the data:

(a) Individual physical records received from the DAA are compiled into *tape buffers* for recording. The tape buffers are also accessed by a series of tasks which extract particular pieces of information (e.g., radar sample data, beacon reports, etc.) to be distributed to the rest of the system.

(b) The data are distributed to the system as a whole via a *data stream* mechanism. Each stream represents a particular type of data, and may be accessed by any task in the system. Data are not dropped from the system until every task accessing that type of data has had a chance to acquire the data, or until data shedding is forced to occur due to exhaustion of buffer space.

The data stream concept and implementation were enhanced during this reporting period to support event driven (in addition to polling) operations. Otherwise, the basic data stream features remain unchanged.

In addition to the data management task, data distribution includes, when necessary, the computation of weather moments for each radar sample gate. This is a highly CPU intensive task, originally intended to be performed in the DAA. Until such a capability exists in the DAA, it is necessary to perform this operation in the 3280 before the moments data are distributed to the system. Considerable effort has gone into making this computation as efficient as possible, and the current implementation is capable of operating in real time in the 3280 at the data rates anticipated for 1988 without the further addition of auxiliary processing units.

With the incorporation of beam indexing as a test-bed capability, the moments computations were modified to accommodate the variable number of pulses collected per radial. This change required an increase in memory usage (for lookup tables), but did not affect the basic computation performance.

During this reporting period, it became desirable to compensate in the moments computation software for radial sweep angle errors generated by various hardware and software latencies inherent in the test-bed front end. The angle correction software accommodates both the non-indexed and indexed beam modes of operation, and does not affect the computation load.

3. Resampling and Display

The resampling and display tasks enable the operators to observe the data-collection process, and to evaluate appropriate scan strategies for collecting meaningful and useful data. Additionally, during 1987 operations the resampled images were downloaded to a local product display workstation for pseudo-real-time perusal.

The resampling process was originally implemented using a spatial averaging technique which provides high-quality, accurate images. This algorithm is extremely CPU intensive, and would have absorbed a significant portion of the available processing resources at the data rates anticipated for the 1987 operations. Consequently, the algorithm was changed to a more CPU efficient, but less accurate, nearest gate approach. This technique does not perform any averaging, so image accuracy is dependent on the relative sizes of the resampling spatial resolution and radar sample spatial extents. For test-bed purposes, this technique is entirely adequate. Additionally, the size of the resampled region was reduced from 448 by 448 discrete bins to 256 by 256 bins. The reduction in image quality significantly improves the ability to produce timely color images on the displays, and does not affect the usefulness of the images.

The 3280 display task, utilizing the Genisco color computer and three monitors (one each for reflectivity, velocity, and spectral width), turns the resampled data into color pictures under limited operator control. This capability remains essentially unchanged from the previous reporting period, with the exception of improvements to the ability to display aircraft beacon information.

4. Operator Interfaces

The operator interface to the RTS is comprised of an operator command entry terminal, and a system status monitor terminal. The command entry terminal is serviced by a task which performs two basic functions:

(a) Interpretation and/or distribution of operator commands, and

(b) Display of command responses including entry errors.

Throughout much of this reporting period, the command entry task processed most commands locally; during the last third of the period, the command handling mechanism was enhanced so that commands are simply distributed to the tasks which are to be affected by the command. In that way the operator interface itself is unaffected by additions to or changes in the system, and individual tasks are themselves responsible for their own command processing.

The status monitor terminal displays system status reports as well as warning and error messages. The system status monitor capability has not changed since the last reporting period.

5. Communication

This portion of the RTS is responsible for exporting weather moments and algorithm product data to external computer systems and workstations. Two ethernet connections are used for all external communications:

(a) A raw ethernet (no handshaking protocol) for weather moments data. The connection broadcasts weather moments data onto a dedicated ethernet cable at real-time rates (~100 kbytes/s).

(b) An FTP and/or TCP/IP-based standard ethernet protocol for algorithm product data.

During the 1987 operations, weather moments were transmitted to the NCAR computers via the moments ethernet. The FTP and TCP/IP were used to transmit resampled images to a local product display Apollo workstation which was used to perform real-time truthing in support of algorithm evaluation.

Early in the next reporting period, TCP/IP connections will be used to disseminate algorithm products (including gustfront, precipitation, and track-and-predict) to a variety of local and remote workstations and computer systems. The moments ethernet function will remain the same (with minor data format changes), but several additional computers will be receiving the data.

I. LOCAL/REMOTE PRODUCT DISPLAYS

The display capabilities of the display computer workstations are relatively new. They take advantage of the workstation's unique environment to provide a much faster, more flexible, and more interactive capability. Zooming, panning, user programming, multiwindow interaction,

larger images, real-time operation, and a greater variety of colors are all available through a combination of the workstation's native capabilities and software designed to exploit them.

The workstation development began in March 1986. The goal was to develop a display capability for real-time operation on some previously purchased Apollo workstations. If possible, the design and the software should also be suitable for use on the Sun workstations that the group was (at that time) considering for purchase. Achieving that goal required a number of functions:

(1) Collection and classification of data from multiple sources in real time;

(2) Functions to display data of various types including radar returns, range/azimuth marks, algorithm outputs, aircraft beacon tracks, and geopolitical maps;

(3) Mechanisms by which the above may be quickly and easily manipulated and monitored.

Our approach has been to develop each of the above elements in a general-purpose form and integrate them to provide the total environment. This approach has the advantage of being rapid to prototype and modify and in providing a large number of modules which are suited to both real-time and offline analysis.

The resulting collection of programs is commonly referred to as *WxShell.* In fact, the name *WxShell* refers specifically to two related processes responsible for the graphic and text data presentations to the user. The true *WxShell* processes run an interpreter which accepts commands and/or scripts at the user's (interactive) request to perform the desired action. Since it is programmable at run time, the same software is suitable for use in both the real-time and offline analysis contexts. The other processes (data base, data gathering, etc.) are each quite independent, but all have a common and flexible network/server/client orientation.

Work in the previous reporting period had progressed such that a single-window (graphic display) environment was running on Apollo workstations with reasonable performance and moderate capabilities and data could be gathered in real time from the host computer. Still missing were more refined versions of the individual functions, a data-base server to index the gathered data, communications and synchronization between windows, and development of software for communications of reduced data between remotely sited workstation displays.

All the above needs were addressed and largely satisfied during the period covered by this report. In addition, the work also evolved to satisfy the following new or additional group needs.

(1) Individual display functions were made faster, had additional functionality added, or both. New functions to annotate radar images and display aircraft beacons were created. Also, provisions of the command environment were combined with existing display functions to create new *cursor correlation* and *slaved windows* functions.

(2) A data-base server optimized for real-time operation was designed and implemented. It permits access to data based on several criteria including data types and

values. Also functions to permit querying and updating of the data base from inside or outside the data display environment were created.

(3) The command environment was expanded to support communications between windows. The general nature of the implementation permits windows on separate machines (even in separate states!) to exchange data and commands.

(4) The systems level remote communications hardware and software were ordered and delivered.

(5) As of March 1987, though there was no definitive plan to use Sun computers as part of the test-bed display system, some work toward merging the display efforts on the Sun and Apollo workstations had been performed. At that time, the group had a few Apollo workstations and a relatively large number of Sun workstations. In that the programming environments are similar and the workstations provide similar capabilities, it was desirable that the code developed should be applicable to both machines for two reasons:

- From the hardware and system software support perspective, maintaining two different types of hardware and software to provide approximately the same capabilities may prove to be more expensive than simply replacing the Apollos with Suns.
- From the applications software development and support perspective, there is minimal difference between displays for the test bed (which are currently on Apollos) and displays for data analysis (to be done on Suns); it is simpler to provide a single environment for both applications.

From the outset, the software has been designed with Apollo/Sun and real-time/offline roles in mind. Around the middle of the month, a formal decision to support the *WxShell* environment on the Suns for offline data analysis was made. The additional work involved porting the software developed for the Apollo to the Sun, making it functional, identifying areas where performance and/or compatibility could be enhanced.

(6) Also by March, it was becoming clear that a similar display effort being undertaken by NCAR to provide for their needs would not be ready in time for the summer 1987 data-gathering operations. At that point, the prime focus of our effort for the entire summer became the developing of additional capabilities required/desired by NCAR and supporting the entire suite of hardware, operating systems, and application software for their use. That required the following:

- Incremental extension of existing functions (e.g., add azimuth line plotting to the range ring plotting function or the addition of a monitoring capability to autonomous processes).
- Streamlining of existing code for better speed.

- Development and implementation of automated *house cleaning* utilities.
- Upgrading and maintenance of the Apollo operating system.
- Development of *scripts* by which the data NCAR wanted displayed were presented automatically.

Of course, the same work also supported Lincoln's work to document gustfronts in real time.

This support was accomplished almost entirely from Lexington since there were no personnel at the site tasked with any particular workstation support duties.

(7) The port of the software to the Sun workstation environment was completed. The source files required for compilation on the Sun are simple copies of the corresponding codes on the Apollo.

(8) A number of scripts were written to support use of the *WxShell* by the data-analysis users at the Laboratory. They began to use it, finding a number of bugs, but were quite pleased with the increased speed and flexibility.

(9) As part of the development for local users, a graphics button/slider/fill-in-the-blank/menu interface was created. It simplified the job of learning *WxShell* and was a very large factor in its quick acceptance.

(10) The hardware and software which provide for communications between the radar site and remote Sun computers were installed and tested. They worked as anticipated and should be quite satisfactory for operations this coming summer (1988).

(11) A sophisticated capability to plot aircraft beacons was designed and implemented.

(12) Support for the Apollo workstations was discontinued and ports of the non-*WxShell* processes required for real-time operation began.

(13) The data base was upgraded to hold queries and notify the requester when the query condition is satisfied. Previously, the client processes had to repeat the query until satisfied.

(14) New functions to interpret and display new algorithm data formats were developed and installed in *WxShell*. Functions were developed to obtain new products from the new/different processes which generated them.

(15) A function to generate radar data images using information from the *base products* ethernet was developed and integrated. This function replaced a much slower, more cumbersome, and less flexible capability which transferred resampled images from the Concurrent computer.

(16) The interpreter kernal of the *WxShell* was replaced with new code which was simpler, much smaller, and more capable.

J. PLANNED TEST-BED ENHANCEMENTS FOR 1988

Several modifications and upgrades have been made to the test bed during the past reporting period, all leading to the present system capability and further pointed toward being able to successfully perform an operational TDWR demonstration during July and August 1988 at the Stapleton Airport in Denver, CO.

Most of the modifications were made to correct errors and problems uncovered during real-time test operations, including such items as logic miscalculations and various hardware errors. Other modifications were made to incorporate planned upgrades, such as adding computer resources to increase throughput and redesigning software for faster operation.

With the recent addition of a second DAA preprocessor, the weather radar test bed is capable of operating at the full rate of 30° (radials) per second and 800 range gates per pulse. Thus, the data-collection and processing functions can be completed in real time. However, before the system can participate in the summer demonstration, the output of the basic test bed must be communicated to (1) various displays within the FL-2 test-bed display room, (2) the NCAR trailer *verifier*/monitor complex, and (3) the airport ATC facilities in the Stapleton tower and TRACON.

Other system upgrades to be completed in the next few months include: (1) installation of the multiclient ethernets connecting the FL-2 radar trailer, display trailer, and the NCAR console trailer; (2) installation of the microburst subsystem workstations; (3) installation of two analysis display Sun color workstations; and (4) installation of a third APU and additional RAM in the Concurrent 3280 computer subsystem.

1. Ethernet Communications

Figure II-8 shows the overall configuration of the Lincoln Laboratory, NCAR, and Stapleton ATC equipment and communication paths. The communication medium between all processors at the Buckley ANG site is via two separate ethernets. One is a high-data-rate (~100-kbyte) minimum protocol net for transferring moments data to all interested clients and is called the *moments* ethernet. The second is a low-data-rate (~20-kbyte) net using TCP/IP protocol for transmitting the various wind-shear product outputs and is called the *products* ethernet. Figure II-8 shows how the various server and client workstations are connected to the ethernets.

2. Microburst Subsystem

The microburst subsystem hardware consists of two Sun 4/260-M workstations for feature extraction, a Symbolics/Lisp processor, and a Sun 3/260-M product coordination processor. The processors are all connected to both ethernets as shown in Figure II-9. The equipment is presently set up in the Lexington facility for software development. It will be transferred to Denver during April 1988 for final integration into the FL-2 system.

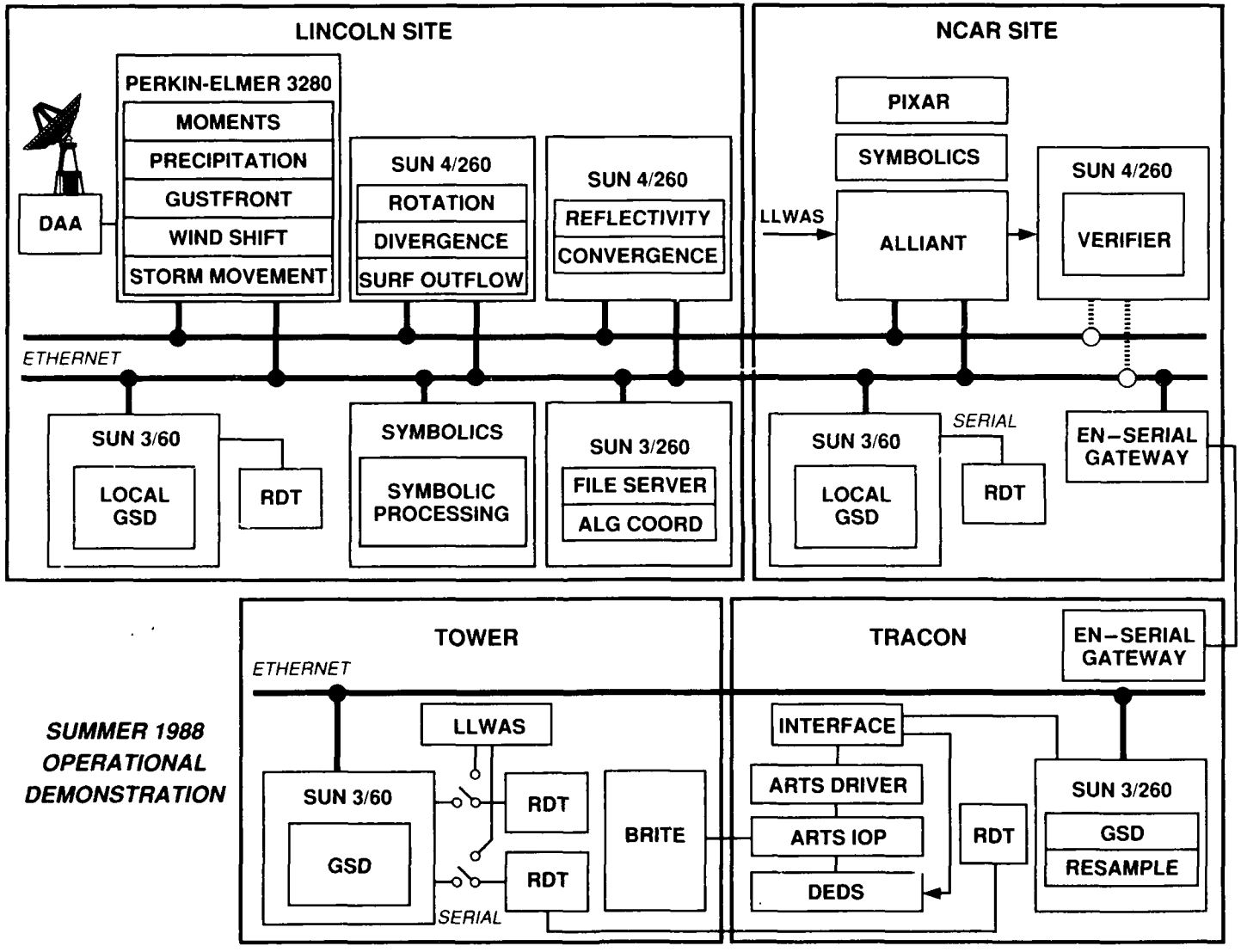

Figure II-8. Configuration of the LL, NCAR, and Stapleton ATC equipment and communications paths.

109733-8

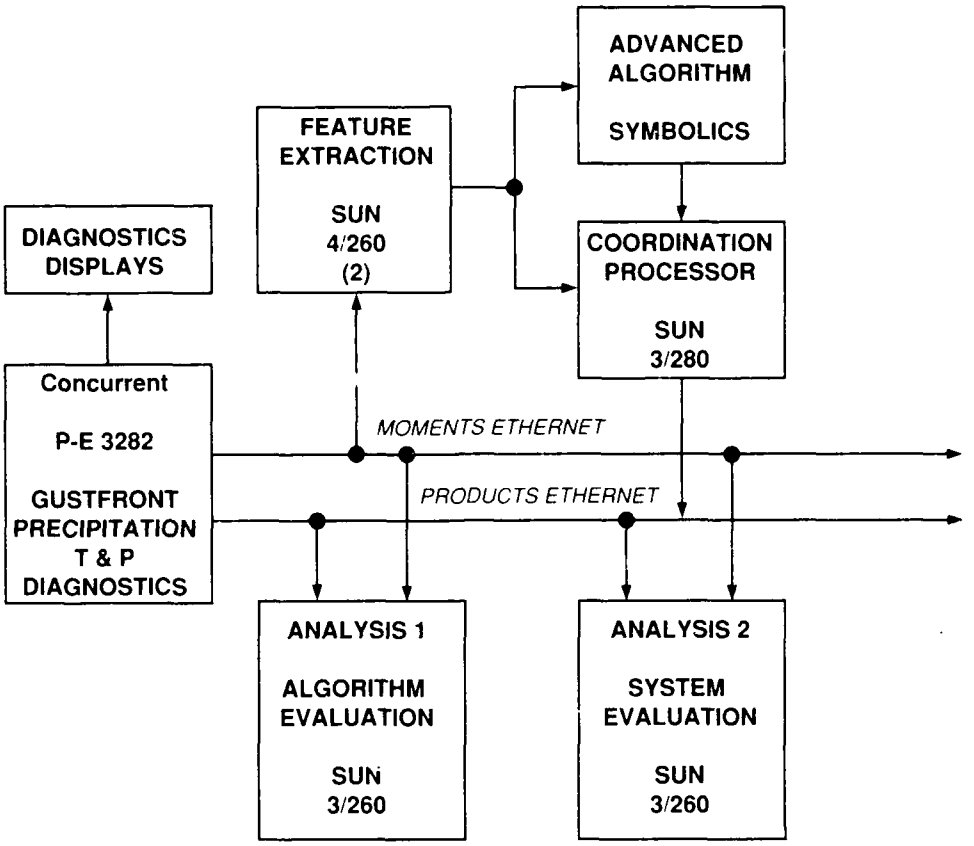

109733-9

Figure II-9. File servers and client workstations connected through ethernets.

3. Analysis Displays

The real-time product verification and analysis displays consist of two Sun 3/260-C workstations. These color displays will be used to display in real time, radar base data, the algorithm product outputs, the Geographic Situation Display output, and various operational overlays. Software to derive the displays is now being developed on similar equipment in Lexington, MA. The displays are scheduled for delivery to the Denver site in April.

4. 3280 Memory Upgrade

Although the present central computer subsystem has sufficient capability to perform the required demonstrable tasks this summer, there is little resource left for expansion or for unforeseen modifications. An upcoming factory upgrade of the Concurrent 3280 computer will provide, among other things, a capability to use more than the present limit of 16 Mbytes of RAM. Therefore, present plans call for installing 16 Mbytes of additional RAM before the summer demonstration. In addition, a third APU will be installed and evaluated during May and June to determine whether purchasing the APU for permanent installation is cost effective.

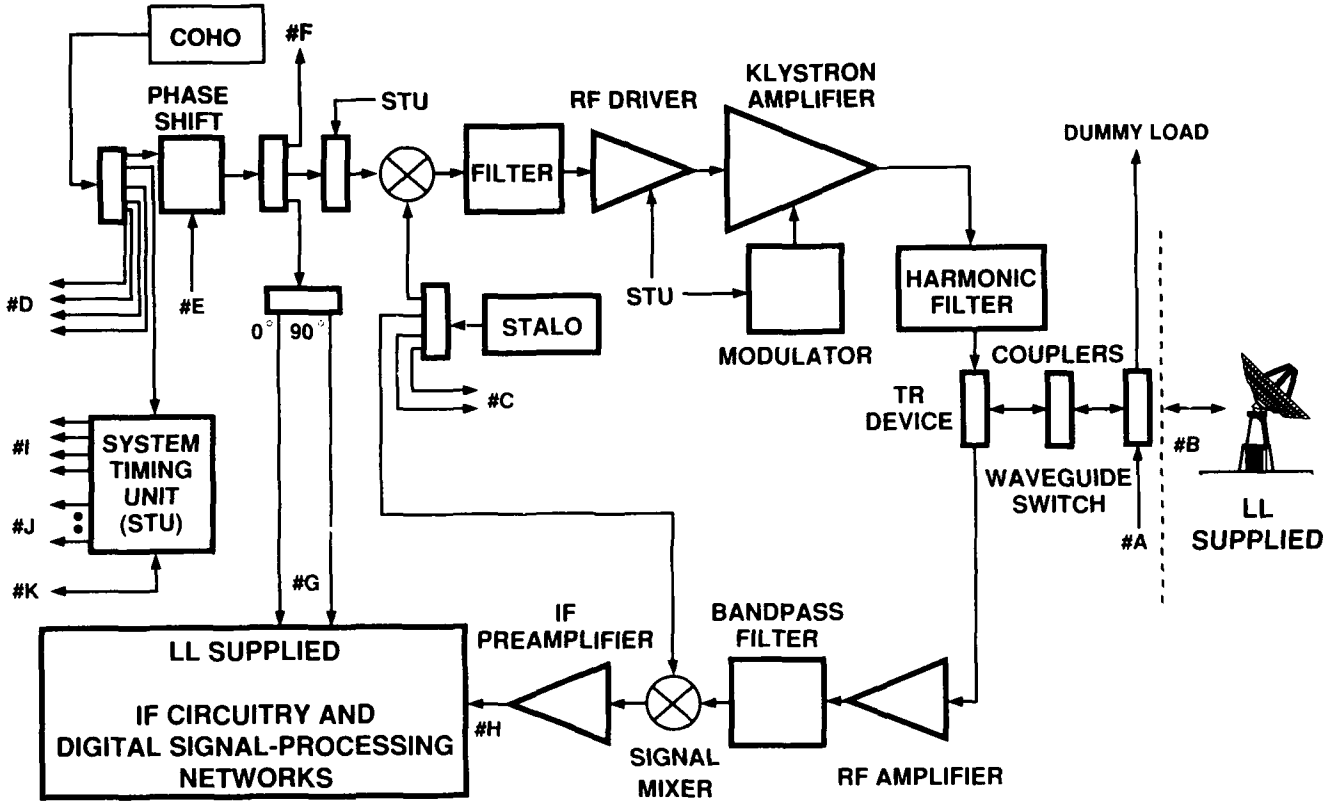

Figure II-10. C-band transmitter/receiver subsystem.

109733-10

K. C-BAND TEST BED

The Terminal Doppler Weather Radar (TDWR) system has been specified to operate in the C-band frequency spectrum (5.60 to 5.65 GHz). The current Lincoln Laboratory TDWR test-bed system operates in S-band (2.70 to 2.90 GHz). In order to more closely simulate a TDWR, we plan to modify the existing test bed after the proof-of-concept tests in Denver in summer 1988.

Initial modification plans center around a changeover of not only the RF transmitter and receiver portion of the test bed, but also the antenna mount as well. (The digital processing portions, i.e., the DAA and the computers, of the test bed will not require any major modifications.) Toward this end, a feasibility study on the use of a surplus AN/MSC-46 Satellite Tracking System, which was designed as a transportable system, was initiated. We felt that the portability would make it convenient to eventually move the system to candidate TDWR locations for site specific clutter and airport visibility analysis.

A decommissioned AN/MSC-46 system was located, obtained, and shipped to Lexington where it was assembled and inspected to assess its applicability to the project. Initial estimates on the cost and time involved in refurbishing the system indicated, however, that the use of the AN/MSC-46 would be cost prohibitive. We decided instead to refurbish the existing test-bed antenna system, and to replace only the RF portion of the radar.

The procurement of a C-band transmitter and receiver subsystem represents the major modification and biggest cost of this endeavor. Equipment will be procured under one contract and the procurement process will be on a competitive basis. The technical requirements document (TRD) which is necessary to conduct a competitive procurement is nearing completion. Several Group 43 personnel as well as recognized experts in the area of transmitter design from outside the Group have been involved in the generation of this document. The formal request for a quotation (RFQ) is expected to be distributed to prospective bidders early in April 1988. Figure II-10 is the block diagram of the transmitter/receiver subsystem showing the equipment to be purchased and indicating where it must interface to the rest of the radar equipment.

A design for the C-band feed horn to fit the existing 30-ft parabolic antenna reflector has been completed, and fabrication costs are being determined. Manufacturing information is also being obtained for the C-band azimuth and elevation rotary joints that will have to be replaced. These items will be formally specified and procured in the spring of 1988. In addition to those efforts, tests have been initiated to characterize and evaluate the existing antenna pedestal servo system by Division 7 personnel.

III. SITE STATUS AND OPERATIONS

A. HUNTSVILLE AND DENVER SITE STATUS

The FL-2 weather radar test bed continued to operate at the Huntsville site through the end of 1986 and into the early months of 1987. The major focus of activity during this period was to work on those hardware/software problems that surfaced during the summer 1986 experimental program and to make upgrade modifications to the system to enhance the radar capability for operations in the Denver area during 1987 and 1988. The ultimate goal was to field the test bed in Denver in such a condition that the system would operate reliably while recording a full set of data (800 range gates) and with the antenna rotating at approximately 30°/s. To achieve this data rate it would be necessary to improve the DAA processor and the Concurrent Corporation 3260 central processor's throughput capabilities. Therefore, plans were made to design and construct a new, faster DAA and to purchase the latest Concurrent computer, the Model 3280, with one additional auxiliary processing unit (APU). The DAA was planned to be developed using off-the-shelf components and software.

The FL-2 radar system was dismantled in Huntsville during February 1987 and shipped to Denver, CO. Reassembly was started on 10 March 1987 at its present site on Buckley Air National Guard (ANG) base. The Buckley site was selected after an analysis of the area around Stapleton International Airport in August 1986. Figure III-1 is a map of a portion of the Denver area surrounding Stapleton. The arc represents the area 15 km from the airport center. During a survey of the area by Lincoln Laboratory and NCAR personnel, nine candidate locations were identified as possible sites for the FL-2 and UND radars. The criteria used in the selection were (1) a range of approximately 15 km from the airport center, (2) a line-of-site view to no higher than 100 m above the runways, (3) a minimum of ground clutter in the sector covering the airport, and (4) a good Doppler viewing angle of the landing/takeoff of the most-used runways.

A fundamental requirement for the TDWR by the ATC and pilot community is for coverage of the runways and the landing/takeoff corridors out to a range of 3 mi from the ends of the runways. Figure III-2 is a schematic of the airport runways with the 3-mi extensions labeled 1, 2, 3, and 4. The large circle represents a 15-km distance from the airport center.

Using a maximum Doppler viewing angle of 60° (i.e., measuring at worst, 50 percent of corridor uniform wind component), the small sectors show areas along the 15-km line where runway extension coverage would be adequate. In making a final choice of sites, we noted that 85 percent of the Stapleton traffic lands from the east (Area 1) and takes off to the north (Area 2). The Buckley ANG site was chosen for the FL-2 radar on the basis of good coverage of the important areas and because it was already government property and its use would not require special leases and local permits in case the FAA chose to site a TDWR unit there.

A considerable amount of RF interference testing was required by existing electronics facilities on Buckley before final permission to use the site was granted. That testing delayed the start of construction until the beginning of January 1987, when we encountered further construction

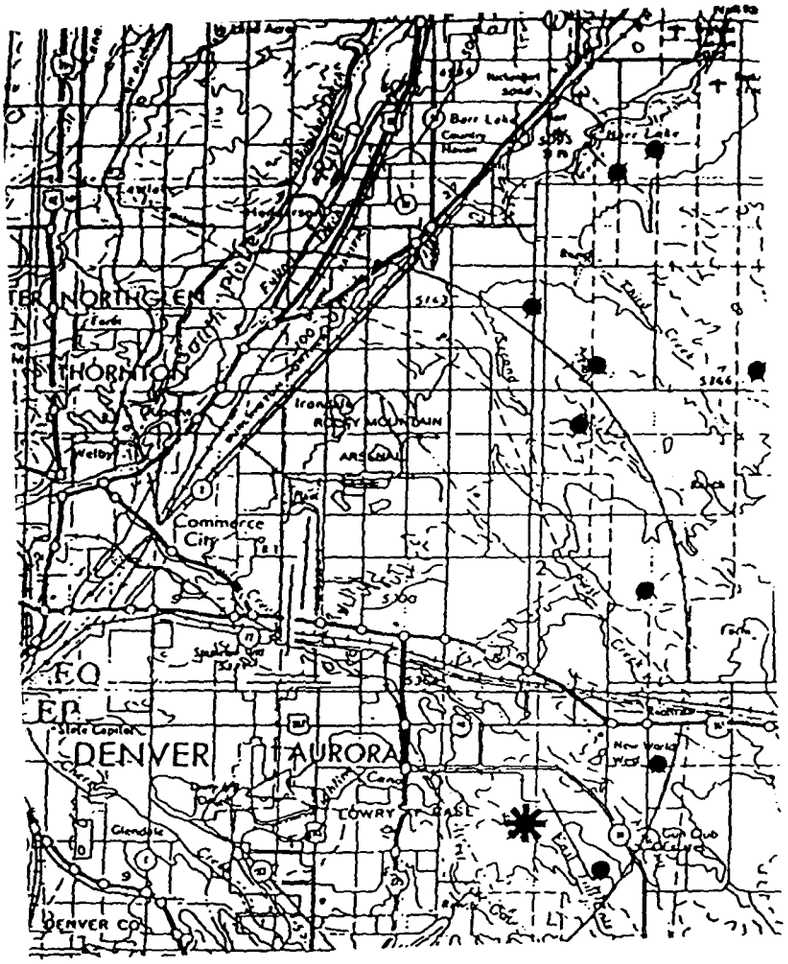

109733-11

Figure III-1. Stapleton International Airport locale near Denver.

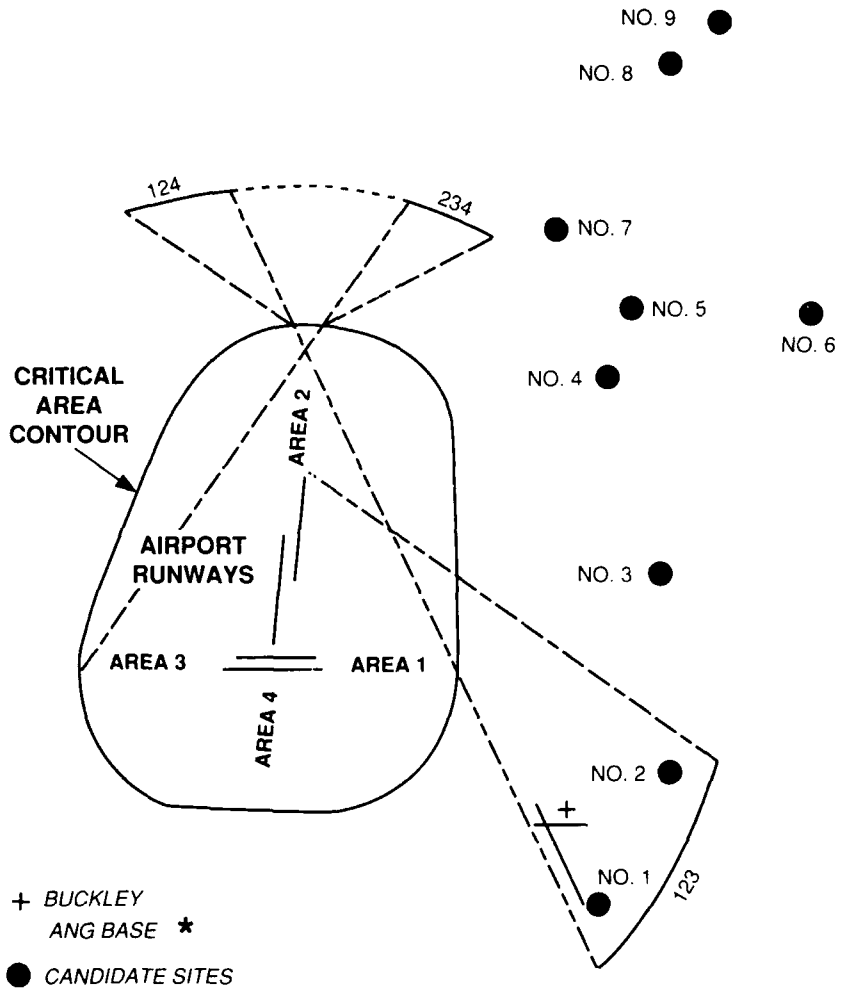

Figure III-2. Critical area for TDWR coverage around Stapleton International Airport.

delays because of inclement winter weather. The site was finally ready for antenna erection on 10 March 1987. All equipment was on-site and interconnected by the end of March.

During the system reconstruction, the new Concurrent 3280 computer system was installed, tested, and certified operational for the 1987 summer experiment. Shipment of the new DAA processing components was greatly delayed, and those pieces that did arrive were so unreliable that plans were made to start the experiment using the existing DAA and to limit the data rate to one-half by processing only 400 range gates (out to a range of 48 km).

The FL-2 test-bed hardware and software operated an average of 6 h/day during June, July, and August 1987. A minimal amount of downtime was experienced due to equipment failure. The causes of the high failure rates in the DAA hardware and software during the 1985 and 1986 summer operations were largely corrected in the 1987 experiments. Only three processing element

hardware failures occurred during the entire 1987 summer. The Concurrent 3280 computer system exhibited some APU failures; however, none affected the test-bed's ability to carry out its operational misisons.

The test bed remained in continuous operational readiness throughout the end of 1987 and through the end of this reporting period (31 March 1988). During the winter months, the UND icing studies program was supported on an *on call* basis. The rest of the time was spent supporting upgrade installations, checkout, maintenance, and system testing in preparation for the 1988 summer operations.

B. HUNTSVILLE AND DENVER SITE OPERATIONS

1. FL-2 Measurements (Huntsville)

The FL-2 radar was operational in Huntsville, AL until 6 February 1987 collecting 54 tapes during the winter period. Approximately half the data involved clutter measurements. The typical weather systems in that period were frontal passages accompanied by abundant rainfall, but very few thunderstorm days. A total of 13 wind-shear events were detected, primarily in October and November 1986. On 1 October, 4 microbursts and 3 gust fronts were recorded. Most of the microbursts were below average intensity. A strong pressure gradient on 15 February caused winds in excess of 55 kn at FL-2. Commercial power was out for several hours. On 28 February, a microburst shear of 24 m/s was detected within a storm tracking northeastward at 75 kn. (Thus, it is possible to detect microburst outflows embedded in strong environmental flow with a single Doppler radar.) Scattered reports of wind damage and power outages were received at the local NWS office.

There were 240 microbursts, 79 gust fronts, and 5 bow-echoes detected in the 1986-87 field season. The most active microburst months were July (74), September (49), August (41), and June (36). More than 92 percent of the shears were recorded from May through September. Research from the Memphis and Huntsville operations indicates that the vast majority of southeastern US microbursts can be expected from the late spring to early fall. The number of outflows in the winter season is dependent on the number of thunderstorm days. Huntsville wind shears like those in Denver are characterized as episodic since more than half of the events occurred on 20 days. In fact, one-quarter of the outflows were detected on 6 days. The highest daily tabulation was 19 microbursts on 21 September when a strong downburst (38 m/s) caused moderate damage in Decatur, AL.

Figure III-3 is a scatterplot of event locations in relation to FL-2 at Huntsville. In general, the events are distributed in all quadrants at a range of 2 to 70 km. There were fewer detections in the northeast sector due to topographic features and scan strategies. One feature that did cause blockage at low elevation angles was Rainbow Mountain located to the northeast. Whenever possible, the scan sequence focused on the western dual-Doppler lobe which contained the surface mesonet. The distribution of events tends to suggest that blockage was not a significant factor at the FL-2 site in Huntsville.

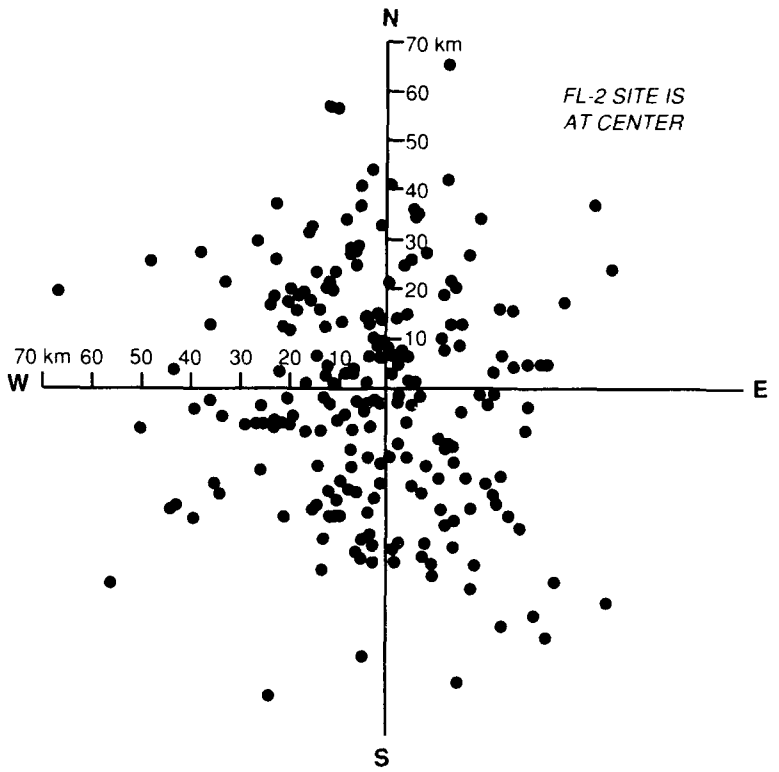

109733-13

Figure III-3. Locations of microbursts occurring within 70 km of the FL-2 radar site.

Microbursts can occur at any time of the day or night in the southeastern US; however, they are most common in the afternoon or early evening as witnessed by the Huntsville data set. Maximum surface reflectivities accompanying the outflows ranged from 40 to 65 dBz, with an average of 55 dBz. Reflectivities aloft were comparable to those at the surface. The majority of microbursts in the southeast are associated with heavy rainfall. At least one case from Huntsville serves to show that high reflectivity is not a criterion for a strong shear. On 6 August, a velocity differential of 24 m/s was recorded with a cell containing a surface reflectivity of 40 dBz. The distance across the outflow at peak intensity was 2 km. This was a dangerous shear since only moderate rainfall was present at the time of the event.

The maximum velocity differential for Huntsville microbursts varied from 10 to 40 m/s with a median of 18 m/s. Thus, the average Huntsville shear is slightly lower in intensity than JAWS microbursts. Within 6 min of initial detection, 50 percent of the outflows peaked, whereas 90 percent had done so by 12 min. The typical southeastern US microburst provides 6 to 12 min lead time from initial to maximum divergence. The average lifetime for 39 FLOWS microbursts was 14 min. One event lasted 3 min, while another was detected for 51 min. In general, microburst lines composed of two to five individual outflows last in excess of 30 min. The typical microburst intensified 1.6 times from its initial divergence.

Forty Huntsville microbursts were examined for precursors. Of these, 96 percent portrayed a descending core, 94 percent divergent tops, 65 percent rotation, and 48 percent convergence. The latter (convergence) does not appear to play a major role in the formation of Huntsville downbursts. Average warning times varied from 12 min for a descending core to 0 min for convergence. The maximum storm reflectivity peaked 9 min before the initial divergence.

Another characteristic of Huntsville microbursts is their ability to re-intensify several times in a life cycle. Of the 35 cases that were examined, one-third showed evidence of strengthening after a gradual decline. Most of those events were characterized as linear. The fact that a microburst can fluctuate in intensity is pertinent for TDWR warnings to pilots. If a microburst is embedded within a line, caution should be advised when reporting an event as decreasing in intensity. After several minutes, the microburst might attain a hazardous level again.

2. FL-2 Measurements (Denver)

From late March until early May 1987, the FL-2 radar system was assembled at the Buckley ANG Base near Denver, CO. The first data were collected on 7 May 1987. There have been 567 weather and clutter tapes gathered at the Denver site. Table III-1 provides a daily summary of test-bed operations during the spring and summer convection season. The primary mechanisms for convection in the Denver region are (a) topographical forcing, (b) boundary-layer forcing, and (c) frontal forcing. On average, a mission lasted approximately 4 h. The most active month was August (29 operational days), while there were only 17 episodes in May. Most operations were conducted between 1300 and 1900 local time. The longest mission on 2 July comprised 9 h of data collection. Occasionally, the radar crew returned in the evening to collect data on nocturnal thunderstorms. While microbursts are not as common after sunset, earlier studies had suggested a secondary peak in microburst activity during the evening in the High Plains area.

An examination of the daily microburst count in 1987 reveals a similar distribution between Denver and Huntsville. There were at least three outflows detected on over 80 percent of the microburst days. In fact, one-third of the total microbursts were recorded on the ten most active days. The 25 wind shears on 12 June represent the highest daily tabulation.

From 7 May 1987 through 7 March 1988, 480 microbursts and 138 gust fronts were identified in the Denver radar data set. The 1987 field season yielded more microburst detections than Memphis or Huntsville. The advancement in system technology (software and hardware), radar operator experience, and extensive event analysis is partially responsible for the increase. Without a doubt, the convective season in the High Plains is the most active locale in which FL-2 measurements have been obtained. Approximately three-quarters of the Denver wind events were detected in June, July, and August.

However, in certain other key respects Denver was similar to Huntsville and Memphis. For one, the temporal distribution of wind events in the High Plains and southeastern US is essentially the same. Both regions reflect a peak in microburst activity during the late afternoon and early evening hours, when convection due to diurnal heating is most prevalent. Second, the intensity of the outflow by categories is similar in each locale. The discrepancy is the greater number of weaker outflows in Huntsville and Denver (see Figure III-4).

TABLE III-1

Test-Bed Operations in 1987

Date	Operating Time (hours)	Tape Numbers	Weather Type	Wind Shear Events
7 May	0.6	001	Mild/Clutter	None
8 May	0.5	002	Warm/Clutter	None
11 May	1.0	003-4	Warm/Clutter	2 GF
13 May	2.9	005	Warm TRW's	3 MB/2 GF
17 May	3.2	006-07	Warm TRW's	4 MB/3 GF
18 May	2.5	008-09	Warm/TRW's	3 MB/3 GF
19 May	3.2	010-12	Mild/TRW's	None
20 May	1.5	013	Mild/TRW's	None
21 May	4.0	014-17	Mild/TRW's	3 MB/2 GF
22 May	2.1	018	Mild/TRW's	3 MB
23 May	3.2	019-21	Mild/TRW's	8 MB/2 GF
25 May	0.5	022	Fair/Clutter	None
26 May	3.7	023-25	Mild/TRW's	2 MB/2 GF
27 May	2.2	026	Mild/RW's	1 MB/1 GF
28 May	4.0	027-28	Warm/TRW's	11 MB/1 GF
29 May	6.0	029-31	Mild/TRW's	1 MB/1 GF
30 May	2.9	032-33	Fair/Warm	8 MB/1 GF
3 Jun	0.6	034	Cloudy/Warm	None
5 Jun	5.2	035-37	Hot/TRW's	None
6 Jun	6.0	038-41	Hot/RW's	1 MB/1 GF
7 Jun	6.8	042-47	Hot/TRW's	8 MB/1 GF
8 Jun	1.0	048	Mild/TRW's	None
9 Jun	3.7	049-51	Mild/TRW's	5 MB/1 GF
10 Jun	5.4	052-55	Warm/TRW's	18 MB/3 GF
11 Jun	6.0	056-65	Warm/TRW's	9 MB/3 GF
12 Jun	7.7	066-71	Warm/TRW's	25 MB/4 GF
13 Jun	2.6	072-73	Hot/RW's	1 GF
14 Jun	4.9	074-78	Hot/TRW's	18 MB/4 GF
15 Jun	4.0	079-82	Hot/TRW's	12 MB/2 GF
16 Jun	3.0	083-85	Hot/RW's	2 MB/1 GF
17 Jun	3.3	086-89	Warm/RW's	15 MB
18 Jun	5.9	090-95	Warm/TRW's	8 MB/1 GF
19 Jun	0.4	096	Clear/Clutter	None
20 Jun	6.5	097-01	Warm/TRW's	13 MB/2 GF
21 Jun	7.0	102-06	Warm/TRW's	17 MB/4 GF
22 Jun	5.0	107-10	Warm/RW's	1 MB/3 GF
23 Jun	6.2	111-16	Warm/TRW's	8 MB/2 GF
24 Jun	1.0	117	Warm/RW's	None
25 Jun	3.9	118-21	Mild/TRW's	2 MB/1 GF
26 Jun	0.5	122	Fair/Clutter	None
30 Jun	5.0	123-29	Cool/RW's	1 GF
1 Jul	3.6	130-32	Warm/RW's	2 MB/2 GF
2 Jul	8.6	133-41	Warm/TRW's	16 MB/4 GF
6 Jul	7.6	142-46	Hot/Virga	1 GF
7 Jul	5.5	147-50	Warm/TRW's	3 MB/2 GF
8 Jul	6.3	151-56	Warm/TRW's	8 MB/3 GF
9 Jul	5.6	157-60	Warm/TRW's	15 MB/4 GF
10 Jul	4.2	161-66	Warm/TRW's	5 MB
11 Jul	5.9	167-74	Warm/TRW's	2 MB
12 Jul	1.6	175-76	Cool/RW's	1 MB
14 Jul	1.2	176-77	Fair/Warm	None
15 Jul	2.8	179-81	Hot/RW's	1 MB
16 Jul	5.7	182-88	Hot/RW's	4 MB/2 GF
17 Jul	5.7	189-97	Warm/TRW's	6 MB/1 GF
19 Jul	0.6	198	Hot/Clutter	None
20 Jul	1.0	199-00	Fair/Hot	None
21 Jul	2.3	201-03	Hot/RW's	None
22 Jul	5.9	204-10	Hot/TRW's	8 MB/2 GF
23 Jul	3.5	211-17	Hot/TRW's	2 MB/2 GF
24 Jul	8.1	218-30	Hot/TRW's	13 MB/2 GF
25 Jul	1.1	231-32	Hot/RW's	None
26 Jul	3.0	233-37	Hot/TRW's	None
27 Jul	5.0	238-44	Hot/RW's	1 GF
28 Jul	6.7	245-53	Hot/TRW's	16 MB/2 GF
29 Jul	5.6	254-61	Hot/TRW's	6 MB/2 GF
30 Jul	7.0	262-69	Hot/TRW's	3 MB/2 GF
31 Jul	5.2	270-76	Hot/TRW's	2 MB/2 GF
1 Aug	2.5	277-80	Hot/RW's	None
2 Aug	4.9	281-86	Hot/RW's	4 MB/2 GF
3 Aug	4.1	287-92	Warm/RW's	None
4 Aug	2.1	293-96	Warm/RW's	None
5 Aug	4.1	297-00	Warm/RW's	None
6 Aug	5.6	301-08	Warm/RW's	8 MB/1 GF
7 Aug	7.4	309-17	Warm/TRW's	3 MB/1 GF
8 Aug	1.9	318-19	Warm/RW's	None
9 Aug	5.5	320-26	Warm/TRW's	2 MB/2 GF
10 Aug	4.5	327-31	Warm/TRW's	2 MB/2 GF
11 Aug	6.5	332-38	Warm/TRW's	5 MB/1 GF
12 Aug	4.7	339-43	Mild/RW's	None
13 Aug	3.5	344-48	Warm/TRW's	9 MB/2 GF
14 Aug	3.0	349-52	Fair/Warm	None
15 Aug	5.4	353-60	Warm/RW's	None
16 Aug	2.6	361-63	Fair/Mild	None
17 Aug	2.5	364-66	Fair/Warm	None
19 Aug	1.4	367-68	Fair/Clutter	None
20 Aug	4.6	369-74	Hot/RW's	6 MB/1 GF
22 Aug	5.3	383-88	Mild/TRW's	None
24 Aug	3.6	389-92	Warm/TRW's	5 MB/1 GF
25 Aug	7.8	393-02	Warm/TRW's	6 MB/2 GF
26 Aug	3.5	403-06	Mild/RW's	None
27 Aug	5.6	407-12	Mild/TRW's	4 MB/2 GF
28 Aug	6.1	413-17	Warm/RW's	3 MB/2 GF
29 Aug	0.8	418	Clear/Air	None
30 Aug	5.0	419-21	Warm/TRW's	1 GF
1 Sep	5.2	422-26	Warm/TRW's	1 GF
2 Sep	7.1	427-33	Warm/TRW's	12 MB/4 GF
3 Sep	5.7	434-39	Warm/TRW's	10 MB/5 GF
4 Sep	6.0	440-45	Mild/TRW's	5 MB/2 GF
5 Sep	5.0	446-50	Mild/TRW's	3 MB/1 GF
7 Sep	1.5	451-52	Mild/RW's	None
9 Sep	3.4	453-55	Warm/RW's	3 MB/1 GF
10 Sep	4.7	456-60	Mild/TRW's	2 MB/1 GF
11 Sep	2.9	461-63	Mild/RW's	None
12 Sep	1.2	464	Warm/RW's	None
13 Sep	3.8	465-68	Warm/RW's	10 MB/1 GF
14 Sep	5.1	469-74	Warm/TRW's	5 MB/3 GF
15 Sep	1.1	475	Mild/RW's	None
16 Sep	4.6	476-81	Warm/RW's	2 MB/2 GF
17 Sep	2.4	482-83	Cool/TRW's	None
22 Sep	0.1	484	Fair/Warm	None
24 Sep	2.2	485-88	Fair/Clutter	None
25 Sep	1.0	489	Warm/RW's	1 GF
26 Sep	2.2	490-91	Warm/RW's	4 MB/2 GF

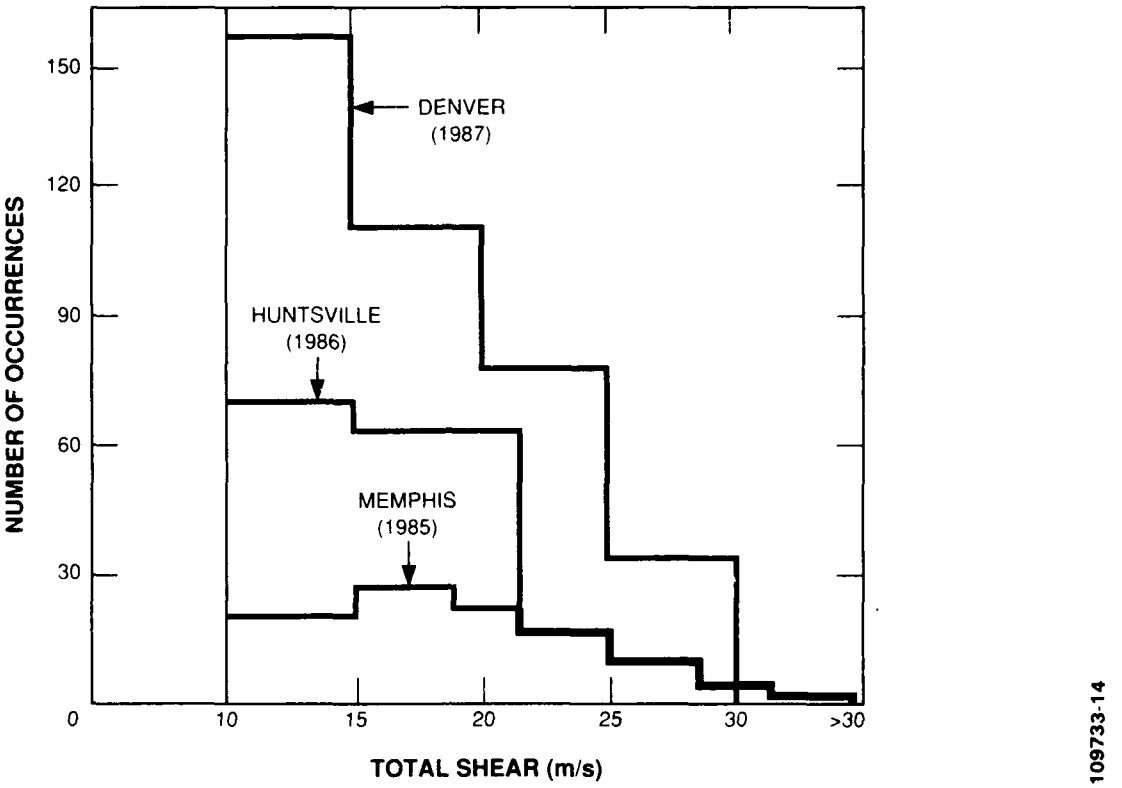

Figure III-4. Frequency distribution of total shears at Memphis, Huntsville, and Denver.

One unique attribute of High Plains microbursts is the prevalence of dry events. The reflectivity distribution of Denver microbursts is presented in Figure III-5. Approximately 50 percent of the cases attained peak surface reflectivities of 40 dBz or less. This frequency distribution is comparable to results from JAWS. In contrast, there were very few low-reflectivity outflows recorded in Memphis or Huntsville. Three low-reflectivity days (17 June, 9 July, and 2 September) from 1987 were selected for the microburst algorithm refinement and testing data base. From these days, 36 dry microbursts were analyzed to determine the approximate reflectivity levels in the surface divergence region. The maximum reflectivity at the surface ranged from 0 to 35 dBz, with a median of 10 dBz. On the other hand, the reflectivity within the outflow varied from -9 to +25 dBz. Lincoln Laboratory is currently assessing the performance statistics of the microburst detection algorithms on these days.

The depth of the microburst outflow is pertinent for radar siting and scanning. The height of maximum velocity in Denver microbursts ranged from the surface to 800 m, with most values in the lowest 300 m. The depth of outflow varied from 200 to 1100 m, with a median of 500 m. Results from the southeastern US suggest a similar depth of outflow.

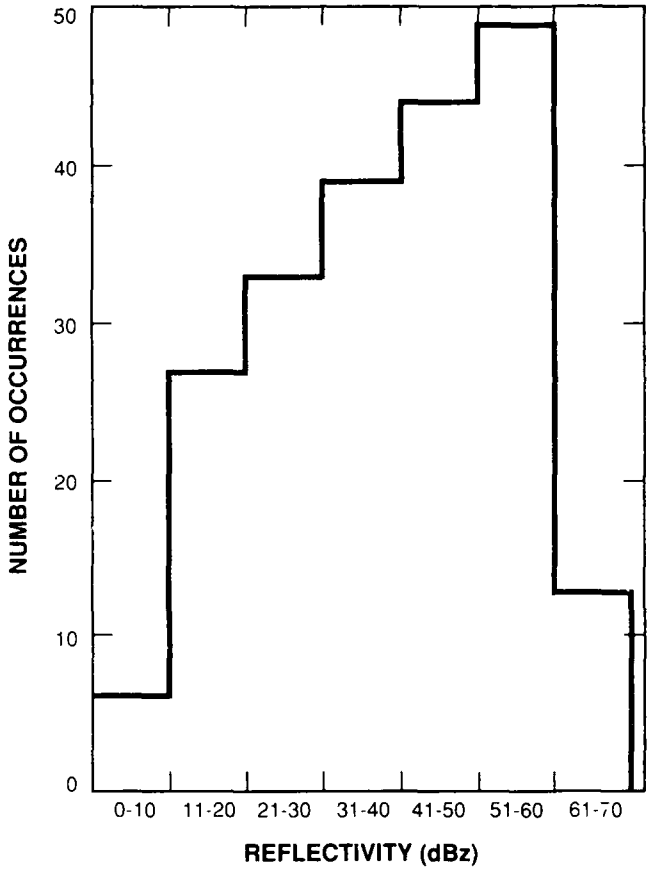

109733-15

Figure III-5. 1987 Denver microburst reflectivities.

In order to evaluate the advanced version of the microburst detection algorithm, 81 events from Denver were examined for possible radar-detectable features aloft (precursors) that precede or accompany the outflow. The inclusion of precursors such as descending reflectivity cores, convergence, and rotation can provide advanced warning of potentially hazardous wind shears. More than half of the cells displayed either rotation or convergence during some phase of the microburst's life cycle. Unlike Huntsville, very few cells obtained divergent tops prior to the surface outflow. Since the scan strategy did not always extend to storm tops, it is difficult to produce reliable statistics on this parameter. The median lead times for rotation or convergence considered separately are 0 and 1 min, respectively. However, the warning time for both features is 3 min. Average warning times for descending reflectivity regions are still being evaluated. The maximum core reflectivity for the 81 cases ranged from 20 to 60 dBz, with a median of 35 dBz. Approximately half the cells attained their maximum reflectivity prior to the outflow. It is expected that additional lead time will be provided once a reflectivity threshold is determined for Denver microbursts. The advanced algorithm based on Huntsville testing associates reflectivity regions of 30 dBz (storm cell) and 50 dBz (storm core). A lower threshold of 15 dBz has been suggested to track descending reflectivity cells in a dry subcloud environment.

The following is a synopsis of selected 1987-88 case studies:

June 17th was a typical dry microburst day with several virga lines tracking eastward off the mountains. A number of outflows exhibited radial velocity differentials in excess of 25 m/s. On 2 July, severe weather developed in the region with numerous reports of heavy rain, hail, and funnel clouds. A tornado touched down a half mile west of the UND site with no injuries. Microburst cells on the 9th of July were categorized as low reflectivity. The UND Citation penetrated several downbursts located north and southeast of FL-2. In addition a strong wind shear developed along the foothills and tracked northeastward. The maximum velocity differential for this event was 38 m/s. Within the core, the reflectivity varied between 20 and 25 dBz. Weak convergence was detected at midlevels in the cell. A strong microburst centered eight km north-northwest of FL-2 was penetrated by several aircraft landing at Stapleton. A number of pilots reported strong downdrafts and loss of altitude. Another active day in terms of airport operational impact was 2 September. At least four virga-type microbursts were detected to the west, north, and east of the airport runways. The longest lived outflow tracked across the north end of the north/south runways. The wind shears east of the airport were close to the arrival end of 26L and 26R.

During the winter season, turbulence data were collected in support of the turbulence algorithm development effort. Several dual-Doppler data sets were gathered to assist the icing algorithm development at UND. Some of the most intense turbulence of the season was recorded with these wintertime storms.

3. Mesonet Operations

The FLOWS weather stations were operational in Huntsville through December 1986. During the first two weeks in January 1987, the mesonet stations were disassembled and stored. Shortly thereafter, the mesonet trailer was trucked to Denver for the 1987 tests. The following accomplishments were achieved this period.

(a) The pressure sensors were calibrated at NCAR using 5-V input voltage. Temperature effects are still apparent at a number of stations. At least two sensors portray diurnal variations up to 14 mb. By the end of the measurements in Huntsville, the absolute difference at individual stations ranged from +4 to -2 mb. Some of the deviation is related to fluctuations within the daily site barometer (standard).

(b) The temperature-humidity sensors were cleaned and calibrated at Vaisala over a humidity range from 12 to 97 percent.

(c) The wind-direction sensors were equipped with 360° linear pots instead of the sine-cosine variety. Wind direction in degrees is now available in the field. Preliminary testing indicates greater resolution will be possible in 1987-88.

(d) During the winter (1986-87), the hardware and sensors for ten additional stations were acquired on interagency loan from the Bureau of Reclamation to support the FL-3 radar left in Huntsville for FL-3 measurements.

(e) A minor software error in the equation to calculate wind speeds was corrected. This modification will be loaded into the DCP software prior to the 1988 operational demonstration.

The 1987 FLOWS mesonet consisted of 29 stations. Urbanization within a 4-mi^2 sector precluded the installation of a 30th station until the spring of 1988. There will be a possibility of missed wind-shear events by the mesonet due to the gap in the southeastern sector. The sensors are spaced 2 to 4 km apart in a quasilinear arrangement around the airport. Thus, it will be possible to directly measure the headwind-tailwind component of wind shears impacting Stapleton.

There were several changes in data-handling format from 1986 to 1987. The humidity sensors were calibrated over a broader range to account for the drier conditions expected in 1987 and 1988. In addition, barometric pressure is now reported as station pressure instead of sea-level. Also, the 9-V power supplies were changed to 5 V. This did not affect the pressure resolution of the sensors. The raw station pressure is corrected in later analyses based on the elevation difference from the NWS (standard). A second correction factor is the average sensor deviation determined from the weekly site microbarograph. The biggest problems with pressure continue to be fluctuation due to temperature change and the inability of a sensor to maintain its calibration. It is likely that daily correction factors will have to be applied whenever an individual event is analyzed.

The sine-cosine pots in the wind-direction sensors were replaced with 360° pots which eliminated gaps at specific azimuths. A number of pots displayed a noise problem whenever the wind direction fluctuated across north. The faulty pots were replaced with new pots from Belfort.

The Denver mesonet became fully operational the first week in July 1987. A station is occasionally off the air due to electrical storms or dead batteries. The typical failure mode involved a faulty data-collection platform, wind speed, or direction sensor.

By the end of September 1987, a number of wind events were recorded by the mesonet. Preliminary analysis of 2 September data revealed several outflows active within the network between 2200 and 2330 UTC. These events were scanned in a coordinated dual-Doppler mode with UND. Microburst outflows on this day were classified as dry with surface reflectivities less than 20 dBz. Data from 2 September will serve as a single, dual, and/or mesonet *truth* case for the microburst detection algorithms. In addition, the ability of the FL-2 system to detect low signal outflows in a clutter environment can be assessed.

After November 1987, the surface network was reduced to ten stations so that sensors could be calibrated for the 1988 operational demonstration. The reduced mesonet grid was used by UND scientists to assist in the icing algorithm development. The entire 30 station mesonet should be fully operational in April 1988.

4. LLWAS Operations

The Huntsville LLWAS functioned adequately throughout the period except for occasional power outages. The average wind speed and direction at six stations is updated at 2-min intervals. Several wind-shear events were captured by the LLWAS after the FLOWS mesonet was taken down.

From March 1987 to March 1988, the advanced LLWAS at Stapleton was recorded at the FL-2 site. The system consists of twelve remote sensors, a central computer, and remote display capability. The average station spacing of 2 km allows for a high spatial resolution of wind events within the network. By combining the LLWAS data with the FLOWS mesonet data, an even denser array is obtained in the airport vicinity. LLWAS information that is displayed on the computer maintenance screen is transmitted by modem from the airport to the FL-2 radar site. This data stream is filtered to select only the wind direction and velocity from each of the twelve sensors, plus the date and time. To assist in off-line analysis of potentially hazardous wind shears, the LLWAS outputs were recorded on tape since 15 July. There was a period of missing data while the advanced LLWAS testing was conducted at Stapleton. A Sun workstation provided a real-time geographical display of LLWAS wind speed and direction. Thus, it was possible to evaluate the timeliness of wind-shift predictions at the airport. No updates or modifications are scheduled during the next reporting period.

5. UND Radar Measurements

There were no UND operations in Huntsville after September 1986. During the winter of 1986-87, the UND radar collected icing measurements in Grand Forks in support of an icing algorithm design.

The UND C-band Doppler system became fully operational in Denver on 4 July 1987. The radar site is located 21 km north of FL-2. The primary focus of UND measurements was dual-Doppler support for low-level wind shears near Stapleton. From 4 July to 29 September, 100 radar tapes were collected and converted to Lincoln Common Format (CFT) for later analysis. Once an event tracked within a dual-Doppler region, both radars scanned in a coordinated mode with a 1-min surface update rate. At least 41 microbursts and 36 gust fronts/boundaries had favorable dual-Doppler viewing angles. The strongest microburst event (29 July) located in a dual-Doppler lobe exhibited a radial velocity change of 28 m/s. Over one-third of the cases attained differential velocities in excess of 20 m/s.

In addition to data collection, UND scientists conducted extensive playbacks to establish a data base of wind-shear statistics. To determine the radial velocity differential recorded by FL-2 and UND, 22 microbursts with favorable dual-Doppler viewing angles were analyzed. The ratio of maximum-to-minimum velocity varied from 1.0 to 1.9. Dual-Doppler analysis of microbursts which occurred on 31 July, 21 August, 3 September, and 4 September will serve to distinguish the maximum asymmetry observed in the Denver measurements.

During the winter of 1987-88, UND radar operations focused on icing studies with the support of the Citation. One of the primary inputs to the icing algorithm is the presence of convergence. Lincoln assisted the UND program by providing FL-2 dual-Doppler support from November 1987 until April 1988.

6. Supplemental Weather Data

Additional weather data [i.e., the DIFAX (weather charts) and LASERFAX satellite images] serve as forecasting tools before and during an operation. Upper-air soundings obtained through WSI assist in microburst forecasting and analysis. Each week, the data are cataloged and shipped to Lincoln Laboratory for archiving.

A KAVOURIS display installed in the operations room provided a continuous loop of NWS reflectivity levels from the WSR-74 at Huntsville (Huntsville site) and WSR-57 at Limon (Denver site). The data loop is useful in determining storm movement and translation speed at times when the FL-2 radar is not operational.

Two Apollo workstations were devoted to real-time wind-shear truthing and algorithm evaluation during the summer of 1987. Software support allowed data such as the event number, location, and intensity to be stored in a file. The information will assist in off-line scoring of the gust front and microburst algorithm. From late July to early September, the Apollo in the Lincoln display room was devoted to the evaluation of LLWAS algorithm alarms. Once an alarm was detected, the event was verified based on radar data such as reflectivity and velocity. Only low-level surface scans were provided in the real-time verification process.

7. Clutter Measurements

Clutter measurements from the FL-2 Denver site began with the first data collected on 7 May 1987. A total of 45 tapes were collected through 7 March 1988. Most of the tapes have been translated to CFT. These data will be used primarily to construct clutter residue maps and to assess the clutter residue variation due to seasonal changes. The data will also serve as a data base of measurements of the clutter environment for future use. Clutter measurements were recorded on a weekly basis when the weather permitted. Daily measurements were made for one week in July to investigate more rapid changes in the clutter environment. The current scan strategy consists of 0.1° elevation steps to an elevation of 1°. The pulse repetition frequency (PRF) and filter option are selected based on the optimal requirements for the TDWR algorithms. Currently, data are collected at PRFs of 1220 and 1050 with the widest stop-band filter for each PRF.

The level and extent of clutter at the Denver site are much more severe than at previous FL-2 test sites. The clutter environment around Buckley (Denver) is displayed in Figure IV-16 in Section IV. These data were collected without the use of clutter filters. Figure IV-17 in Section IV displays clutter residue measurements on the same day using a high-pass FIR filter with a maximum attenuation of 50 dB and a stop band width of 1 m/s. The range rings in the figure are at 20-km intervals. Both data sets were recorded when there was no visible weather in the area.

8. Aircraft Measurements

The UND Cessna Citation II, an instrumented research aircraft, was used to gather data from 13 July through 4 September 1987 in support of the turbulence algorithm development

effort. In addition, the aircraft was available for icing/turbulence data collection from November 1987 through April 1988. During this reporting period, the Citation flew approximately 25 missions in support of the TDWR program. The strategy was to deploy the Citation to regions (within 60 km of FL-2) where radar measurements indicated the possibility of turbulence. The aircraft was then requested to fly in search of moderate (or greater) turbulence while the radar scanned the volume of the airspace in which the Citation was located. The goal of the experiment was to sample turbulence associated with a variety of weather phenomena. Of particular interest was the likelihood and severity of turbulence between the cells of a convective line. Data were also collected from isolated convective echoes, microbursts, and gust fronts.

A special scan strategy was developed for use during the Citation missions. A volume scan consisted of three tilts: (1) at elevation of the airplane, (2) 1° below the airplane, and (3) 1° above the airplane. The azimuth limits of the sector were ±30° from the azimuth of the Citation. Such a scan strategy combined the advantages of *spotlighting* the airplane while scanning a volume. It was not only possible to collect data in the immediate vicinity of the airplane, but also to relate the observed turbulence to storm structure and development.

An initial inspection of real-time observations reveals that the Citation occasionally encountered moderate turbulence while penetrating intense convective elements. A number of turbulence missions during the winter seemed to show a correlation between icing and the degree of turbulence. Once the airplane data tapes arrive from UND, there will be more analysis of the 1987-88 flights.

9. Lightning Measurements

During the period from September 1986 to March 1987, lightning measurements were displayed in real time at the FL-2 Huntsville site. An additional array of corona point sensors was installed the latter half of the season at selected mesonet sites. This will allow for a comparative data set on lightning activity in microburst producing storms over the FLOWS surface network.

An IBM-PC system was installed at the Denver site to display the location of cloud-to-ground lightning strikes from the NOAA/PROFS LLP system in real time. A combination of hardware and data format problems prevented the system from coming on-line in 1987. Work continues with PROFS to ensure that the system will be operational for the 1988 storm season.

IV. EXPERIMENTAL DATA REDUCTION AND ALGORITHM DEVELOPMENT

A. GENERAL-PURPOSE SOFTWARE

Early in this reporting period, a general-purpose software committee was formed to more effectively manage the development of new software, the maintenance of existing software, and the transition of data-analysis efforts from the Concurrent computers to the Sun system. One of the basic tasks of the committee was to review requests for new software or maintenance of old software, and to allocate programming and hardware resources as appropriate; the relative importance, near-term desirability, and difficulty of the programming tasks had to be assessed. Additionally, the committee considered design and review policies for the development of new software.

By the end of the reporting period, the general-purpose software committee had been superceded by the Data Analysis Systems Committee. This new committee is concerned with data-analysis support facilities in general, with emphasis on Lincoln software maintenance and development, computer system hardware and software maintenance, and near- and long-term needs for additional software and hardware.

By the end of the reporting period, much of the important data-analysis software originally executed on the Concurrent computers had been ported to, or rewritten on, the Sun system. Foremost among the software packages are:

(1) The common format type (CFT) radar data read and write packages.

(2) The Cartesian (CAR) data read and write packages.

(3) The CAR display function (used to display CAR data on color workstations). (This facility is known as the *WxShell* on the Sun system.)

(4) NCAR plotting software.

(5) CFT to CAR (polar to Cartesian) data resampling utility.

Source code on the Sun system was placed under the Unix Source Code Control System (SCCS). Most software locally supported (i.e., not supplied by Sun Microsystems) is now centrally located to facilitate documentation, modification, and enhancement.

B. CONCURRENT COMPUTER SYSTEMS

Figure IV-1 shows the present computer configuration at the Lexington facility. The three Concurrent Computer Corp. (formerly Perkin-Elmer) computer systems used to support data reduction and algorithm development continued to experience heavy use. The operating configuration at the end of this reporting period was as follows.

(1) A 3260MPS with one APU and 16 Mbytes of memory was used for algorithm development, and batch processing during three shifts.

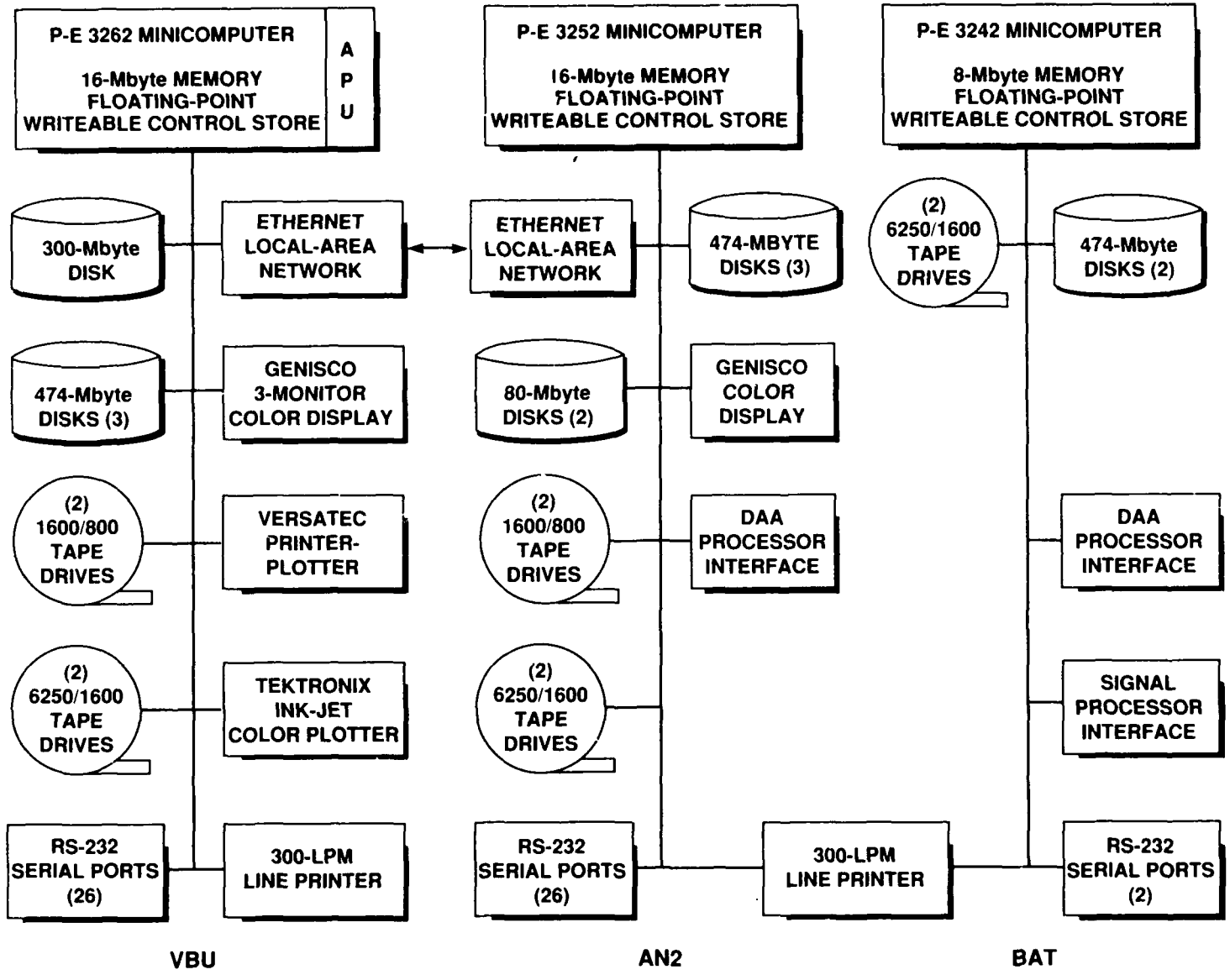

Figure IV-1. The three-computer configuration at Lexington.

109733-16

(2) A 3250 with 16 Mbytes of memory was used for test-bed real-time software (e.g., DAA and real-time program) development, algorithm development, and batch processing during three shifts.

(3) A 3240 with 8 Mbytes of memory was used for test-bed real-time software (e.g., DAA and radar control) development, and batch processing during three shifts.

During this reporting period, the following enhancements were made to the Concurrent systems:

(1) One 375-Mbyte disk each was added to the 3250 and 3240.

(2) One 6250-bpi tape drive each was added to the 3260 and 3250.

(3) Revision 8.1.3 of the OS/32 operating system was installed on all three systems.

Reliability of the systems was generally good throughout the period, with the only serious problem being a power supply failure in the 3250 which rendered the system unusable for three days. Additionally, for several weeks in early 1987 an intermittent memory-access-board failure caused problems in the 3260, affecting both tasks running in the computer and communications with a number of peripherals.

Additional major upgrades in the systems are not anticipated for the next reporting period, although experience would indicate the likelihood of a requirement for additional disk storage.

C. SUN WORKSTATIONS

Prior to September 1986, the Sun network consisted of two fileservers, each with its own dedicated ethernet, and a total of thirteen desktop workstations. Disk storage capacity was approximately 1520 Mbytes.

The period from October 1986 through March 1987 was marked by a steady increase in utilization of the Sun network, addition of new hardware and software, and the identification of further system requirements.

The hardware enhancements during this period included two floating-point accelerator boards, necessary to increase the execution speed of many computation intensive data analysis algorithms.

Several improvements were also made to the software environment during this time period. The operating system was upgraded from Sun Unix Version 3.0 to Version 3.2. The IMSL computation library was installed on one of the fileservers. Six Interleaf Word Processing licenses were purchased for the purpose of preparing and maintaining all documentation.

In the following six-month period beginning in March 1987, a third fileserver was installed, increasing the total on-line disk capacity to over 2600 Mbytes. Desktop workstations were added steadily, bringing the total number of personal workstations in use to 34 by the end of September 1987.

A 280-Mbyte local disk drive was added to one of the office workstations for the specific purpose of supporting the microburst algorithm work. The identification of similar, specific project needs became the main expansion strategy. A remote Sun workstation with a 220-Mbyte disk installed at the FL-2 site in Denver has been linked to our local network via a synchronous data link which permits remote operations to be orchestrated from our local network in Lexington.

Miscellaneous hardware and software upgrades were also initiated during this period. The IMSL computation library was upgraded with the latest IMSL release. Four licenses to run Sun Common Lisp were purchased. Eight workstations received local memory upgrades to improve processing speed for memory intensive software (such as Lisp, and locally written data-reduction software). Finally, the local laser printer was upgraded to process 20 pages per minute (formerly 8 pages per minute).

The most recent six months from October 1987 through March 1988 have been marked by an accelerated network expansion. Sun released Unix Version 3.4, which was installed on all network machines. A fourth fileserver and four additional desktop workstations have been added, bringing the total to 38 personal workstations in use at present.

To address the growing need for on-line disk storage space, six large-capacity disk drives were purchased. The redistribution of disk resources will provide 5300 Mbytes of general-purpose disk space, with 100 Mbytes of local storage allocated to the microburst algorithm group.

A request has been issued to purchase a color, thermal wax, plotting system for the purpose of generating hard copy of images produced on the Sun network. The color plotter is expected by mid-April 1988.

The strategy of addressing specific project needs has continued with the purpose of three new stand-alone Suns for the microburst project, which, after local testing, will be shipped to the Denver test site. Two high-speed Direct Memory Access boards are being tested in a stand-alone Sun workstation by the DAA group.

D. RADAR DATA ANALYSIS

1. Algorithm Verification

To verify the microburst detection algorithm output we must analyze the data manually to determine *truth*. There are two types of radar-data-based truth analysis that we currently use. The first type is called truth verification and is the identification by location, shape, and strength of wind-shear events based on the eyes of a trained observer. Verified truth is used to define what events the algorithm should see. The second type of truth is called dual-Doppler truth for which two radar scans are combined (providing they meet certain scanning criteria) to provide a two-dimensional, wind flow of a microburst or gust-front event. This type of truth is used to study the structure, shape, and evolution of microbursts. Both types of truth are used not only to increase the understanding of the microburst itself, but also to better evaluate the performance of the microburst (MB) algorithm.

Three veins of algorithm truth verification currently taking place involve surface divergences, upper- and mid-level features, and gust fronts. In each case a trained observer examines played-back radar data to determine what features are distinguishable in the radar image. These events are then compared with their respective algorithm output and scored according to a predefined set of scoring rules.

Surface divergence truth is utilized to evaluate the performance of both the surface only and advanced microburst algorithm. An observer visually scans all surface tilts for a specified time period looking for microburst strength divergent signatures. The divergence must be greater than 10 m/s along a number of radials to be classified as a microburst divergence. A microburst divergence is recorded by its strength (the highest maximum differential velocity from all radials within the microburst) and the outline enclosing all radials with greater than 10-m/s differential velocities. From 1986 and 1987 radar data, 23 days of surface divergence truth, encompassing some 83 h of observation, have been extracted. A detailed listing of the truth days, times, and status may be found in the discussion of microburst algorithm performance (Section IV-F).

In addition to surface divergence, upper- and mid-level feature truths are needed to evaluate the advanced algorithm's performance. The features truthed include convergence, rotation, divergence, and reflectivity cores. Features aloft are considered to be precursors to some microburst events and are used by the advanced algorithm to declare early weak divergences as microbursts before the surface only algorithm would have. An observer visually examines all scans aloft (1° elevation or higher) for any of the above features and attempts to associate them with a microburst event. For 1986 and 1987, we gathered 16 days of upper-level truth, covering more than 78 h of observations. A detailed listing is in Section IV-F.

The newest type of truth observation is for gust-front events. Again, a trained observer examines all surface tilts looking for gust fronts distinguishable in the radar images. The gust front is characterized by its maximum convergence and by the outline defined by the extent of associated convergence. Some 12 days, including more than 40 h of radar observations, are detailed in Section IV-I of this document.

Dual-Doppler analyses are performed on selected microburst events which are considered good for two-dimensional analysis. The two-dimensional wind flow can exhibit the characteristics of the flow within the microburst. Dual-Doppler studies were performed on a dozen cases in 1985 and 1986. Approximately 15 microbursts have been processed through dual-Doppler from the 1987 season. More days will be processed shortly in support of the asymmetry study discussed in the next section. The analyses are also used to examine the performance of the microburst algorithm in relation to the entire outflow.

2. Other Studies

a. Asymmetry Analysis

The aspect-angle dependence (asymmetry) of some microburst events has raised some serious questions about the effect of asymmetry on TDWR system performance. In an effort to evaluate

possible degradation to system performance, we have begun looking at asymmetry over the lifetime of some twenty Denver microburst events. The study will gather statistics on the frequency, magnitude, and life cycle of microburst asymmetry and any possible single radar observable characteristics which indicate the existence of asymmetry. The asymmetry cases will then be examined in relation to the TDWR detection system to help determine whether or not asymmetry seriously inhibits system performance.

b. FL-2 Sidelobes off Downtown Denver Buildings

During the operation of the FL-2 radar in Colorado, unusual sidelobe echoes have been detected from the large buildings in downtown Denver. The echoes are located 90° to 120° clockwise and counterclockwise of the downtown Denver area and appear to have velocities associated with them. The velocities are a function of the scanning direction and speed and are caused by the motion of the feedhorn as the antenna rotates in azimuth. The equivalent weather from these buildings is very strong. Quantitatively, they are in reasonably good agreement with what might be expected based on the sizes of the buildings in downtown Denver. Finally, the use of the clutter filters with the FL-2 radar effectively eliminates these spurious echoes from the data.

3. Translations

Raw radar data received from a variety of radar installations are translated into CFT format to provide a common format for processing within MIT Lincoln Laboratory. Normal translations are performed on days of high activity or special interest. Although processing of the 1987 FL-2 data was delayed until an angle variation problem was corrected, normal processing for 1985-87 has now been completed. Some tapes remain in RAW format only because the data are either of poor quality or of little interest. Additionally, we receive mesonet, LLWAS, and UND radar and aircraft data tapes which are translated into their respective common formats and placed in our data library. Table IV-1 lists the number of raw tapes received from a particular source for

TABLE IV-1

Translation Status 1985-87

	1987 Raw Tapes	1986 Raw Tapes	1985 Raw Tapes
FL-2* (percent)	511 (80)	249 (81)	963 (48)
UND* (percent)	110 (96)	113 (73)	312 (32)
LLWAS (percent)	15 (100)	43 (100)	87 (100)
Mesonet (percent)	39 (100)	91 (100)	137 (100)
UND Aircraft	—	68	50
RRWDS	—	—	58

* Raw tapes during 1987 had a density of 6250 bpi as opposed to 1600 bpi in past years.

1985-87. The table also identifies, where applicable, the percentage of raw tapes which have been translated into common format.

4. Outside Distributions

All the data collected by Lincoln Laboratory in support of wind-shear studies are available to organizations, institutions, or individuals with a demonstrated need for the data. Requests for data are generally approved for any group working in wind-shear-related studies; other requests are also handled but are placed at a lower priority. The Laboratory has gathered a wide variety of wind-shear data ranging from mesonet weather-station recordings to in-depth, dual-Doppler analyses. We have made a conscious effort to make these data available to outside organizations on a timely and efficient basis.

Outside distributions of radar and mesonet data have increased dramatically over the past year. Over ninety requests from some seventeen organizations were received and filled by Lincoln Laboratory. They ranged from copies of microburst videotapes to multiple, dual-Doppler analyses. Most of the data requested were for combined radar and mesonet data for specific events. A request by the FAA Technical Center for dual-Doppler analyses over Stapleton airport for 25 and 28 August, and 2 September 1987 was the longest and most difficult to fill. More cases have been requested by the Technical Center and they will be filled in the coming months. Table IV-2 summarizes the data requested by each research organization.

E. MESONET/LLWAS DATA ANALYSIS

Surface meteorological data were continuously collected by the mesonet and LLWAS networks over specific periods during 1985 in Memphis, TN; 1986 in Huntsville, AL; and 1987 in Denver, CO. The mesonet surface wind data, collected during these years, were compared with Doppler radar data that had been collected during convectively active weather periods. The results of the comparison study have been, and are being, used for the following:

(1) Confirm low-altitude wind shear (LAWS) and other possible hazardous weather events observed by the radar.

(2) Determine wind-shear events not observable in Doppler radar data.

(3) Provide support for the microburst, and to a lesser extent, the gust-front detection algorithms.

The additional meteorological data collected by the networks (excluding the LLWAS) will be used to diagnose the relationship between temperature, barometric pressure, relative humidity, rainfall rates, and winds during these events. Thus, a better understanding of the causes and circumstances of the low-altitude wind shear may be gained.

1. 1985 Data

A report by J. DiStefano[1] focuses on the observability of microbursts using pulse Doppler weather radars and surface anemometers. The data used for the study were collected in the

TABLE IV-2

Outside Distributions
(March 1986 through February 1988)

Organization	Recipient	Data Requested	Organization	Recipient	Data Requested
AFGL	Paul Desrochers	FL-2 Universal data for 31 Jul, 26 Sep 86; 2, 4 Sep 87.	NSSL	David Rust	FL-2 Universal data for 12 Mar 86.
FAA TC	Paul O'Brien	FL-2 and UND Universal format data for 30 Apr, 25 Jun, 8 Sep 85. LLWAS for 1984-85.		Dale sirmans	FL-2 Universal data for 24 Jul, 86.
	Rick Page	Dual-Doppler* analyses for 21, 25, 28 Aug; 2 Sep 87. Mesonet and LLWAS data for 5, 20 Aug 87		Steve Smith	FL-2 Universal data for 29 Jun, 28 Jul 87.
MIT	Earl Williams	1986 FL-2 CFT data for 13, 28, 29, 31 Jun 86. Raw mesonet data for 28 Apr, 4 May 87.		Arthur Witt	FL-2 Universal data for 2 Oct, 9 Nov, 9 Dec 86; 21 Jun 87.
MITRE	Sadegh Kavoussi	CEF and color plots for 23 Jun, 24 Jul 87.	Purdue University	Diana Klingle	Resampled images of 11 Jun 86. FL-2 color slides for 28 Jul 86.
	Doyle Peed	FL-2 Universal data for 24 May 86.	Sierra Nevada	Floyd Williams	FL-2 Universal data for 13 Jul, 1, 20 Aug, 22 Sep 86; 20 Aug 87.
NASA/MSFC	Steve Goodman	1986 FL-2 Universal data for 24, 25, 29 May, 11, 17, 24 Jun, 13, 26, 28, 31 Jul 86.	TPS (Turbulence Prediction Systems)	Pat Adamson	Mesonet data for 11 Aug 84; Jun, Jul 86.
NCAR	Cleon Biter	FL-2 Universal data for 6, 13, 31 Jul 86, 28, 30 May, 18 Jul 87.	UCLA	Roger Wakimoto	Mesonet and LLWAS date for Jun, Jul 86; Jun, Jul 87.
	Kim Elmore	UND Universal data for 31 Jul 87. Dual-Doppler* for 21 Aug 87.	U. of Alabama	Steve Williams	Mesonet data for Jun, Jul 87.
	Bill Mahoney	FL-2 CFT data for 9, 24, 31 Jul, 2, 6, 20 Aug 87. FL-2 color plots for 30, 31 Jul, 25, 27 Aug 87.	U. of Chicago	Ted Fujita	Dual-Doppler for 24 Aug 86. Mesonet data for Jun, Jul 86, and B-Scans for 6 Mar 87. Color Slides for 7 Jun, 25 Jul 86. FL-2 data for 25 Aug 87.
	John Tuttle	UND Universal data for 20 Jul 86.		Brian Smith	CMF for Jun, Jul 86.
	Wayne Sand	CEF and color plots for 25 Jun, 24 Jul 87.	U. of Florida	Peter Ray	FL-2 Universal data for 20 Jul 86.
NSSL	Mike Eilts	FL-2 Universal and CFT data for 28, 29 Jul, 28 Aug, 2, 4 Sep 87. FL-2 and UND Universal data for 13 Jul 87. Mesonet and LLWAS for 13 Jul 87. FL-2 Universal and LLWAS plots for 26 Aug, 2 Sep 87.	U. of Wisconsin	John Anderson	FL-2 CFT data for 10 Jun, 9 Jul 87.
			UND	Dave Bernhardt	Mesonet data for Jun, Jul 86.
			USAF	Jim Warnke	MB videotape for 26 Jun 85.

Memphis, TN area during the FLOWS project of 1985. The methods used for declaring a microburst from both Doppler radar and surface anemometer data were described.

A main objective in this report was to identify the results that were generated by comparing the 1985 radar observed microbursts (which impacted the surface mesonet) with the surface mesonet observed microbursts. The results of this study revealed that, in the period of 5 April to 31 December, a total of 45 microbursts impacted the Memphis mesonet. We observed that 42 of these events had accompanying radar data and therefore were of primary interest. They broke down as follows:

(a) 95.2 percent (40 of 42) were detected by both the radar and surface mesonet systems.

(b) 4.8 percent (2 of 42) were not observable in the radar data.

(c) Zero percent (0 of 42) was undetected by the mesonet surface sensors.

2. 1986 Data

During the 1986 data-collection period in Huntsville, AL, surface mesonet (30 stations) and LLWAS (6 stations) data were available from 6 April through 9 December. In addition, PAM (Portable Automated Mesonet) data were also recording continuously during the months of June and July. There were 41 surface meteorological stations that comprised the PAM network. In order to incorporate these PAM data into the already-existing mesonet and LLWAS data sets, adjustments had to be made on the mesonet analysis software package. The PAM data ultimately enhanced the surface coverage, and therefore provided an increased likelihood for detecting any microbursts that impacted the network's dense coverage center.

The analysis work performed on the 1986 data sets centered on the comparison between mesonet and radar detected microbursts. The software package, mentioned above as being implemented on the 1987 surface mesonet data, had also been implemented on the 1986 data. It was revealed that during the period 6 April through 9 December, 129 microbursts impacted the mesonet (71 of them were observed between June and July when the surface coverage was increased by the addition of the PAM stations). Of these events, 105 had accompanying radar data. To determine microburst observability, a comparison analysis (using both the radar and surface data sets associated with these 105 events) was performed, with the following results:

(a) 85.7 percent (90 of 105) were observed by both the radar and surface mesonet sensors.

(b) 1.9 percent (2 of 105) were not identified by the radar, corresponding to a radar observability percentage of 98.1 percent.

(c) 12.4 percent (13 of 105) were not observed by the mesonet surface sensors.

In each of the two cases not identified by radar, the featured microburst was very weak and, although a microburst-strength differential velocity was not observable by radar, in both instances

the divergent wind pattern associated with the event was clearly evident in the radar velocity data field. All microbursts which exhibited a differential velocity in excess of 13 m/s were identified by radar.

3. 1987 Data

During this 1987 data-collection period, an investigation revealed that 102 microbursts and 42 gust fronts impacted the mesonet. When focusing only on the microburst events, it was observed that 66 of these had accompanying radar data. Comparing the two data sets (radar and surface mesonet) to determine the status of microburst observability showed the following:

(a) 92.4 percent (61 of 66) were observed by both the radar and surface mesonet sensors.

(b) 6.1 percent (4 of 66) were unobserved by the radar, corresponding to a radar detection percentage of 93.9 percent. [Two of the four unobserved microbursts were very weak (less than 13 m/s peak velocity difference) and short lived.]

(c) 1.5 percent (1 of 66) were unobserved by the mesonet surface sensors.

All four microbursts not observed by the radar were classified as "dry" events with low surface reflectivities and with three of the four being relatively weak (peak velocity differences $<$20 m/s). The strongest event exceeded 20-m/s velocity differential for 2 min and appeared to have been missed due to a combination of very low reflectivity and a very shallow depth outflow.

A report, which will identify the results that were generated by comparing the 1987 radar-observed microbursts (which impacted the surface system) with the surface mesonet-observed microbursts, is being compiled by J. DiStefano and should be completed shortly.

4. FAA Technical Center Support with Mesonet and LLWAS Data

During 1987, support was given to the FAATC by Lincoln Laboratory to assist in their evaluation of the upgraded Denver LLWAS system. The support was the provision of meteorological data (mesonet, LLWAS, single Doppler, and dual Doppler) to the Tech Center which would be helpful during their evaluation process. The data consisted of specific low-level wind-shear cases (i.e., microbursts and gust fronts) which occurred within the 1985 and 1987 data-collection periods. Table IV-3 lists dates and times for which mesonet and LLWAS data were provided to the Tech Center.

A report is being prepared which discusses the events for four salient days.

5. Software Status

Other than the adjustments made to the mesonet analysis software package (mentioned earlier in this section) for the incorporation of PAM data, work was also performed on several other programs as well as the generation of new ones.

TABLE IV-3

Joint Mesonet and LLWAS Data

Date	Time (UT)
30 April 1985*	2133 to 2153
25 June 1985*	1755 to 1843
26 June 1985*	1947 to 1958
8 September 1985*	1846 to 1924
5 August 1987	1800 to 2030
11 August 1987	1950 to 2105
20 August 1987	2100 to 2200
21 August 1987*	2138 to 2245
26 August 1987*†	0000 to 0055
28 August 1987*	2205 to 2235
2 September 1987*†	2200 to 2330

* Dual and single (FL-2 and UND) Doppler radar provided to FAATC.
† These data sets were also sent out to NSSL in Oklahoma.

Some of the mesonet analysis software packages have been changed over the last several months. The mesonet storage and retrieval package (NETPAC) has been updated to accommodate the network characteristics package (NETCHAR). Due to the changes in these packages, it was necessary to update all the existing mesonet software. MBGRAF, a program utilized in the analysis of mesonet and/or LLWAS data, was adjusted to display wind and lightning data from the ASR-9 mesonet in Huntsville, AL.

Over the last six months, several new data translators were written. One was designed to transpose NESDIS (the National Environmental Satellite, Data, and Information Service) generated mesonet data into the Synergetics-formatted mesonet data. This translator has been used in the recovery process of two valuable segments of Huntsville mesonet data from 1986, and could be useful in the future should the need arise to retrieve mesonet data directly from NESDIS. Another translator was written for the data from the ten ASR-9 mesonet stations in Huntsville. These data include 1-min wind and lightning averages. A translator that will convert Synergetics-formatted data into Common Mesonet Format (CMF) has also been written.

Two new mesonet analysis software programs have been written over the last few months. The first was called WINDAVG and uses mesonet data as input. It is a command-driven program that will compute an average of the wind speeds (both average and peak) and their corresponding u and v components over a user-specified area. The program will be utilized intially as

an aid for the gust-front truthing process, but may be used during microburst analysis in the future. The other program, MESOPLOT, is currently being designed to plot any products available from the mesonet and/or the LLWAS data sets for user-specified time periods.

Some of the 1987 mesonet data were observed as being contaminated with sporadic noise caused predominantly by malfunctioning wind-direction potentiometers. The only data fields affected were pressure, temperature, relative humidity, and precipitation. A filter, described by F. Brock,[2] has been tested and finally implemented on our data. The filter appears to work satisfactorily.

Some work has gone into a program that will further enhance our mesonet analysis capability. This program will allow the analyst to generate, from the input of mesonet or mesonet and LLWAS data, a uniform grid of interpolated data. This will ultimately lead to better computations of such parameters as surface divergence and vorticity. The work on this program, however, has been given a low priority. Over the past six months, when time allowed, progress with this software package continued.

6. Future Work

During the next several months, emphasis will be placed on analyzing the 1988 Denver data sets as well as finishing the reports on the 1986 Huntsville and 1987 Denver data. The task will be similar to that of recent work, namely, the comparative study between Doppler radar and surface-detected microbursts where the subject of detectability is addressed. Also planned for the coming months will be a comparative study between the radar and mesonet observed microburst winds. The wind histories as well as the wind magnitudes vs time will be analyzed for select cases. The analysis should help in the understanding of the headwind/tailwind estimation for microbursts. Also, the time delay (lag) which occurs between the time that the microburst is observed aloft by radar and the time at which it impacts the surface will be investigated.

F. MICROBURST DETECTION ALGORITHM DEVELOPMENT

The microburst detection algorithm development effort is aimed at producing an automatic procedure for recognizing hazardous, low-altitude, wind shear resulting from microburst downdrafts, using Doppler weather radar measurements. This effort is primarily intended for application to the Terminal Doppler Weather Radar system being procured by the FAA. Over the last few years, two major approaches have been investigated. The first approach is based on the detection of microburst surface outflows, by searching the radar measurements near the surface for the characteristic divergence signature. The second approach extends the surface outflow detection method by employing velocity and reflectivity signatures aloft, as well as those at the surface. This advanced detection algorithm is able to provide more reliable detection of weaker events, and to detect microbursts somewhat earlier in their lifetime than is possible using the surface information alone.

Executable implementations exist for both the surface outflow and three-dimensional algorithms, and these algorithms have been subjected to extensive performance evaluations. Algorithm

performance is assessed by applying the algorithm to actual weather radar measurements, and comparing the algorithm produced microburst alarms with *ground-truth* information derived by experienced radar meteorologists studying the radar observations. Results of these performance analyses are presented below.

In addition to this off-line performance analysis, the surface outflow algorithm has been implemented in the FL-2 weather radar test-bed system, and has been routinely operated during the past two summer data-collection seasons: Huntsville, AL in 1986 and Denver, CO in 1987. This operational field experience has provided considerable insight into the real-time computational requirements, reliability, and day-to-day performance of the surface outflow algorithm. Real-time implementation of the three-dimensional algorithm is currently in progress, and will be demonstrated during the 1988 TDWR operational test and evaluation in Denver.

The salient accomplishments in the algorithm development effort during this reporting period are summarized in Table IV-4.

1. Surface Outflow Algorithm

The surface outflow detection algorithm identifies microbursts by locating their divergence signature in radar velocity measurements made at the surface. The three main steps in the algorithm are diagrammed in Figure IV-2. The first step in the detection process identifies regions of strong divergent shear, which are manifest as a rapid increase with range in the velocity measurement along a radial of measurements. The second step involves the spatial association of shear segments which are identified on adjacent radials, to form two-dimensional regions of strong divergent shear. The third step correlates these shear regions in time, across consecutive scans of the radar. The time-correlated regions of shear identified by this process are finally tested against strength and area thresholds to provide microburst alarms. A detailed description of the algorithm operation was presented in Merritt.[3]

The detection process has been found to perform quite well on a large sample of microburst cases. Performance may be improved, however, by merging information from radar measurements aloft with the surface outflow features detected by this algorithm.

2. Advanced Algorithm

The advanced microburst algorithm development work began in 1984 as part of an investigation into the use of artificial intelligence techniques for air traffic applications. A microburst recognition system called WX1 was developed, which coupled a rule-based expert system to an object-oriented feature database. This system, implemented on a Symbolics 3670 Lisp machine, performed feature extraction on Cartesian resampled radar data to identify reflectivity and shear regions. It combined these regions into three-dimensional structures in order to increase the reliability and timeliness of microburst warnings. The WX1 system is described in detail in Campbell and Olson.[4]

TABLE IV-4

Milestones for Microburst Algorithm Development

Date	Milestone
June 1986*	Formal documentation of outflow detection algorithm submitted to NEXRAD JSPO (Version 1)
July 1986*	Outflow algorithm operational in FL-2 test-bed radar
	NCAR scientists independently evaluate outflow algorithm performance at Huntsville field site
December 1986	Time association stage added to outflow detection algorithm (Version 2)
January 1987	Version 2 outflow algorithm scored against LL and NCAR ground-truth data sets
March 1987	Ground-truth data sets refined, and Version 2 algorithm rescored
	Formal documentation of Version 2 algorithm submitted to NEXRAD JSPO
April 1987	Feature extraction algorithms implemented on Sun computers for locating convergence, rotation, and reflectivity regions from polar data
	Advanced algorithm (on Symbolics Lisp machine) restructured to accept polar-based feature inputs computed on Sun computer
June 1987	Outflow algorithm began routine operation and evaluation in FL-2 test-bed radar
	Initial version of advanced algorithm documented in AEL and submitted to FAA
October 1987	Design and implementation of real-time advanced algorithm system (feature extraction and symbolic processing) begun
February 1988	Final version of advanced algorithm AEL submitted to FAA
March 1988	Initial system testing begun for real-time advanced microburst implementation

* These activities were previously reported in the Semiannual Technical Summary, "Weather Radar Studies," Lincoln Laboratory, MIT (30 September 1986).

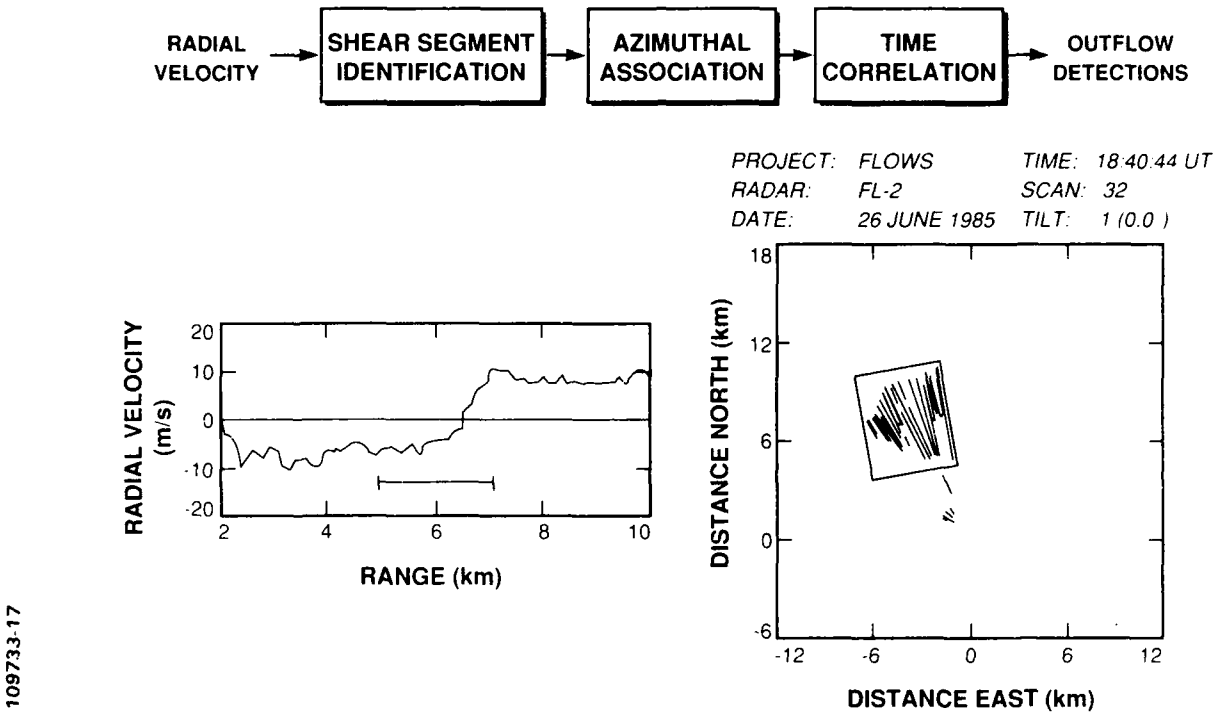

Figure IV-2. Outflow detection algorithm.

Although the WX1 system demonstrated that significant performance improvements could be obtained through the use of features aloft, the system had two major shortcomings. First, the system used features extracted from Cartesian resampled data rather than the polar data likely to be used in an operational system. Second, the feature extraction operations performed on the Lisp machine were much too slow to be employed in real time. Accordingly, we decided to modify the system to use polar-based features generated on a Sun workstation. The ultimate aim of this effort was to achieve a real-time implementation of the advanced algorithm.

The new system, called WX2, employs a feature database containing reflectivity and shear features extracted by a Sun workstation from the input polar radar data. The expert system rules assemble these features into three-dimensional structures, such as storm cells, reflectivity cores, convergence aloft, and rotation aloft. The rules use these structures to recognize microburst precursor signatures and to aid surface outflow recognition. The use of precursors allows the system to make a microburst declaration while the surface outflow is still weak, thereby increasing the timeliness of the warning.

a. Microburst Precursors

Microburst precursors are features aloft which indicate that a microburst is about to occur in the near future, i.e., in 5 to 10 min. Roberts and Wilson[5] presented conceptual models for the

evolution of three types of microbursts typical of the Denver area. Isaminger[6] has identified precursor signatures associated with microbursts in Huntsville.

Figure IV-3 shows a conceptual diagram for the evolution of a prototypical microburst of the type found in the southeast United States. In the first stage of development, a reflectivity core appears aloft in the parent storm of the microburst at about 5 km AGL (above ground level). At the same time, a convergence or inflow begins to develop at or above the level of the reflectivity core.

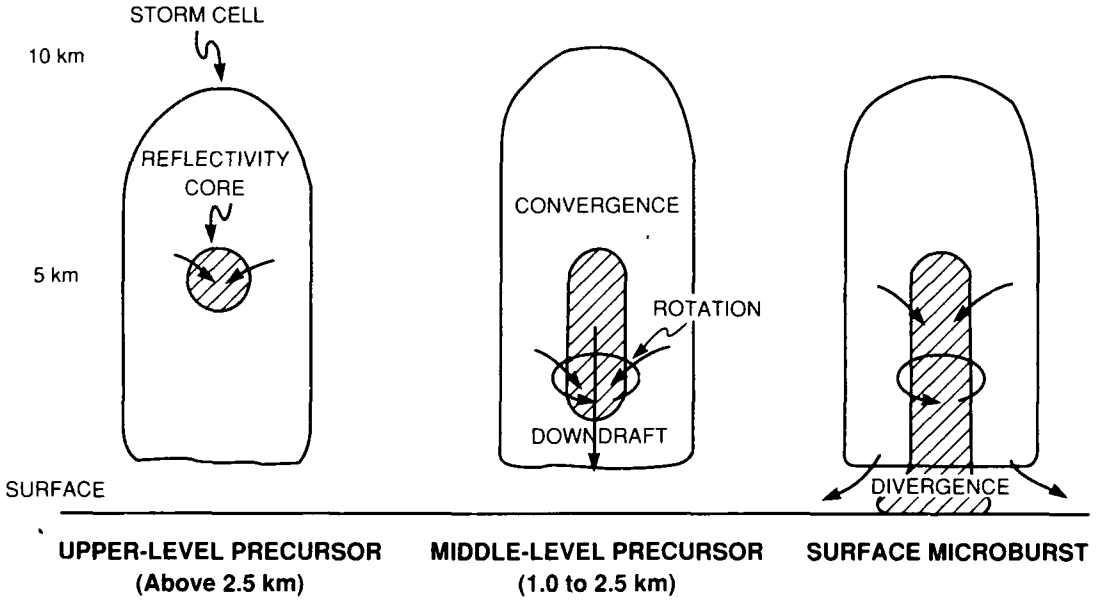

Figure IV-3. Conceptual diagram for microburst evolution in southeast US.

In the second stage of development, the reflectivity core has begun to sink to middle level (about 3 km). Convergence is evident now at this level and rotation often also begins to develop. Taken together, the descent of the reflectivity core and the development of the middle-level velocity signatures are indications that a strong downdraft has developed. It is this strong downdraft which will produce the hazardous outflow at the surface.

In the third stage of development, the reflectivity core has reached the surface and divergent flow at the surface is now evident. The outflow will typically reach maximum intensity in the next 5 to 10 min. As a general rule, the strongest surface outflows intensify the most rapidly.

Thus, by detecting precursors aloft, it should be possible to provide an early microburst warning based on the initial surface outflow. This sort of tactic was adopted by meteorologists from the National Center for Atmospheric Research (NCAR) during the CLAWS (Classify, Locate, and Avoid Wind Shear) project at Denver during the summer of 1984 (McCarthy and

Wilson[7]). During the CLAWS project, NCAR meteorologists provided microburst warnings for the Stapleton airport area by monitoring a single S-band Doppler weather radar.

In the absence of a microburst precursor signature, the meteorologists waited until a surface outflow signature reached 10 m/s (20 kn) before declaring a microburst hazard. However, if a microburst precursor was present and a weak surface outflow was detected, the meteorologists declared the microburst hazard immediately.

b. Radar Signatures

Figure IV-4 summarizes the radar signatures that the WX2 system uses for microburst recognition. There are two classes of signatures: reflectivity features and shear features. Reflectivity signatures consist of storm cell features and reflectivity core features. Storm cell features are regions of 30 dBz or greater reflectivity; reflectivity core features are regions of 50-dBz or greater reflectivity. Reflectivity features are recognized for all scans, except for surface scans (due to clutter contamination).

Shear signatures consist of divergence, convergence, and rotation features. Surface divergence signatures are recognized only for surface scans. Lower-level divergence signatures below 1 km AGL are recognized for scans aloft. Convergence signatures are recognized for middle and upper levels. Rotation (cyclonic and anticyclonic) signatures are recognized also at middle and upper levels, although over slightly lower limits. Finally, divergence signatures above 7 km AGL are recognized for storm cell divergent tops.

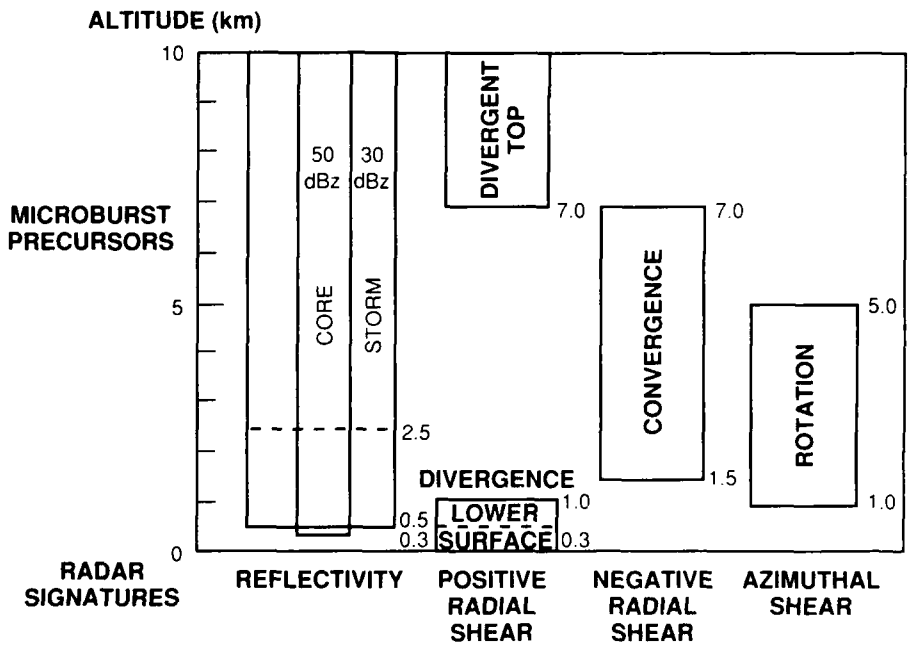

109733-19

Figure IV-4. Radar signatures for microburst recognition used by WX2 system.

c. Scanning Strategy

Figure IV-5 shows an idealized picture of the scan strategy assumed by the WX2 system. As seen in the figure, the scan strategy consists of L surface scans and M scans aloft. Multiple surface scans are used to provide rapid updating for microburst surface outflows. The scan strategy employed for most of the data used to validate the present algorithm consisted of 16 scans (4 surface and 12 aloft). The interval between surface scans was about 1 min, and the time to complete a volume scan was about 4 min.

The use of multiple surface scans within a volume scan necessitates the introduction of the *sliding-window* volume scan concept. For each surface scan, the sliding-window volume scan consists of the surface scan plus the M most-recent scans aloft.

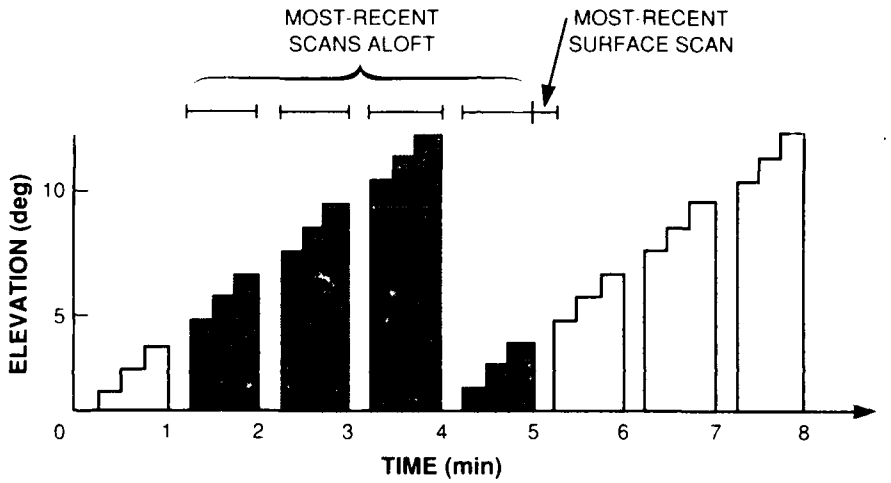

109733-20

Figure IV-5. Idealized scan strategy showing sliding-window volume scan.

d. System Design

As shown in Figure IV-6, the WX2 system is divided into two components: feature extraction and symbolic reasoning. The feature extraction is performed by a Sun workstation using conventional programming techniques. The symbolic reasoning is performed by a rule-based expert system implemented on a Symbolics Lisp machine. The expert system is implemented

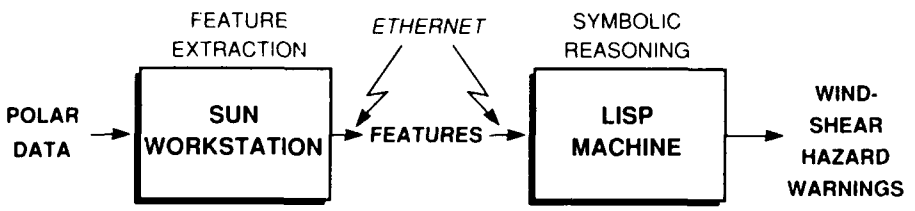

109733-21

Figure IV-6. WX2 system design.

using the YAPS (Yet Another Processing System) production rule language. Features are transmitted from the Sun workstation to the Lisp machine either via magnetic tape or ethernet file transfer.

Feature Extraction:— Feature extraction consists of processing the base radar measurements to produce sets of features. Each feature is a two-dimensional region of a particular type, such as a convergent shear or storm cell region. Attributes are computed for each feature such as the area, mean radius, centroid, and bounding box, as shown in Figure IV-7. Additional attributes are computed for particular types of features, such as the velocity difference for a shear feature.

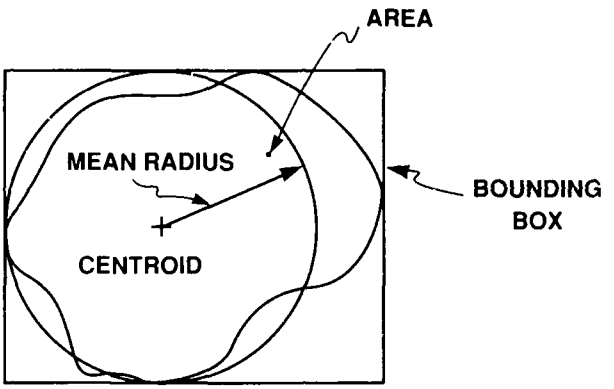

109733-22

Figure IV-7. Feature attributes.

The algorithms for extracting shear features operate on radial velocity data to extract divergence, convergence, and rotation features. The divergence and convergence algorithms process the velocity data radially to identify sequences of increasing and decreasing velocity. Segments thus recognized are associated together in azimuth to produce regions of outflow and inflow. Similarly, the rotation algorithms process velocity data azimuthally, then radially to identify regions of cyclonic and anticyclonic circulation.

The reflectivity feature extraction algorithms process reflectivity data to identify storm cell and reflectivity core regions. These regions are identified by thresholding the reflectivity data at 30- and 50-dBz levels. The thresholded data are then associated radially and then azimuthally to produce the desired reflectivity regions.

Symbolic Reasoning:— Symbolic reasoning consists of combining two-dimensional features to produce three-dimensional structures. The first stage in symbolic processing is to vertically correlate features of the same type to produce velocity and reflectivity structures. Velocity structures are constructed from convergence, divergence, and rotation signatures. Reflectivity structures are assembled from 30- and 50-dBz regions. Figure IV-8 illustrates the vertical integration process for storm cells.

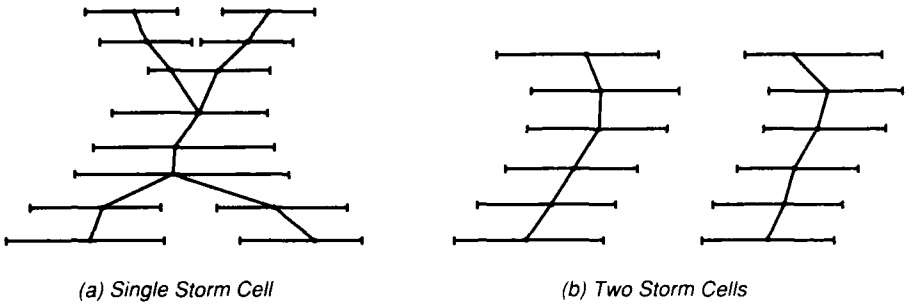

Figure IV-8. Vertical integration.

The second stage of the symbolic processing is to create complex structures. A complex structure is one which contains features of different types. For example, a middle-level precursor signature can be recognized from a convergence aloft combined with a descending reflectivity core.

e. Microburst Precursor Recognition

This section will illustrate how the WX2 system recognizes microburst precursors and how precursor signatures can be used to provide an early microburst hazard warning.

Figure IV-9 shows a hypothetical example of a reflectivity core descending from aloft. A series of sliding-window volume scans is shown illustrating the descent of the core. The rule for recognizing the descending core is that the bottom of the reflectivity core must be above an

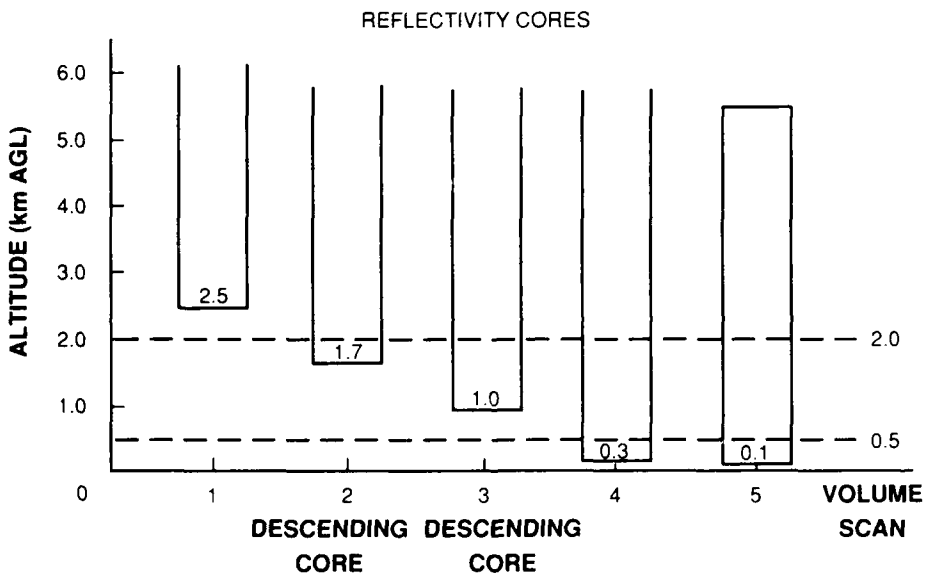

Figure IV-9. Descending reflectivity core recognition.

upper-threshold altitude (e.g., 2 km AGL) on the previous volume scan and below the threshold on the present volume scan. The reflectivity core continues to be recognized as descending until the bottom descends below a lower threshold (e.g., 0.5 km AGL).

Figure IV-10 illustrates how middle-level precursors are recognized. In this case, the middle-level precursor is recognized from an upper-level downdraft (convergence or rotation aloft above 3.5 km AGL) and a descending reflectivity core. When these two signatures occur together, a rule fires which recognizes the middle-level precursor.

The rule for recognizing the middle-level precursor (in simplified form) would appear as follows:

```
(if (goal recognize-middle-level-precursors)
        (volume-feature -ud :upper-level-downdraft)
        (volume-feature -dc :descending-core)

        test (send -ud :overlaps-p -dc)

then (setq -mp (make-volume-feature (list -ud -dc))
        (fact volume-feature -mp :middle-level-precursor)
        )
```

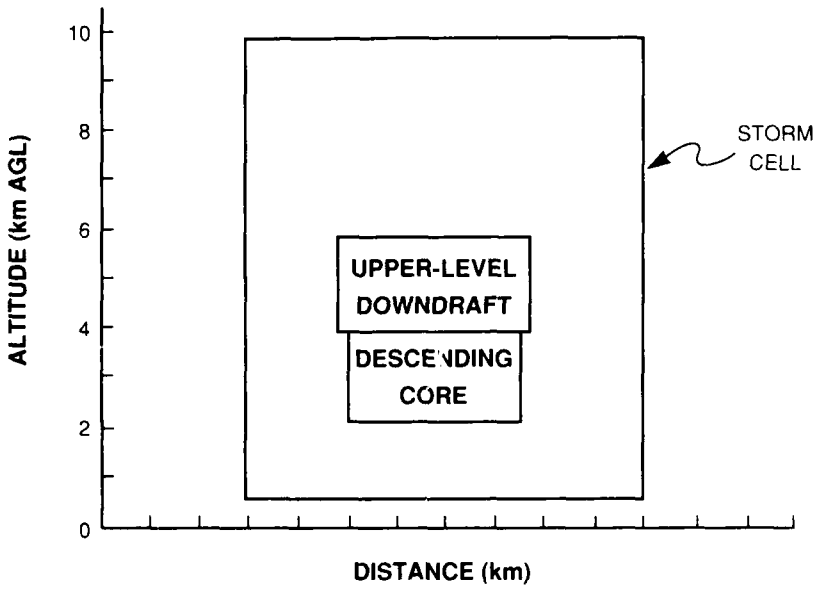

109733-25

Figure IV-10. Middle-level precursor recognition.

This rule matches facts in working memory for an upper-level downdraft and a descending reflectivity core, and binds the variables -ud and -dc to the corresponding Lisp objects pointed to by these slots in the facts. A test is then applied which checks whether the two structures overlap; the test is invoked by a message to one of the Lisp objects.

If the test passes, then the right-hand side of the rule fires, causing two actions to be taken. First, a new structure (volume-feature) is created from the original two structures and bound to the variable -mp. Second, a new fact is added to the expert system memory representing the middle-level precursor signature which has been recognized.

Figure IV-11 shows how an early microburst declaration can be made using precursor signatures. If a middle-level precursor is associated with a weak surface outflow, then a rule fires which produces a microburst declaration. The rule is a mechanization of the procedure used by NCAR meteorologists in the CLAWS project to declare a microburst based on a weak surface outflow combined with the observation of a precursor signature.

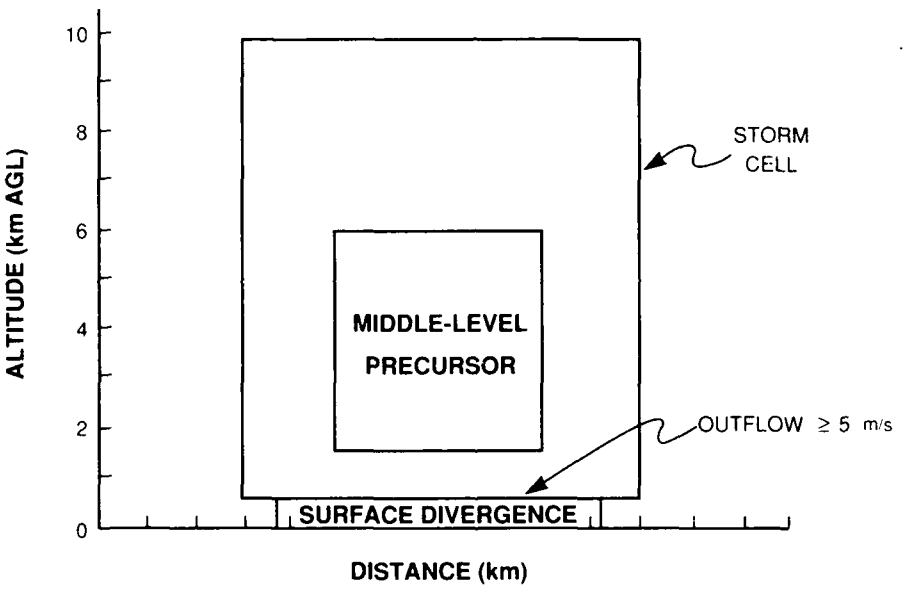

Figure IV-11. Early microburst hazard declaration.

An example of output from the WX2 system for three successive volume scans is shown in Figure IV-12. The data processing in this case was obtained by the FL-2 S-band radar at Huntsville, AL on 7 June 1986. At 16:49:09 CST, the system recognized a middle-level precursor from a descending reflectivity core combined with convergence and rotation signatures aloft. On the subsequent surface scan at 16:50:28, a weak surface outflow (8 m/s) is detected along with the middle-level precursor. The system therefore makes an early declaration of the microburst hazard while the outflow is still below the 10-m/s threshold. Finally, on the subsequent surface scan at

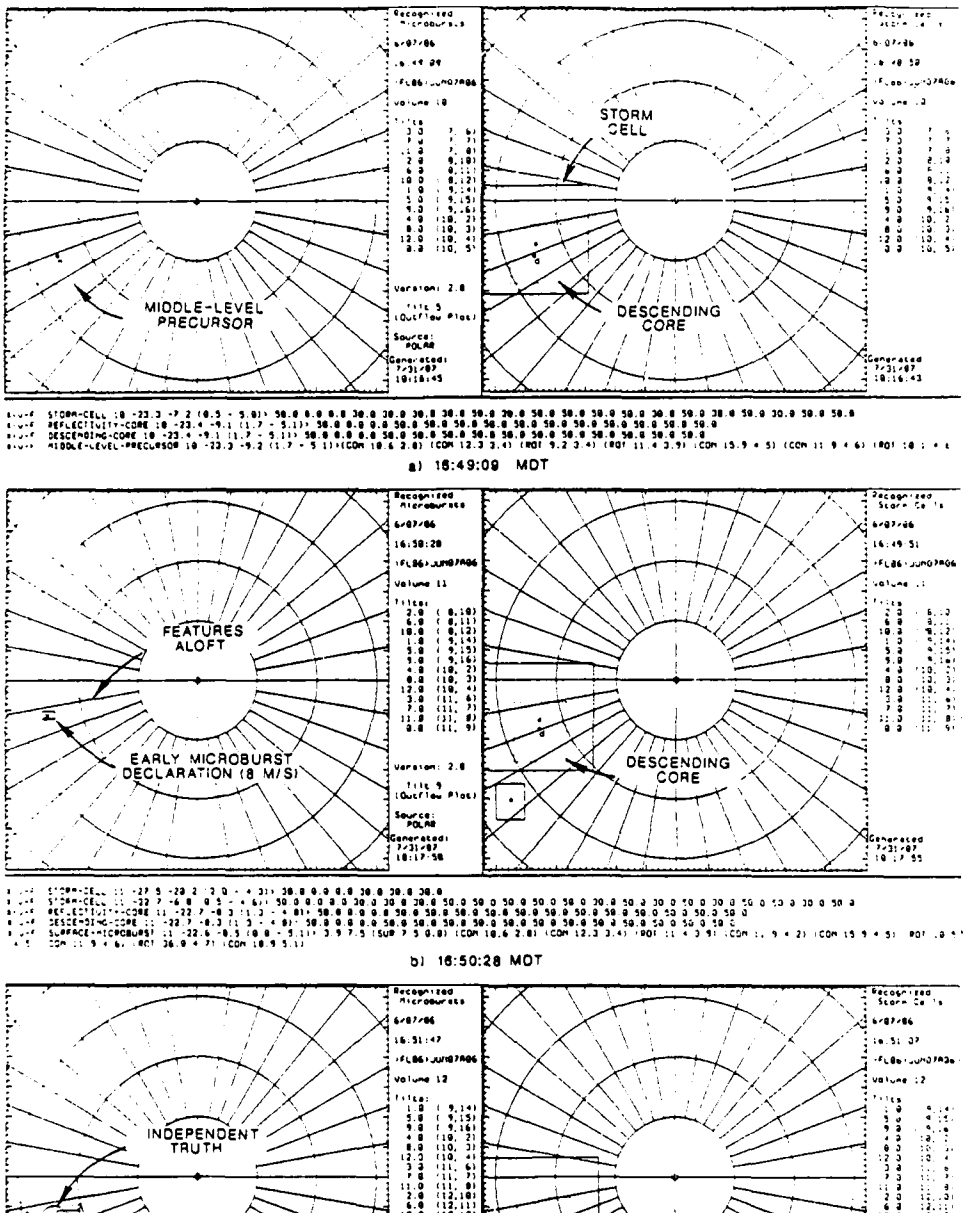

Figure IV-12. Example of results from Huntsville, AL microburst on 7 June 1986.

109733-27

16:51:47 the microburst outflow reaches 12 m/s, as indicated both by the WX2 output and the circle indicating independent truth generated by NCAR meteorologists.

Note that the use of precursors in this case allowed the WX2 system to declare the microburst hazard 1.3 min earlier than would have otherwise been possible. In addition, the system began declaring the middle-level precursor 7.5 min before the outflow reached the 10-m/s threshold.

3. Performance Evaluations

The detection performance of the microburst algorithms has been extensively evaluated on a large number of recorded data cases. The evaluation process consists of a comparison between the microburst alarms generated by the algorithm under test with the contents of a *ground-truth* database. The database contains the location, extent, and strength of all microbursts present in the radar viewing area, on each radar scan. It was created by experienced radar analysts, who carefully examined the recorded radar data for the test cases.

a. Ground-Truth Database

For the purpose of this performance evaluation, a microburst event has been defined (by joint LL and NCAR agreement) as a wind shear which produces a velocity change of at least 10 m/s over a distance of less than 4 km. Given such an event, the boundary (or edge) of the event is defined by the contour of horizontal divergence above the level 2.5 m/s/km. Divergence is computed as the maximum linear divergence (i.e., $\Delta V/\Delta R$ along a line) in any direction at each point (as opposed to the standard two-dimensional definition of divergence: $\Delta U/\Delta X + \Delta V/\Delta Y$). The purpose of using the maximal linear divergence is to more accurately characterize the hazard experienced by an aircraft encountering the microburst event. A microburst is considered *ended* after its outflow has not met the 10 m/s in 4-km criteria for at least 2 min of observation.

A substantial number of microburst events from the 1986 and 1987 data-collection programs in Huntsville, AL and Denver, CO, respectively, have been closely examined to determine the location and duration of true microbursts. The examination was performed by analysts from both Lincoln and NCAR. Several passes have been made through most of the radar data, to provide reliable indications of the locations and strengths of all microbursts involved. Table IV-5 lists the days for which microburst ground truth has been created, from both the 1986 and 1987 data-collection programs.

The process of examining the base radar velocity and reflectivity images to identify microbursts is an extremely tedious, and hence error-prone, process. Several iterations are typically required to produce a reasonably accurate identification of the microbursts present. In those cases where numerous events are present in the same area (e.g., a microburst line), the ground-truth information often simplifies the actual conditions, identifying clusters of microburst outflows, rather than meticulously delineating the boundaries and temporal histories of individual events.

TABLE IV-5

1986 and 1987 Ground-Truth Database

Date	Date Available	Truth Type (UT)	Truth Period	Weather Synopsis (UT)	Truth Grade	Truther
7 Jun 86	1625-2150 (5.4)	Surface	1651-1749 (1.0)		A	LL
1 Jul 86	1102-1425 (3.3)					
	1732-2339 (6.1)	Surface	1734-1940 (2.1)		A	LL
6 Jul 86	1804-2228 (4.4)	Precursors	2043-2121 (0.7)		C	LL
11 Jul 88	0012-0107 (0.9)	Precursors	0012-0034 (0.3)		C	LL
	1205-1234 (0.5)					
	1618-2245 (5.5)	Precursors	1720-2042 (3.3)			
24 Jul 86	1733-2032 (3.0)	Surface and precursors	1756-1935 (1.7)		A	NCAR/LL
25 Jul 86	1448-2258 (8.2)	Surface and precursors	1853-2216 (3.3)		A	NCAR/LL
31 Jul 86	1637-2050 (4.3)	Surface and precursors	1741-1923 (1.7)		A	NCAR/LL
7 Aug 86	1802-0022 (6.3)	Precursors	2109-2200 (0.9)		C	LL
24 Aug 86	1749-2211 (4.3)	Surface and precursors	1845-2011 (1.5)		A	LL
5 Sep 86	0023-0147					
	2044-2120 (0.3)	Surface	2045-2058 (0.2)		A	LL
20 Sep 86	1708-2159 (4.9)	Precursors	2113-2131 (1.3)		C	LL
21 Sep 86	1722-2201 (4.7)	Surface and precursors	1832-2046 (2.2)		C	LL
22 Sep 86	1923-0006 (4.7)	Surface	2121-2354 (2.5)		A	LL
26 Sep 86	1628-2007 (3.5)	Surface	1733-1945 (2.2)		A	LL
23 May 87	2037-2344 (3.1)	Surface	2100-2218 (1.3)	Thunderstorms	A	LL
28 May 87	2051-0048 (4.0)	Surface and precursors	2149-0026 (2.6)	Thunderstorms	A	NCAR
30 May 87	2323-0205 (2.7)	Surface	2346-2060 (2.3)	Wet thunderstorms	A	NCAR
7 Jun 87	2138-0238 (5.0)	Surface and precursors	2323-0158 (2.5)	High reflectivity, line	A	LL
10 Jun 87	1901-0017 (5.2)	Surface and precursors	1919-2322 (4.0)	Dry line	A	LL
14 Jun 87	1933-0058 (5.4)	Surface and precursors	1953-0057 (5.0)	Hot, thunderstorms	B	LL
17 Jun 87	2103-0036	Surface and precursors	2124-2333 (2.1)	Weak thunderstorms	A	LL
18 Jun 87	1934-0123 (5.9)	Surface	2147-2327 (1.7)	Supercell thunderstorms	A	NCAR
21 Jun 87	1759-0100 (7.0)	Surface and precursors	1941-0046 (5.0)	Dry MBs	A	LL
9 Jul 87	2051-0222 (5.5)	Surface and precursors	2342-0014 (0.5)	Warm, thunderstorms	C	LL
25 Aug 87	1919-0047 (5.5)	Surface	2309-0033 (1.5)	Wet, line	A	LL
2 Sep 87	1722-0039 (7.3)	Surface and precursors	2223-2310 (0.9)	Line thunderstorms	A	LL

Notes

Truth Grades: A = several review passes completed; B = initial pass only; and C = incomplete surface truth available.

To insure agreement between the various analysts involved in the ground-truth process, a workshop was held at Lincoln on 1-2 March 1988. A number of cases were examined by a group of analysts to resolve remaining problems and to jointly discuss the various finer aspects of the ground-truthing process. As a result of the workshop, the majority of the Denver 1987 test cases were refined, and considerable agreement on the resulting ground-truth data (and the procedures by which the data are to be judged in the future) was achieved.

b. Scoring Procedure

The scoring process involves the comparison of the algorithm-generated alarms with the microbursts indicated by the ground-truth database. On each surface scan of the radar (roughly once per minute), the alarms and truth are compared to determine the number of hits, misses, and false alarms. The statistics are then tallied for each of the days under evaluation, and reported as a function of microburst strength. The two quantities derived by this comparison are the probability of detection (POD) and the probability of false alarm (PFA), defined as follows:

POD = number of hits ÷ number of true events

PFA = number of false alarms ÷ total number of alarms

For these statistics, an *event* is considered to be a single radar scan through an active microburst. Since most microbursts exist for several radar scans, each microburst is counted multiple times (in proportion to its duration) in these statistics.

c. Performance Results

Both the surface outflow and advanced algorithm have been evaluated by the above procedure on five test days each from the Huntsville (1986) and Denver (1987) ground-truth cases. The test sample includes roughly 125 microbursts, with a wide range of peak strengths and surface reflectivities. Table IV-6 presents performance statistics for the test cases.

We see that both algorithms perform quite well, with the advanced algorithm showing larger relative improvement on those microburst observations with weaker differential velocities.

TABLE IV-6

Performance Statistics for Huntsville and Denver Test Cases

	Surface Outflow (percent)	Advanced (percent)
POD for $\Delta V < 20$ m/s	87	90
POD for $\Delta V > 20$ m/s	99	100
POD for All Events	89	92
PFA	3.8	5.2

4. Real-Time Implementation for TDWR OT&E

An operational test and evaluation of the TDWR microburst detection system will be conducted during July and August 1988, using the FL-2 radar at Denver. The advanced microburst detection algorithm is currently being transitioned to a real-time environment so that it may be used in this evaluation.

A block diagram of the real-time microburst system is shown in Figure IV-13. Radial format base data (reflectivity and radial velocity measurements) are supplied to the microburst system from the FL-2 central processor, and the basic feature extraction modules are applied. These modules will be executed using two Sun 4/260 workstations. The resulting features are then transmitted to a Symbolics 3600 processor, where the advanced algorithm symbolic processing is performed. The resulting alarms are then coordinated with the surface divergence shear segments (used by the display processing algorithms) and transmitted to the end-user display system.

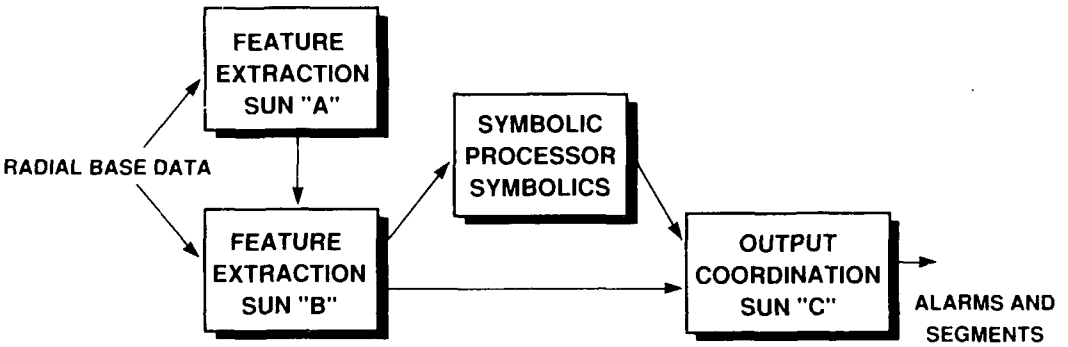

Figure IV-13. Microburst real-time system.

Design and implementation of this system began in late 1987, and the completed system will be delivered to the Denver field site in April 1988. Final integration testing of the major components is currently being performed on the hardware located at Lincoln.

The real-time implementation effort has required that considerable effort be devoted to restructuring the various feature extraction tasks, speeding up the Symbolics processing, and implementing intermachine communications handling. Benchmarks on the Sun 4/260 processors were used to determine that the feature extraction tasks could execute in real time for worst-case datasets. Considerable optimization efforts on the Symbolics yielded a tenfold increase in speed over the previous implementation of the advanced algorithm ruleset. The improvement in execution speed lowered the worst-case average processing time to less than half of the data-collection time. These efforts resulted in assurance that the advanced algorithm would be able to operate in real time.

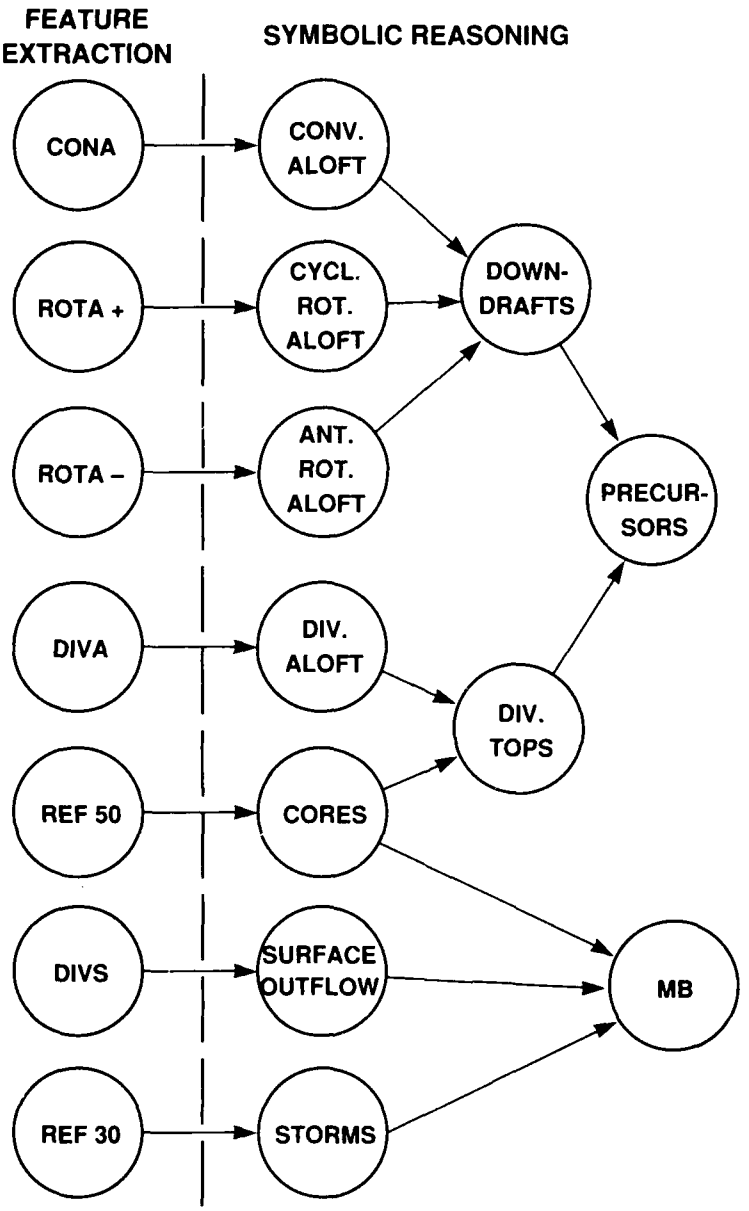

Figure IV-14. Algorithm organization.

5. Formal Documentation of Algorithms for TDWR and Terminal NEXRAD

The microburst detection algorithm development efforts are directed at the TDWR and Terminal NEXRAD applications. The algorithms developed at Lincoln are supplied to these FAA programs via a formal documentation and validation process, as was used for the NEXRAD program. Each algorithm must be described in a structured Algorithm Enunciation Language (AEL), which is then submitted to the Government for validation and, ultimately, inclusion in the system specification.

An early version of the surface outflow detection algorithm (not including time correlation) was documented in this manner, and submitted to the FAA in June 1986. In late 1986, a time correlation module was added to the surface outflow process, and the improved algorithm documentation was resubmitted to the FAA in March 1987.

In early 1987, the advanced detection algorithm was reorganized to accept polar format base data, and documented in the AEL form. This version of the AEL was submitted to the FAA in June 1987. Recent improvements in the algorithm, as well as numerous corrections to the previous descriptions, resulted in a revised advanced algorithm AEL package, submitted to the FAA in February 1988.

The advanced algorithm is documented as a set of eleven separate processing modules, as shown in Figure IV-14. A project report describing the advanced algorithm has been submitted to the FAA in draft form.

G. TURBULENCE DETECTION ALGORITHM DEVELOPMENT

The purpose of the turbulence detection algorithm effort is to develop an effective, weather-smart algorithm that detects turbulence from Doppler radar data. In support of this goal, the major thrust of the work over the past 18 months has been in the following areas: the development of turbulence data preprocessing capabilities, implementation of the option to use various spectrum width estimators and turbulence algorithms (Bohne, Labitt), the continued analysis of 1985 Memphis turbulence data, the comparative analysis of turbulence associated with microburst outflow regions, data collection during coordinated aircraft-radar experiments, and the development of an algorithm to identify possible turbulence encounters by aircraft of opportunity.

In an effort to ensure that the data on the turbulence detection algorithm contain only weather echoes associated with isotropic turbulence, a data preprocessor was developed that allows various spurious signals to be suppressed prior to turbulence processing. A point target filter was incorporated into the data analysis software. This filter removes transient, high-velocity echoes (due to aircraft, birds, and insects) from the data. While reflectivity information could also be used as a discriminant, only velocity discontinuity detection has been exploited. Analysis of the Memphis turbulence data shows numerous instances in which point targets evidently gave rise to erroneous indications of strong turbulence. A feature was added to the software to monitor the frequency with which the point target filter was used on a per-radial basis. The rate of point target filtering was usually low (less than five per radial), but for a significant number of

radials there were much higher numbers indicating that aircraft were not the only targets causing sharp velocity field discontinuities. The numbers generally decreased with increasing elevation angle, further suggesting that birds and insects were responsible for corrupting the weather products.

Several FL-2 (FAA-Lincoln Laboratory Doppler) and UND (University of North Dakota Doppler) radar cases were analyzed as part of an aspect sensitivity study of turbulence to assess the validity of the isotropic assumption. Initial results at low altitude suggested that isotropic behavior dominated the spectrum width comparisons, but departures from isotropy were also evident.

An initial comparative analysis of the FL-2 and UND data of 9 August 1985 indicated that the detection and interpretation of low-reflectivity targets at low altitudes required caution. Large spectrum width values were detected in regions not believed to be associated with strong turbulence.

Several cases were studied as part of a microburst turbulence investigation. Little turbulence was noted in the outflow regions of microbursts. This contradicts turbulence models that have been developed by other organizations for use with JAWS data. The wet microbursts of the southeast may differ from the dry microbursts of the southwest regarding outflow turbulence characteristics. This comparison must be pursued in the future.

A quantitative comparative analysis of spectrum width estimators based on 0-1 and 1-2 correlation lag estimates and of the Bohne and Labitt turbulence parameter estimates was begun. The effect of turbulence outer-scale parameter values in the Bohne algorithm must be assessed relative to sensitivity and consistency in the radar turbulence measurements. Documentation of the turbulence analysis software package to support these analyses has been completed and distributed.

The data-collection effort, which took place in Denver during the summer of 1987, was supported by the instrumented UND Cessna Citation II. The mission of the Citation was to fly in and around various weather phenomena (e.g., gust fronts, isolated convective cells, and lines of convective cells) measuring turbulence.

A scanning strategy was developed for use during the coordinated aircraft radar experiments. This strategy, shown in Table IV-7, provided both high-resolution coverage (in time and space) of the airspace occupied by the Citation and storm surveillance. The scan strategy consisted of two scan sequences: the turbulence scan and the surveillance scan.

The turbulence scan was composed of three 60° sector scans. The elevation angles and sector centers were defined by the altitude and range of the Citation, as determined from the ATCRBS data. The first sector scan was centered on the aircraft. The second and third sectors were 1° in elevation above and 1° below the aircraft, respectively. The tilt sequence (which took about 24 s) was then repeated using an updated aircraft location.

TABLE IV-7 Turbulence Volume Scan	
Elevation Angle	**Azimuth Limits**
AC*	AC ± 30°
AC + 1°	AC ± 30°
AC - 1°	AC ± 30°
Surveillance Volume Scan	
0.2	WX† ± 60°
2.2	WX ± 60°
4.5	WX ± 60°
6.7	WX ± 60°
8.8	WX ± 60°
11.0	WX ± 60°
13.1	WX ± 60°
15.6	WX ± 60°
* AC = aircraft † WX = weather	

The surveillance scan was conducted once every 5 min and was designed to gather data on storm movement and development. This scan contained ten 120° sector scans whose centers were determined by the location of the weather.

The scan strategy outlined above could not be used in support of the other missions of the TDWR 1987 Summer Experiment (e.g., microburst and gust-front algorithm testing) and, in fact, conflicted with those missions. As a result, the turbulence experiments could only be conducted infrequently and under special circumstances (i.e., when there were no storms in the vicinity of Stapleton Airport or moving into the dual-Doppler lobes). Also, due to the congested airspace around Denver, it was often impossible to position the Citation where moderate (or greater) turbulence was expected to be found. Even so, data were gathered for eight case studies.

The work to collect coordinated radar aircraft turbulence data continued throughout the winter of 1987. While the UND Citation conducted icing studies for the FAA, the FL-2 scanned the airspace around the Citation. During December and January, data were collected on three days when moderate or greater turbulence was reported by the Citation.

In addition to the data-collection effort, an algorithm was developed to identify possible turbulence encounters by aircraft of opportunity. This algorithm used data from the Air Traffic Control Radar Beacon System (ATCRBS) or Mode-C data. The MODEC algorithm was designed to search the ATCRBS altitude data for all aircraft for deviations of greater than or equal to 300 ft from an established flight path. The planes were required to be in level flight since the data resolution was insufficient to allow the detection of altitude deviations during climbs and descents.

The MODEC algorithm was tested using the flight path of a Citation flight conducted in 1986 in Huntsville, AL (Figure IV-15). For example, during the time between about 18:50 and 19:30 GMT, the Citation was flying at 9000 ft. The Citation crew reported encountering moderate (M) turbulence at 19:05 GMT. This corresponded to the flight altitude deviations identified from the ATCRBS data and indicated on Figure IV-15 by an X.

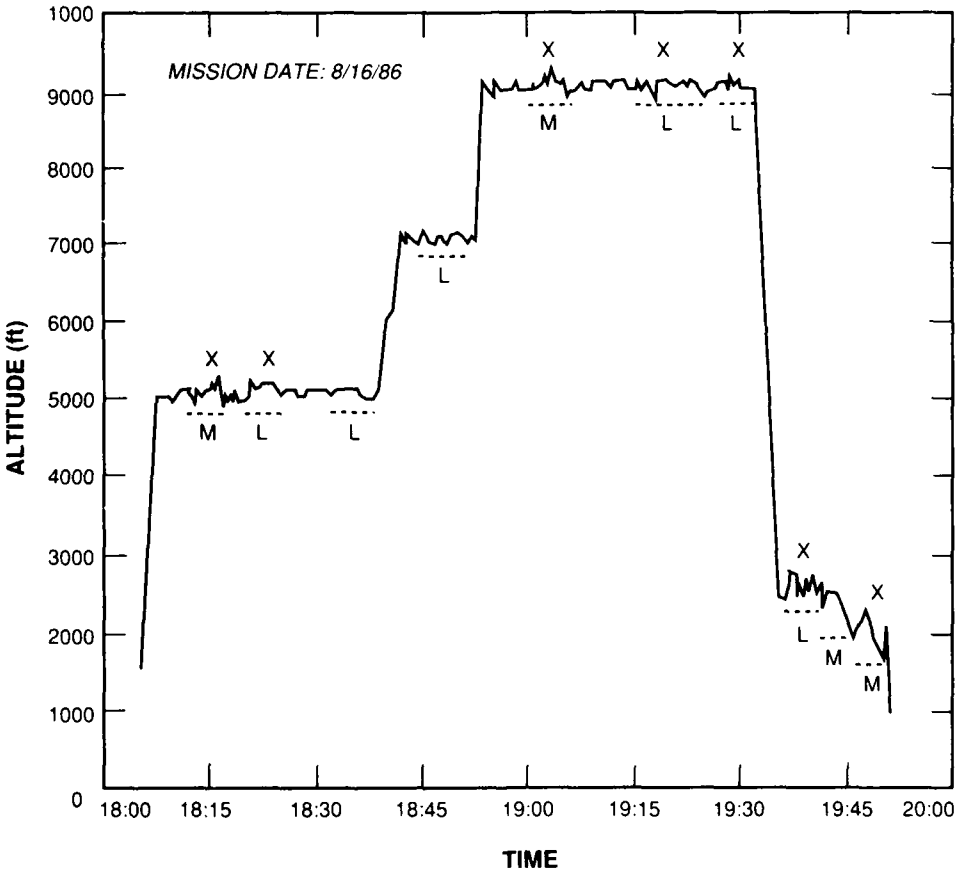

Figure IV-15. ATCRBS (C-mode) data showing altitude deviations corresponding to moderate turbulence.

The MODEC algorithm was run on the ATCRBS 1987 Denver data and did not perform as well as hoped. This was due in part to the traffic patterns (that may be characteristic of Denver). Aircraft departing from and arriving at Denver almost always executed continuous climbs and descents, thus altitude deviations could not be measured. The algorithm had a high probability of false alarms, often generated by bad data. However, these false alarms were easily identifiable in the plotted output. Although the algorithm demonstrated shortcomings, it can still be a useful tool and may prove more effective at different airports.

Future plans for the turbulence detection algorithm work include investigating (1) the possibility of suppressing wind-shear contributions to spectrum width, (2) the validity of the isotropy assumption at higher elevations, (3) the use of reflectivity to identify high spectrum widths due to weather rather than weak signal, and (4) turbulence associated with wet vs dry microbursts. Effort will also be expended in continued collection of aircraft radar turbulence data through mid-May, analysis of the 1985 (Memphis) and 1986 (Huntsville) data that have been processed, and processing and analysis of the 1987 data.

H. CLUTTER MAPPING AND ENVIRONMENT ASSESSMENT

Ground-clutter suppression is a major challenge to the terminal Doppler weather radar. Clutter measurements made by Lincoln Laboratory near major airports indicate that a mean clutter suppression in excess of 56 dB for C-band and 65 dB for S-band (see Mann[8]) is necessary for the TDWR. Figure IV-16 displays a clutter cross section near the Denver test site, expressed in equivalent weather reflectivity units (dBz).

The magnitude of clutter suppression needed is in excess of what is typically achieved from the clutter filter defined in the TDWR specification.[9] Figure IV-17 shows the clutter residue equivalent reflectivity measured with a high-pass filter characterized by a stop-band width of 1 m/s and attenuation of over 50 dB. The clutter has been suppressed to a great extent. However, the residual clutter still poses a problem to wind-shear detection. Figure IV-18 displays a sector of weather data recorded with a high-pass filter and processed with an experimental version of the gust-front algorithm. There are three events of interest. There is a gust front near the lower-right-hand corner labeled GF. There are several thunderstorm signatures labeled TRW. Finally, there is a gust-front false alarm labeled FA which was caused by clutter. The true gust front was not detected at this time due to its radial orientation and lack of radial shear.

Clutter returns can trigger wind-shear alarms by creating an apparent wind shear. The anomalous zero-velocity value due to clutter in an otherwise uniform wind field may be interpreted as a convergence or divergence depending on the location and wind direction. In the case of Figure IV-18, the clutter residue zero velocity was interpreted as a convergent gust front. A clutter residue map editor can reduce the number of false wind-shear detections by removing clutter residue, thus eliminating an apparent wind shear.

The clutter residue editor uses a polar map of post-filtered clutter as a spatial threshold for weather data. The map is constructed on a clear day when there is no visible weather. A mean

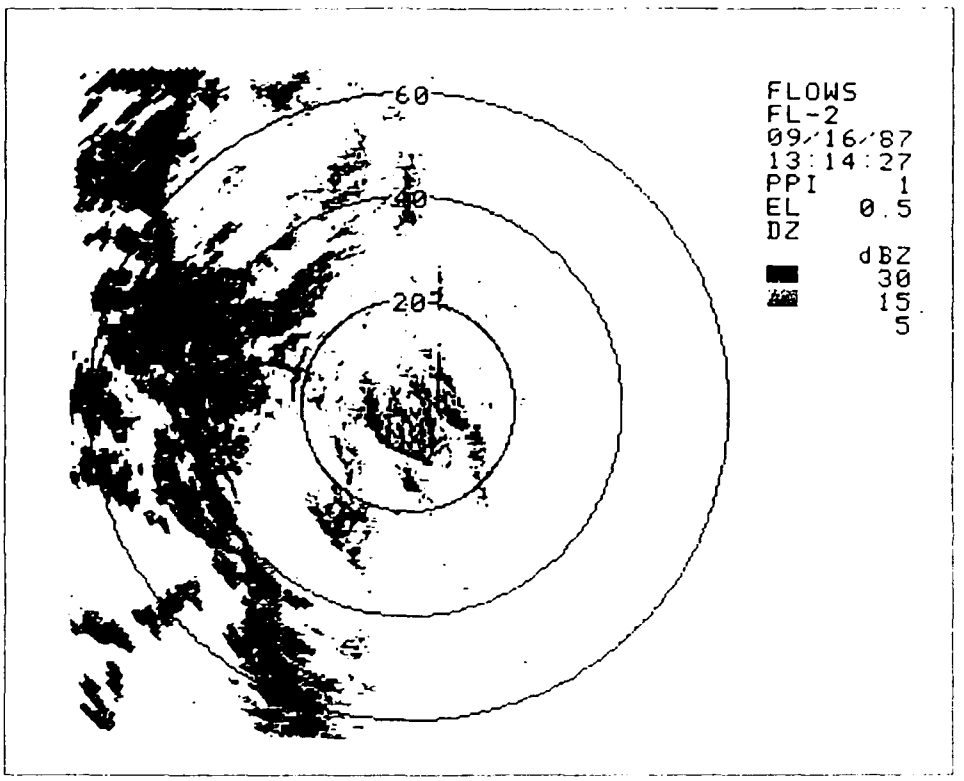

109733-31

Figure IV-16. Clutter cross section near the Denver test site.

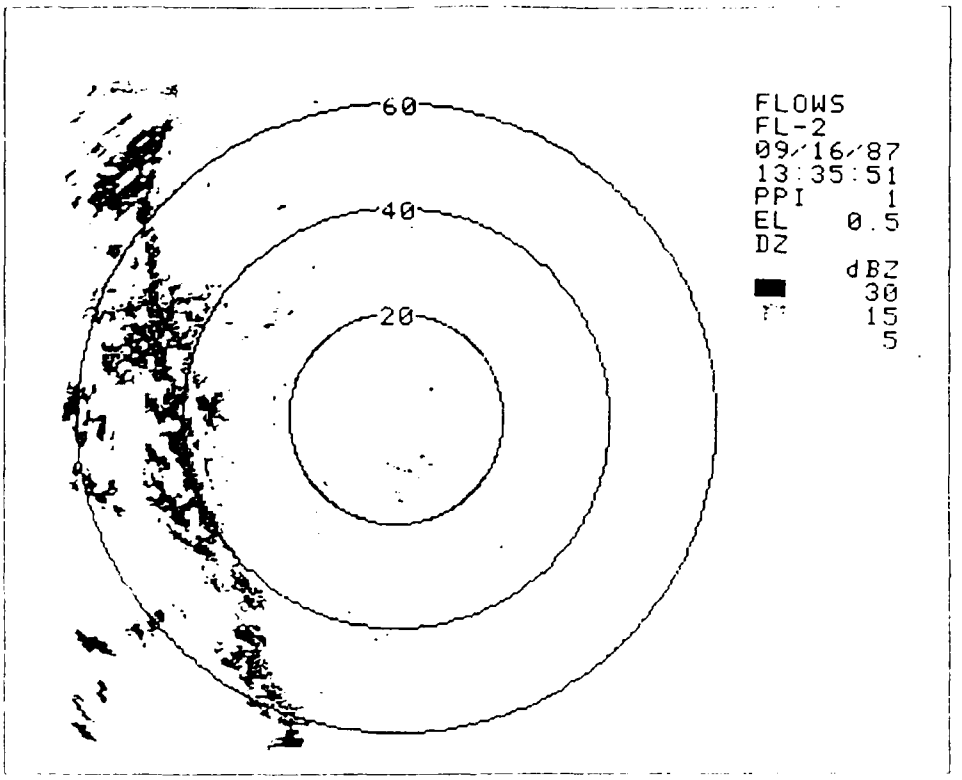

109733-32

Figure IV-17. Clutter reflectivity near the Denver test site measured with a high-pass filter with a stop-band width of 1 m/s and attenuation of 50+ dB.

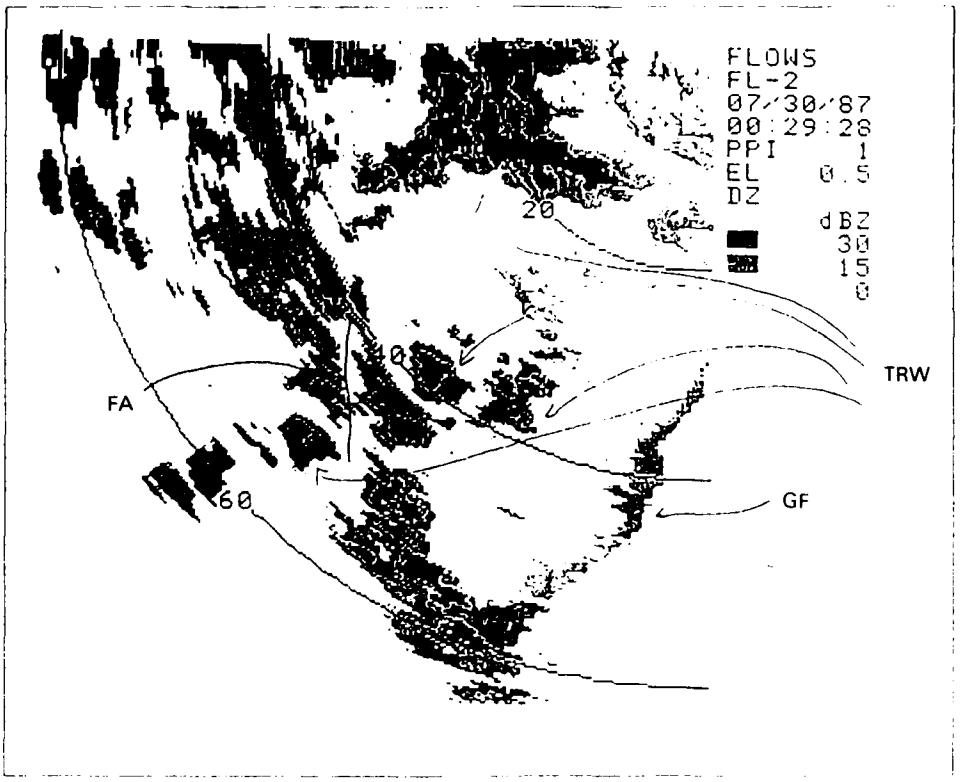

109733-33

Figure IV-18. Sector of weather data recorded with a high-pass filter and processed with an experimental version of the gust-front algorithm.

estimate of the clutter residue is made for each individual range and azimuth cell. Figure IV-19 shows a mean clutter residue of the Denver area. New weather measurements are compared with the corresponding map cell during operations. If the magnitude of the measured value is less than the map value, it is flagged as invalid.

The effects of a clutter residue map editor can be viewed in Figure IV-20. These data are the result of editing the data in Figure IV-18 with the clutter map in Figure IV-19 and reprocessing them with the same gust-front algorithm. The false alarm was eliminated without affecting the true gust front or the thunderstorm signals. A more complete discussion of the clutter residue map editing algorithm is presented in Reference 8.

The complete clutter residue mapping algorithm was defined and implemented as three separate algorithms: the clear-air estimation, map generation, and map utilization. The clear-air estimation algorithm computes an estimate of the clear-air reflectivity. That value is used as a data threshold when constructing a clutter residue map. The intent is to exclude the clear-air measurements from the clutter residue data set. If the measurements were included in the maps, the clutter cross-section estimate would be biased. Furthermore, that would lead to the deletion

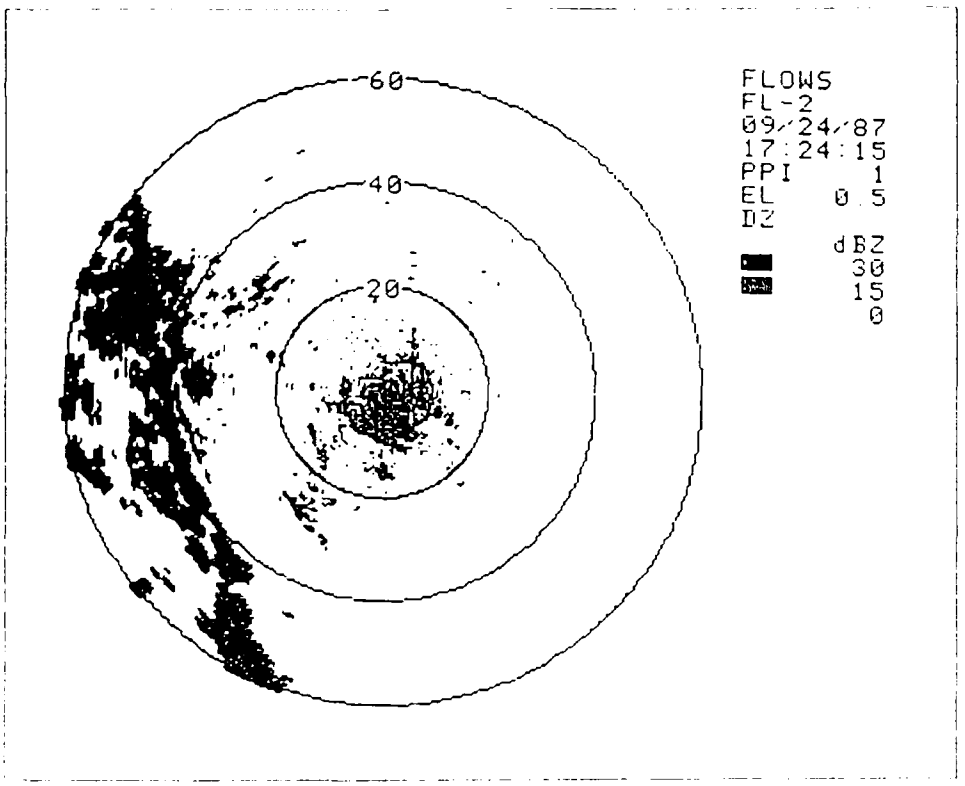

109733-34

Figure IV-19. Mean clutter residue map of the Denver area.

of the useful wind tracers from weather data. The generation algorithm applies the map to the weather data.

A great deal of work has gone into the development of these algorithms. The initial implementations are designed for off-line use. The clear-air reflectivity estimator, as well as the generation algorithm, is interactive and runs on the Sun computer network. The utilization algorithm has been implemented on both the Sun and the Concurrent systems. The utilization program is designed for batch operation and is based on the CFT data format. Many analysis programs have been created to support the development effort and to aid in analyzing the results.

While great strides have been made in developing the algorithms, much work remains to be done. First, the performance of the algorithm needs to be quantified. The results from editing weather data that have been obtained so far have shown that the algorithm is effective at reducing gust-front false alarms such as occurred in Figure IV-18. The next step is to develop a method of scoring the performance of such a system. An initial measure of performance will be assessing the extent the temporal variation in clutter magnitude allows the clutter to pass through the editor without being flagged as invalid.

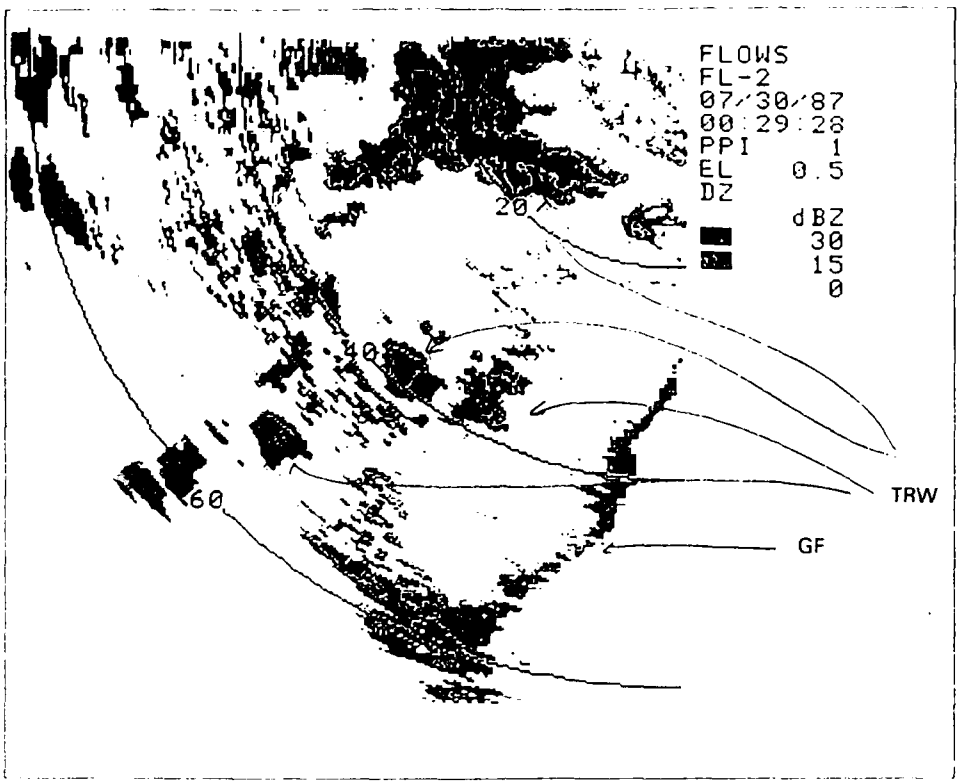

109733-36

Figure IV-20. Result of editing Figure IV-18 with the clutter map in Figure IV-19.

Considerable effort has also gone into the better control of equipment factors which can create apparent clutter residue variations. Analysis of clutter residue variations for the 1986 measurements in Huntsville showed that cells with very high-level clutter would occasionally have extremely large variations in residue level. These variations were found to arise from improper limiting in the IF and A/D converters.

When the clutter level exceeds the system linear dynamic range, the clutter residue map and the measurement to be edited can also create large apparent variations in the clutter residue levels. For example, we find that variations of as little as 0.1 beamwidth in elevation angle can produce clutter residue changes as large as 6 dB. Figure IV-20 compares the clutter residue in the vicinity of Denver's Stapleton International Airport using a clutter filter which provides 50-dB suppression for stationary (fixed) targets. We see that the clutter residue for buildings near the airport increases some 20 dB as the elevation angle decreases from 0.3° to 0.1°.

Similar variations in clutter residue level as a function occur when the coherent processing interval (CPI) angle boundaries for the clutter residue measurements do not coincide with the corresponding angle boundaries for the measurements to be edited. The test-bed measurements made from 1985 to 1987 did not align the CPIs to angle boundaries, so it was necessary to have

a clutter residue map with an azimuth angular resolution of approximately 0.1 beamwidth. This, in turn, requires a tenfold increase in measurements to create the clutter residue map and in real-time memory required to hold the map over that for fixed CPI angle boundaries. Consequently, the test-bed processing system has been modified to have the angle CPI integration always lie between fixed angle boundaries (i.e., the integration period is now inversely proportional to the angular velocity).

Second, there are several site adaptable parameters specified in the algorithm which need to be optimized. In particular, the factor Xcr is used to increase the magnitude of the clutter residue map values. This factor decreases the number of times that the temporal variation in clutter magnitude allows the clutter to pass through the editor. Both factors are dependent on the time statistics of the residual clutter. Studies of the temporal variation of the clutter residue will aid in the selection of optimal parameters. Analyses carried out in the context of ASR weather sensing[10] suggest that a value for Xcr of approximately 8 dB will suffice if the principal variation is due to statistical fluctuations.

The implementation of the algorithms needs to be improved. Currently, the programs are designed for off-line use. A real-time version is being designed for real-time use at the test site in the summer of 1988.

Finally, the impact of the clutter residue editing algorithm performance needs to be addressed in greater depth. The results with clutter residue edited data sets will be compared with the corresponding results with unedited data sets to verify the appropriateness of the site adaptation parameters.

I. GUST-FRONT DETECTION ALGORITHM DEVELOPMENT

The purpose of the gust-front detection algorithm effort is to produce an automatic procedure for recognizing low-altitude convergence (produced primarily by thunderstorm gust fronts) and estimating the associated wind shift using Doppler weather radar measurements. To this end, the focus of the work over this reporting period has been the modification and enhancement of the original gust-front algorithm developed at the National Severe Storms Laboratory (NSSL) by Uyeda and Zrnic',[11] the development of ground truth for data sets against which the algorithm performance would be assessed, and the preparation of software for an Operational Test and Evaluation (OT&E) to take place during the summer of 1988.

The original gust-front algorithm was tested on four data sets (8, 9 November, 9 December 1986, and 28 February 1987) collected in Huntsville during the 1986 COHMEX program. Preliminary results were poor, so significant effort was directed toward improving the algorithm performance in anticipation of an experiment in Denver during the summer of 1987. Various algorithm thresholds were lowered to increase the detection rate for weaker gust fronts. At the same time, the scanning strategy was modified to reduce the false-alarm rate.

Two full 360° tilts were collected (0.5° and 1.0° in elevation). A convergent line had to be detected in approximately the same location on both tilts for a valid gust front to be identified.

In many cases, the convergent line was fragmented due to noise and other data problems. This problem was resolved by implementing a segment joining algorithm which connected fragmented shear features (on the same tilt), based on endpoint proximity and line orientation.

The gust-front algorithm was also restructured to improve modularity and processing speed in preparation for a much-improved, real-time system in Denver. The initial tracking and prediction portion of the algorithm was based upon the concept of centroid tracking. Since the centroid position associated with a gust front was quite unstable from one detection to the next, the tracking results were also unstable. For this reason, the tracking code was modified to use an orthogonal projection from the last centroid position to the current position when computing future positions.

The wind-shift algorithm was added to the gust-front algorithm for testing in Denver. The algorithm was a modified version of the NEXRAD Sectorized Uniform Wind algorithm developed at NSSL, and was used to estimate the wind shift associated with the passage of a convergent line.

As illustrated in Figure IV-21, the algorithm attempted to identify gust fronts by first locating areas of radial convergence (radial shear segments) from the base velocity data (polar coordinates). Segments which exhibited a large value of peak shear and which were spatially close were

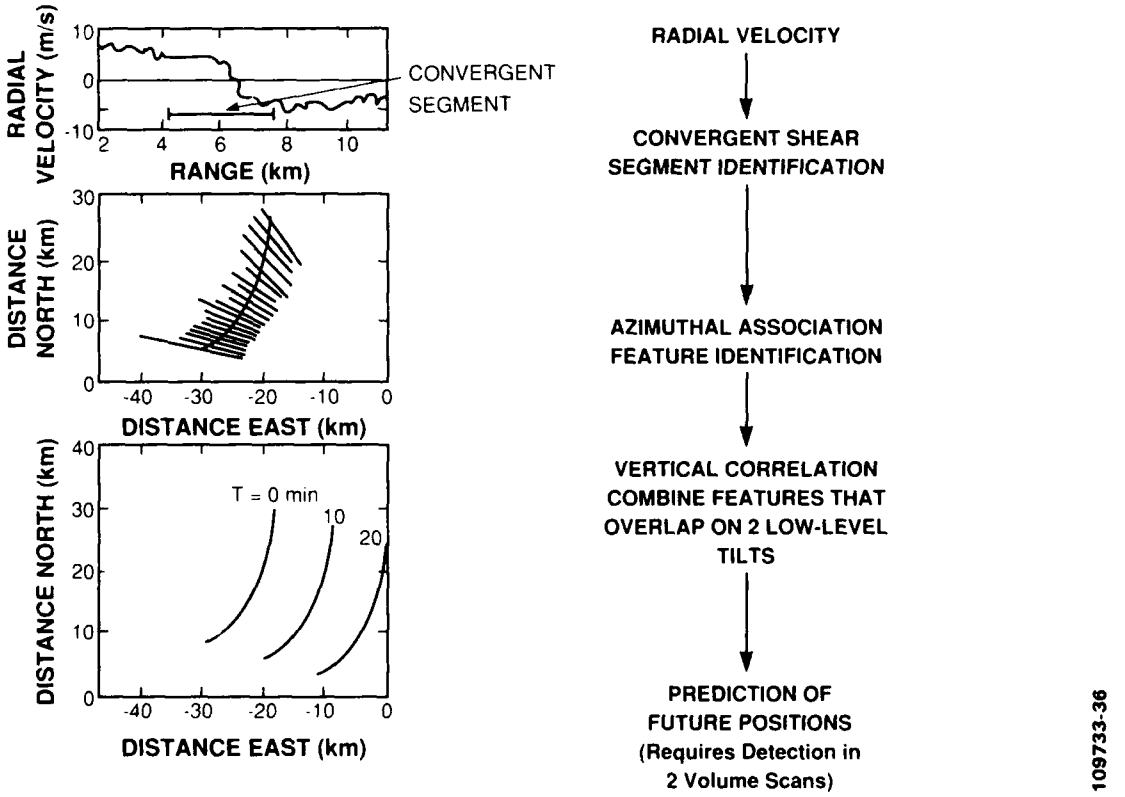

Figure IV-21. Gust-front detection algorithm.

combined into *shear features*. Features found on different tilts (0.5° and 1.0° in elevation) and which exhibited reasonable overlap were combined into a gust front. The feature containing the largest number of radial shear segments was used to represent the gust front. The gust front was then approximated with a least-squares curve fitted to the peak shear values associated with the radial segments (Cartesian coordinates). After a gust front was located in at least two consecutive volume scans, future locations of the gust front were predicted.

A considerable effort was directed toward the preparation of the updated version of the NEXRAD PDL for the gust-front algorithm, which was mailed to the FAA in June 1987. The PDL corresponds to the version of the algorithm that was implemented in Denver on 1 June 1987.

The gust-front algorithm was run in real time during the 1987 Denver experiment, and a performance assessment was conducted. Five data sets were used to generate probability of detection (POD) and probability of false alarm (PFA) statistics. POD was defined as the number of detections divided by the total number of gust fronts (detected + missed). PFA was the number of false detections divided by the total number of detections (true + false). These statistics were gathered on a tilt-by-tilt basis. The gust fronts were classified as weak (ΔV less than 10 m/s), moderate (ΔV between 10 and 15 m/s), strong (ΔV between 15 and 25 m/s), or severe (ΔV greater than 25 m/s). A detection was considered successful if any part of the gust front was found. However, fragmented and partial detections were noted. Scoring was performed on gust-front detection only, not on prediction and wind shift. The POD for strong, moderate, and weak gust fronts was 73, 54, and 30 percent, respectively. The PFA for the five days was 44 percent.

This analysis and the real-time evaluations by NCAR personnel both concluded that there were significant problems with the gust-front algorithm tested in 1987. These included the intermittent detection of a gust front, partial and/or fragmented detections, the strong dependence upon the 1.0° tilt for detection, kinks in the fitted curve, unrealistically high wind-shift estimates, and the inability of the algorithm to detect radially oriented gust fronts. The high PFA was due primarily to ground clutter.

A group was set up to coordinate efforts of Lincoln Laboratory, NSSL, and NCAR to improve, test, and verify the gust-front algorithm to be used in the 1988 OT&E. The effort focused on improving the detection of moderate and stronger gust fronts and on reducing false alarms. (Improved detection of weak gust fronts was a goal of the Gust Front Group that would not be met in time for the 1988 OT&E.) In general terms, Lincoln coordinated the gust-front algorithm effort.

Five cases (28, 29 July; 28 August; 2, 4 September 1987) containing gust fronts that were not well detected by the 1987 algorithm were supplied to NSSL for analysis. In order to maintain consistency, the version of the algorithm that ran in the test bed in 1987 was implemented at NSSL. Lincoln analyzed data (mesonet, UND radar, dual Doppler) to determine the true wind

shift. The results of these analyses were supplied to NSSL to verify the wind-shift algorithm. Lincoln also established a database of twelve cases (10, 14, 18 June; 27, 30, 31 July; and 25 August 1987) to be used for algorithm verification and for POD and PFA statistics.

The work at NSSL focused on improving the detection capabilities and reducing the PFA of the algorithm. Different thresholds for the 0.5° and 1.0° tilts were instituted. Kinks in the fitted curve were smoothed by using a higher-order polynomial to fit the data. Unrealistic wind-shift estimates were caused primarily by improperly de-aliased Doppler velocities, so a new velocity de-aliasing algorithm was implemented and error reduction was employed. A technique for estimating the wind shift for gust fronts whose azimuthal extent did not exceed that required by the wind-shift algorithm was developed. Clutter suppression windows were introduced as an option for reducing clutter-induced false alarms. The 1988 gust-front algorithm was received at Lincoln and implementation begun. A revised PDL was submitted on 31 January 1988.

By consensus between Lincoln, NSSL, and NCAR, the following set of ground-truth rules was developed and applied to the twelve data sets.

(1) To be entered into the truth files, a gust front had to be at least 10 km long.

(2) Two gust-front outlines were entered into the truth files. The first outline consisted of points along the entire length of the gust front, as determined from convergence, azimuthal shear, and/or the presence of a reflectivity thin line. The second outline consisted of the convergent portion of the gust front.

(3) In order for a portion of the gust front to be considered convergent, radial convergence of at least 5 m/s within 5 km of (i.e., perpendicular to) the gust front had to exist over a length of 10 km (along the gust front). If the criteria were not met, the gust front was said to contain no convergent part.

(4) The ΔV of the gust front was determined subjectively as the average peak change in Doppler velocity perpendicular to and along the convergent portion of the gust front.

(5) Truth for the wind-shift algorithm and wind-shear estimates were compiled from mesonet data. Those stations that fell along and behind the front were recorded in the truth file, and the wind data for these stations were processed.

These rules will be applied to real-time truthing during the 1988 OT&E.

Software was developed for generating ground truth in real time and will be used during the 1988 OT&E. An output file is created that contains the tilt date and time, location of the gust fronts, gust-front strength, and (where appropriate) identifiers for mesonet stations behind the gust front. The file is then processed to create two files; one is compatible with the object database, and the other is used to generate ground truth (for the wind-shift estimate) from mesonet data via the program WINDAVG.

Scoring criteria were outlined whereby a detection would be compared with ground truth and the determination of a valid detection would be based upon the length of the true detection.

Similarly, the predicted location would be compared with the truth at the time for which the prediction was valid. If the gust front dissipated by the time of the prediction, a false alarm would be declared. The wind-shift algorithm would be scored against mesonet or dual-Doppler data. The exact details of the scoring method are to be determined. Software to aid the scoring process was developed on the Sun computer. The utility (score_tool) reads the ground truth and algorithm output from an object database and produces plots.

A format was specified and software written that prepares the algorithm real-time output for archiving and ethernet transfer. The new format was similar to the feature exchange format generated by the microburst feature extraction Suns. Integration into the gust-front algorithm was begun.

A great deal of progress was made during this reporting period, but much remains to be done. Implementation and debugging of the algorithm and transport to the Denver site will continue. The algorithm will be run on the twelve cases, the results scored, and reports written. The scoring and real-time truthing software will be finalized. Improvements to the gust-front algorithm will be made and tested in an off-line version throughout the OT&E.

A second focus of the gust-front detection effort has been the development of an advanced gust-front algorithm. The advanced gust-front algorithm consists of an AI-based, expert system which is used to integrate multiple low-level pattern-recognition algorithms. These include algorithms for recognizing convergent shear, azimuthal shear, and reflectivity thin lines. The base gust-front algorithm relies on recognizing only convergent shear and, thus, is vulnerable to situations where a gust front exhibits little convergence.

Gust-front cases from the Denver area often exhibit prominent reflectivity thin lines, so the advanced algorithm should do quite well on these cases. The advanced algorithm is now being run on the same 1987 Denver test case against which the upgraded base algorithm is being tested. Software has been developed that allows results from the advanced algorithm to be scored against ground truth in exactly the same manner as the base gust-front algorithm. That will allow us to determine the improvement in performance provided by the various enhancements in the advanced algorithm.

J. RANGE OBSCURATION AVOIDANCE

One of the major factors leading to the degradation of the quality of Doppler radar weather data is range obscuration by *distant* storms. The storms are located beyond the range interval being sampled by the radar, yet the radar echoes from them are of sufficient strength to ambiguously fold within the range interval of interest. These range aliased echoes could trigger false detections by the algorithms and cause actual hazardous situations near the airport to remain undetected.

By carefully selecting the pulse repetition frequency (PRF) of the radar, range obscuration from distant storms can be minimized over specified airport regions. One of the goals for FL-2 operation at Denver during the summer of 1987 was to be able to automatically and adaptively

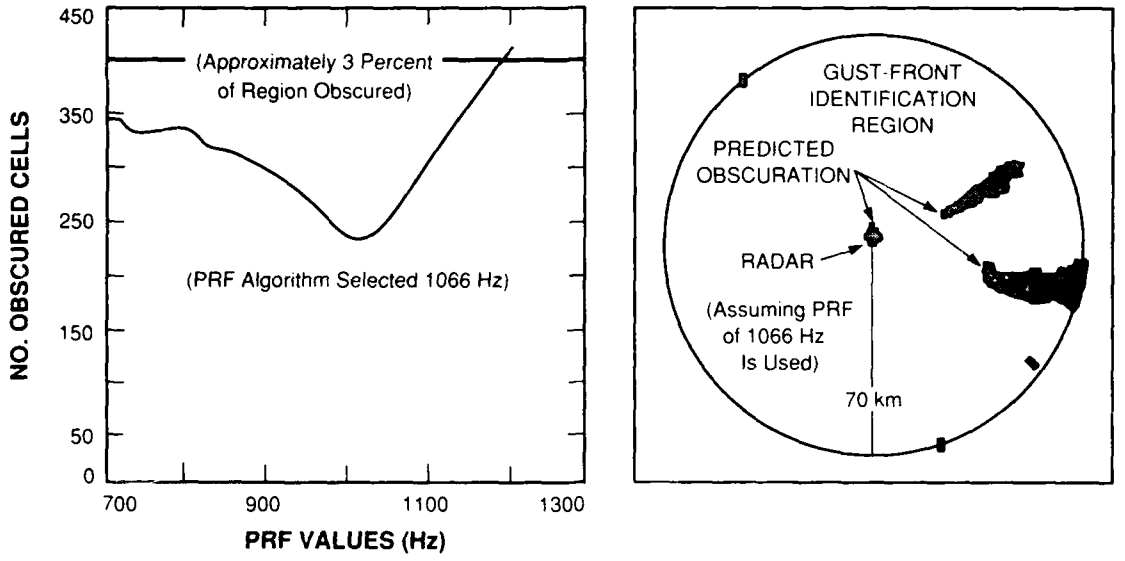

(a) Obscuration Assessment (b) Obscuration Map

Figure IV-22. Selection of PRF for gust-front region for 13 June 1987 at 0107 UT.

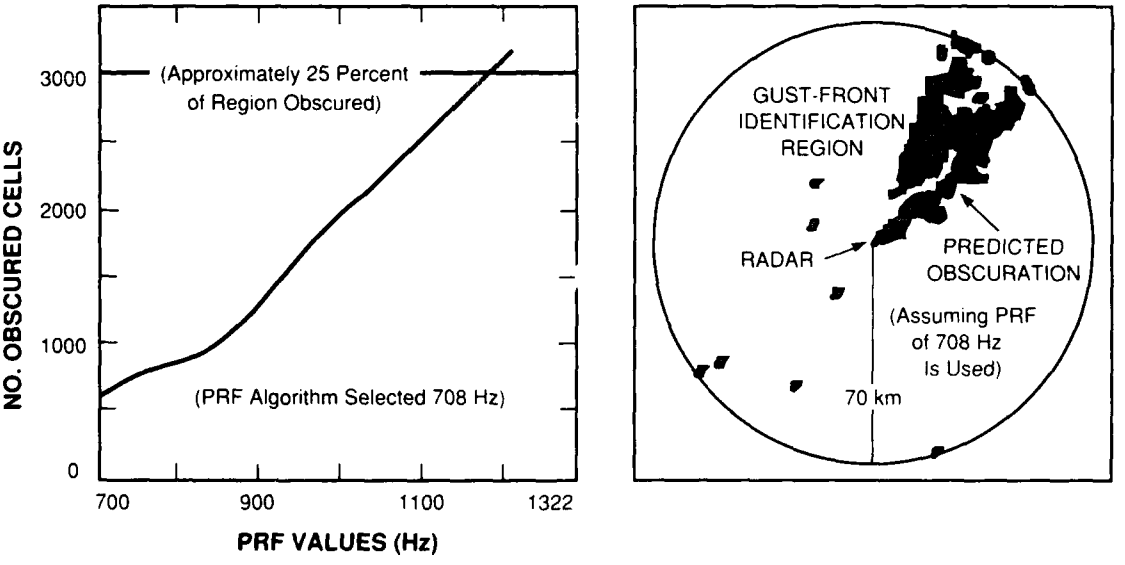

(a) Obscuration Assessment (b) Obscuration Map

Figure IV-23. Selection of PRF for gust-front region for 3 July 1987 at 0118 UT.

select the PRF of the radar. The PRF selection strategy was to be based on minimizing range obscuration over the airport region due to n^{th}-time-around returns from distant weather. *The design of this technique began in January of 1987, and a preliminary design review ws conducted on 12 February 1987. Coding and subsequent testing of the technique commenced in March 1987.*

Four basic steps are associated with the design of the PRF selection technique. These steps involve: first, the identification of the distant weather; second, the assessment of obscuration which will be attributed to this distant weather as a function of PRF value; third, the selection of the PRF value which will minimize obscuration; and fourth, the generation of an obscuration map.

Following the coding of this technique, the algorithm was initially tested on a specially requested data set from Huntsville. (These data were collected before the FL-2 system was dismantled at the Huntsville site.) The results appeared promising, and the algorithm was prepared for real-time implementation at the FL-2 Denver site. Implementation of the algorithm into the FL-2 real-time processing system, during the week of 8 June 1987, went smoothly. The algorithm was found to comfortably keep up with the real-time data stream, and no contentions over system resources were seen to exist between the PRF algorithm and the various real-time meteorological algorithms.

The algorithm entered a two-month shakedown phase, during which time the PRFs which were being selected in real time by the algorithm were carefully scrutinized by the site personnel. (Site personnel continued to be responsible for manual PRF selection.) In addition to the site scrutiny, off-line analysis of the PRF output was being conducted in the Lexington processing environment. Several minor anomalies were discovered and subsequently corrected during this time, and a new scan was devised and implemented to better support PRF selection. By the end of July, the scan strategy and PRF algorithm were declared to be ready for automatic, real-time PRF choice, which meant that the PRFs selected by the algorithm were automatically used on subsequent tilts.

Two examples of obscuration assessment as a function of PRF value, and two subsequently generated obscuration maps, are illustrated below using data gathered during the 1987 summer exercises at Denver. The first example (Figure IV-22) uses data from 13 June 1987, and illustrates obscuration assessment for a situation where several distant storms are located approximately 220 km from the radar. As seen in Figure IV-22(a), obscuration is minimized (to within ϵ) when a PRF of 1066 Hz is selected. The obscuration map generated for this situation is illustrated in Figure IV-22(b). Data from 3 July 1987 are used to illustrate the second example. For this situation, distant weather began approximately 120 km from the radar and covered a tremendously large region out to nearly 250 km from the radar. The obscuration assessment for this situation appears as Figure IV-23(a), and the obscuration map follows as Figure IV-23(b).

The distant weather surveillance scan was initially conducted at an elevation of 0.6°, yet information from this scan alone was found to be insufficient for PRF selection at higher elevations. Storm characteristics change with altitude, but more specifically for the Denver environment; blockage due to the Rocky Mountains affected the algorithm's understanding of the prevailing distant weather. It was therefore recommended to vary the elevation placement of the low-PRF scan, from 0.6° to 1.2° and then back again, thus enabling a more complete set of information to be gathered. Every 5 min a distant weather surveillance scan is conducted. Beginning in August, the elevations of this scan varied between 0.6° and 1.2°. Each elevation is thus revisited every 10 min. (Initial studies of the evolution of distant storms in the Denver area indicate that this revisit time is acceptable.)

The basic functions of the PRF algorithm were felt to be fully verified by August, and attention turned to becoming more selective in the obscuration avoidance issue. Rather than merely minimize obscuration over a region in general, obscuration avoidance over specific areas (i.e., the Stapleton runways) was implemented. An example to illustrate this modification is presented as Figure IV-24, using FL-2 data from 4 September 1987.

Recent efforts associated with the PRF algorithm have focused on implementing a capability to provide real-time graphic output of various diagnostic profiles which are generated by the PRF algorithm. The profiles are similar to those routinely generated and used during off-line development and analysis efforts. This display capability will be an optional feature which will be enabled/disabled by the FL-2 operators using previously established message-passing protocol. This feature is to be a part of the FL-2 operational demonstration planned for July and August 1988.

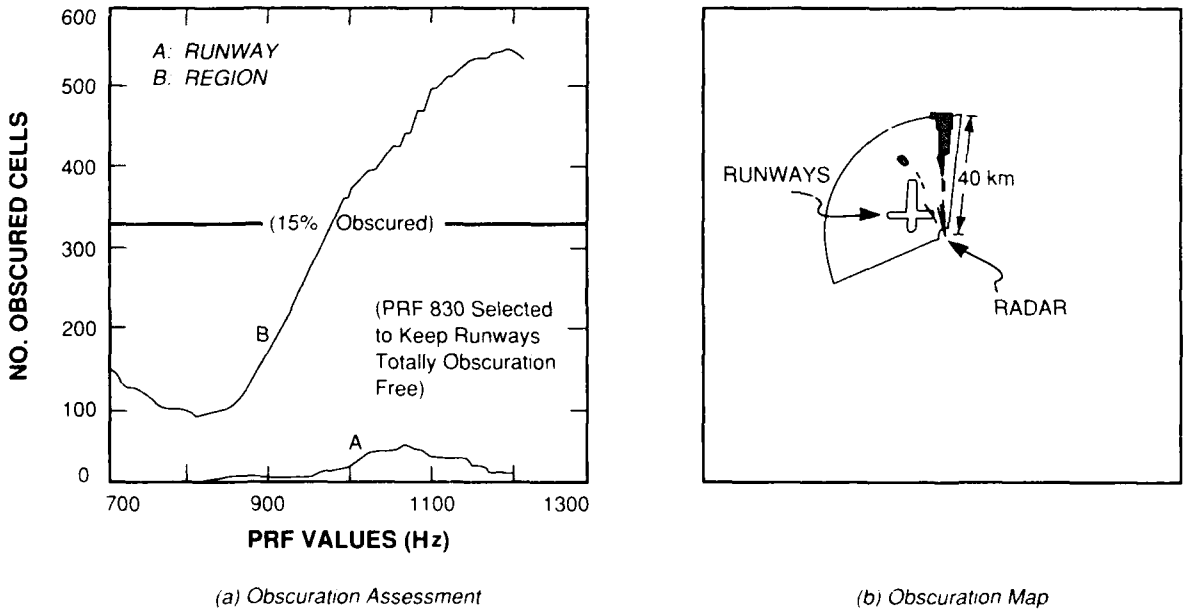

(a) Obscuration Assessment

(b) Obscuration Map

Figure IV-24. Selection of PRF for microburst region for 4 September 1987 at 2021 UT.

Formal documentation on the adaptive PRF selection technique began in June 1987. Additional analysis and a complete set of examples of the performance of the technique on varied weather situations were subsequently added. This documentation, in the form of a Lincoln Laboratory Project Report,[12] has completed all formal review and is awaiting publication.

Initial indications are that adaptive, automated PRF selection works well in the S-band environment at the FL-2 radar. The eventual goal, however, is for this technique to work within a C-band system, i.e., the Terminal Doppler Weather Radar (TDWR) system. The effectiveness of the technique at C-band can be loosely assessed by analysis of the Denver data, under the assumption that a higher set of PRF values is to be used. This can be done off-line in the Lexington processing environment, and is being planned for the next reporting period.

Pseudorandom phase modulation is yet another technique being investigated for its effectiveness in mitigating the effects of range obscuration.[13] This technique has been implemented in hardware at the FL-2 site by W. Drury. A test of the technique using a known out-of-trip source, the Cheyenne Ridge, was conducted on 25 June 1987. The results of this test indicate that the implemented hardware does indeed produce the expected results; i.e., the spectrum of the out-of-trip source becomes *whitened.* This is illustrated in Figure IV-25. Under certain situations, it is anticipated that this may enable valid velocity estimates to be derived from in-trip targets, even in the presence of obscuration by out-of-trip targets. Additional tests are planned for the coming reporting period in order to determine the effectiveness of this approach within a C-band TDWR environment.

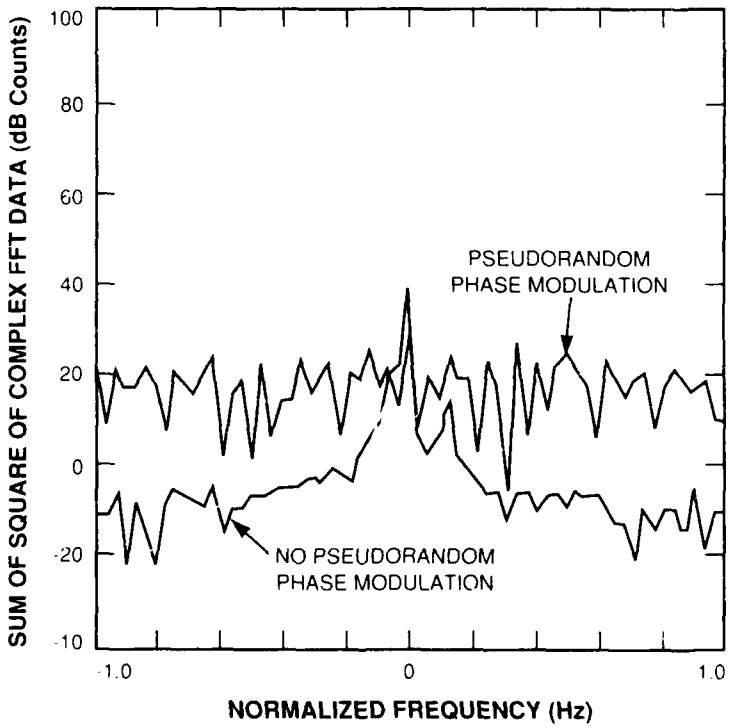

109733-40

Figure IV-25. Range obscuration from Cheyenne Ridge with and without phase modulation.

K. LIGHTNING DATA ANALYSIS*

This investigation is examining possible uses of thundercloud electrical measurements as an adjunct to Doppler radar for detection of hazardous aviation weather conditions. Analysis to date has focused on the temporal relationship between the lightning flash rate and microbursts in a thundercloud, with emphasis on lightning features which may permit accurate predictions of microburst outflows.

Corona current probes on the Lincoln Laboratory mesonet stations in Huntsville were used to measure the surface electric field. Discontinuities in the electric field produced by lightning can be sensed to provide a measurement of the total (cloud-to-ground and intracloud) lightning flash rate. In addition, scientists at NASA/Marshall Space Flight Center operated an array of cloud-to-ground lightning magnetic direction finding sensors. Together, these two sets of measurements define separately the intracloud and cloud-to-ground lightning activity for thunderstorms within 15 km of the center of the ASR-9 mesonet in Huntsville.

Previous investigations had shown that a thundercloud's total lightning flash rate tracks the vertical development of the precipitation echo as measured by radar (and, by inference, the updraft intensity). In contrast, microburst outflows correlate with the descent of precipitation cores and are typically most intense during the late-mature or dissipating stage of a thunderstorm. Thus, it was reasonable to speculate that a temporal history of a thunderstorm's light flash rate might be used to forecast microbursts, or at least confirm a radar's direct detection of the surface outflow. The Huntsville experiment provided the first opportunity for a direct comparison between lightning activity and radar measurements of microbursts.

Data from thirteen 1987 summer thunderstorms were examined, with the following results.

(1) In two cases, the time of maximum total lightning activity preceded the beginning of a microburst outflow as measured by radar.

(2) In seven cases, the time of maximum total lightning activity occurred after the outflow commenced, but well in advance of the peak microburst winds.

(3) Two electrically active storms did not produce microbursts. These, however, were organized squall-line storms which do not characteristically result in small-scale outflows.

(4) Two storms with microbursts did not produce lightning.

There were no cases where the peak lightning activity occurred after the most intense phase of the microburst. Thus, in three-quarters of these thunderstorms, a well-defined maximum in the lightning flash rate preceded the time of peak microburst intensity by an interval of 5 to 10 min.

---

* The FY87 work was performed by Lincoln Laboratory under support of the USAF. The results are reported here because the lightning work is supported by the FAA in FY88.

Future work will be directed toward incorporation of this temporal relationship into an integrated lightning/radar automatic microburst recognition algorithm. The lightning data would have the following potential uses:

(1) Adjusting thresholds for the radar-based detection algorithm,

(2) Generation of a forecast for future intensification or weakening of an outflow.

We also desire to install corona probes on some of the Denver mesonet stations to extend this analysis to the dry microburst environment.

L. STORM TRACKING AND EXTRAPOLATION

1. Introduction

Our interest in meteorological trackers lies in the development of a storm-tracking tool that will function as a planning aid for air traffic control. Our interest in *correlation* trackers was stimulated by the need for a tracking and prediction methodology that would perform well in *extended storm situations*, complementing the performance of centroid trackers which, being *object* oriented, have been shown to perform erratically in such situations.

The typical correlation tracker is founded on methods developed for the processing of arbitrary digital images, and is therefore *weather independent*. In the meteorological setting, a sampled (time-1) two-dimensional reflectivity field is subdivided into smaller, nonoverlapping, equally sized regions (*correlation boxes*) that are correlated independently with a time-2 field to obtain uniformly spaced sample estimates of a *horizontal wind field*. The horizontal wind field is then used to obtain short-term ($\leqslant$30 min) predictions from the time-2 field by extrapolation.

The MIT Lincoln Laboratory (LL) tracking algorithm CARCOR is an example of this type of tracker and, combined with the storm extrapolation map (SEM) algorithm, represents the current state of our tracking and prediction (TP) project.

Our efforts can be organized into four categories. First, we are continually seeking refinement of the tracking algorithm. As an example, we note that modifications making the algorithm more robust with respect to weather pattern/storm type would obviate the need for complementary trackers. Second, input/output product definition and real-time implementation issues are being investigated. The proper format for presentation of the algorithm's output is a primary concern. Third, we are involved in the acquisition and processing of real weather data, and the evaluation of algorithm performance. Finally, the effects of growth and decay are considered separately since an algorithm that could account for their influence would represent a major advancement. In the context of NEXRAD, there is a wealth of weather product data available; hence, our efforts are directed at using available *side information* for improving the TP algorithms.

The description of our achievements and goals is organized into six-month segments which are presented sequentially.

2. October 1986 — March 1987

a. Algorithm Refinements

Motivation for an Object-Oriented Correlator:— The correlation-box size is an algorithm parameter that critically influences performance. It determines the resolution of the wind-field estimate, but is (functionally) bounded from below by *object sizes* within the image and, ultimately, by image quantization. It is important to note that there is a trade-off between resolution of the wind-field estimate and robust generation of *valid* velocity samples. The selection of an optimal correlation-box size is, therefore, an *ad hoc* choice requiring knowledge of the weather-map content.

An alternative solution, which avoids the need for correlation boxes, combines an object-oriented approach with the correlation method: it first defines objects in the map and then estimates samples of the horizontal wind field by correlating and tracking the motion of those objects between two time frames. The design of a tracker based on the correlation and tracking of objects, defined by *groups* of above-threshold pixels (*storms*), was begun during this period. This added sophistication over CARCOR/SEM does not increase computational requirements for two reasons. First, the method for grouping pixels into storms is precisely that which is used by SEM for storm extrapolation. Second, all correlations are done with binary maps (e.g., thresholded layer reflectivity fields). Preliminary results indicate that the performance of the *standard* correlation tracker using binary maps is comparable to its performance using full reflectivity fields.

The Storm Correlation (STORMCOR) Algorithm:— Operation of the algorithm can be divided into three steps. First, time-2 binary weather maps are analyzed for the presence of storms. Second, storms in a time-2 map are correlated spatially with corresponding regions in the time-1 map to identify displacement vectors yielding maximal correlation. Lastly, selected displacement vectors are used to derive velocity estimates, located at the time-2 storm binary centroids, which are taken as samples of the horizontal wind field. As mentioned above, the extrapolation of time-2 storms is accomplished by the SEM algorithm.

A storm is identified as any contiguous group (fulfilling a threshold-in-size criterion) of above-threshold pixels plus the surrounding border of below-threshold pixels. (The contiguity criterion can be relaxed so that groupings are affected less by small regions of *dropouts*.) Each storm in the time-2 map is displaced over a local region (defined by a maximum acceptable storm velocity), and a correlation coefficient with the corresponding time-1 region is computed. That displacement which results in maximum correlation is used to compute a velocity estimate which is identified with the binary centroid of the time-2 storm. If storm extrapolation only makes use of the most recent velocity estimate, then each time-2 storm is translated by means of the velocity estimate that is associated with its center-of-area. This is what is done in the current implementation. Small storms that do not receive velocity estimates, because of threshold constraints, are currently translated using a velocity that is interpolated from the nearest estimated velocities.

The coding of this tracking algorithm, for off-line study, was begun during this reporting period. While CARCOR remains our primary tracking algorithm, evaluation of STORMCOR is considered a parallel effort with potential long-term benefits.

b. Data Processing and Algorithm Performance

Data Acquisition for Tracker Evaluation:— Data sets simulating NEXRAD-like scans were acquired from three different geographical regions: Massachusetts, Alabama, and Oklahoma. The entire reporting period was spent obtaining the raw data and developing software that would convert all data tapes to the CFT format used at Lincoln Laboratory. The processing of these data sets provides a preliminary evaluation of both CARCOR and STORMCOR in a NEXRAD setting.

Algorithm Scoring:— The scoring of TP uses two methods of evaluation. Both compare SEM predictions with a *truth* map, and both summarize performance using probability-of-detection (POD) and false-alarm-rate (FAR) statistics. The first method uses a straightforward comparison based on areal overlap. The second method, which was developed and refined during this reporting period, scores a prediction based on its usefulness for determining flight-path interference. Straight-line segments, of varying length, are randomly positioned within the area of coverage and are treated as potential flight paths. Scoring is achieved by using the predicted image to mark a flight path as being either safe or dangerous. We felt that the latter scoring method more accurately describes the effectiveness of the extrapolated map as a planning aid.

3. March — October 1987

a. Algorithm Refinements

Completion of STORMCOR Coding:— The coding of the tracker STORMCOR, for off-line study, was completed during this reporting period. An SEM algorithm, compatible with STORMCOR, was also coded.

b. Acquisition and Processing of Weather Data

Comparative Analysis of CARCOR and STORMCOR:— A preliminary examination of the STORMCOR algorithm was made with four case studies: NSSL (Norman, OK, 13 May 1983), MIT (Cambridge, MA, 5 August 1981), FL-2 (Huntsville, AL, 9 July 1986), and UND (Memphis, TN, 25 June 1985). These four cases span a range of storm sizes from large extensive storm elements (NSSL and MIT) to small compact storm elements (UND). The FL-2 case falls in-between, exhibiting a linear structure but having many small transitory *storm elements* due to extensive splittings and mergers. The performance of STORMCOR, CARCOR, and *persistence* (i.e., no storm extrapolation) was scored for 10-, 20-, and 30-min forecasts. All computations were done using binary maps generated by a 30-dBz threshold. Scoring followed an area criterion or a *strategic flight path* criterion as indicated above and as described in greater detail by Brasunas.[14]

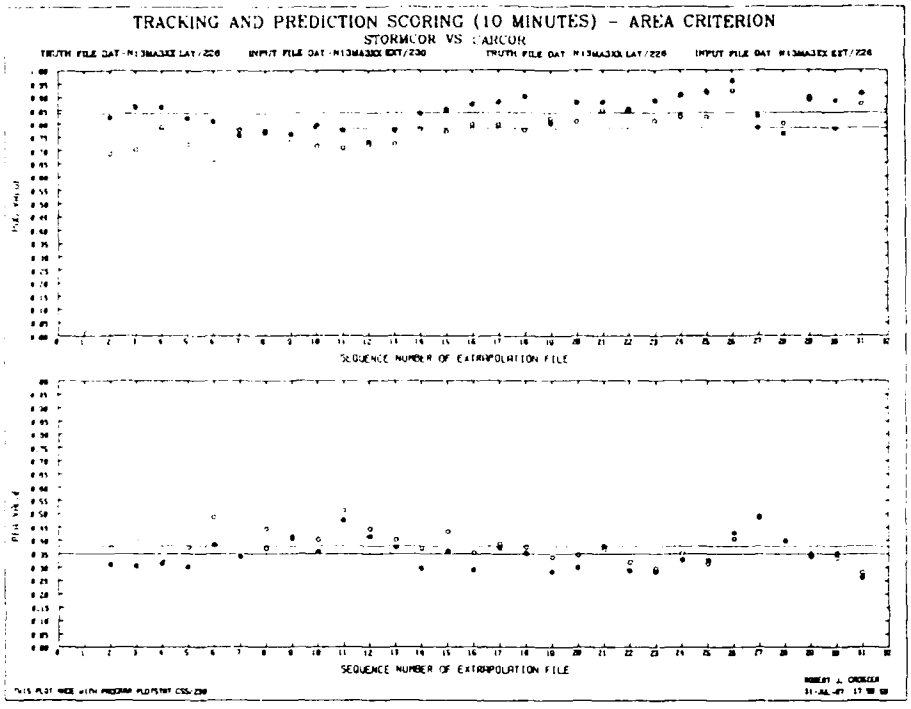

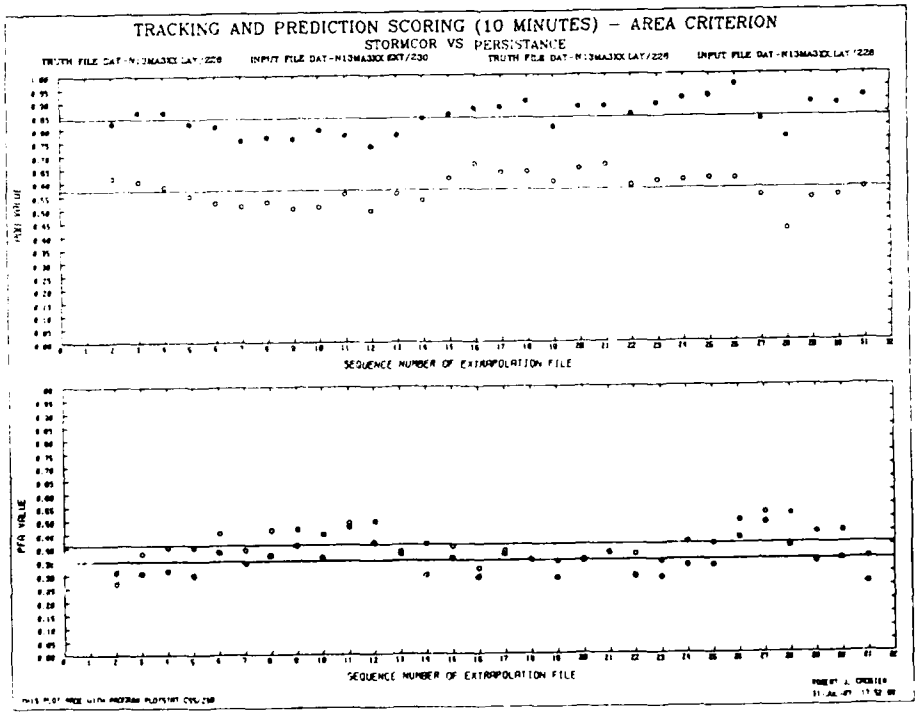

109733-41

Figure IV-26. Tracking and prediction scoring: STORMCOR vs CARCOR and persistence.

An example analysis is presented in Figure IV-26 where 10-min forecast POD and PFA values are computed for a sequence of 32 volume scans (taken at approximately 10-min intervals). Circles indicate individual values (solid circles represent STORMCOR results), and horizontal lines represent average POD and PFA values (POD and PFA, respectively). For this example, there is a clear performance advantage using the STORMCOR algorithm. It should also be noted in Figure IV-26 that fluctuations about POD (respective PFA) of the STORMCOR sequence parallel the behavior of the sequence for persistence. This was characteristic of all the results obtained in this preliminary analysis, and clearly indicates that the variation of POD and PFA values about their respective averages was, in large part, due to factors independent of the tracking method used (growth/decay effects, for example). Since this effect was not accounted for in this preliminary analysis, it should be kept in mind when examining Figure IV-27, which is a summary of the area criterion performance results for all four data sets; this figure is a bar chart plotting average POD and PFA values for all three forecast times and all three forecast methods. Error bars indicate maximum and minimum values obtained for each data set. The STORMCOR algorithm exhibited improved POD and PFA values corresponding to 10-, 20-, and 30-min predictions, as compared with both CARCOR and persistence, for the two data sets containing large-scale weather patterns (NSSL and MIT). The improvement in POD and PFA values was not as marked for the Huntsville data, and may not be significant in the UND case. However, these preliminary results should be interpreted as encouraging, and should lead to continued study. Similar results were also obtained using the *flight-paths* criterion. Comprehensive timing estimates for STORMCOR have not yet been obtained; however, as stated earlier, we do not expect this to have a large impact on any decision to implement STORMCOR.

c. Growth/Decay Effects

During this reporting period, our efforts focused on the development of software for the analysis and incorporation of lightning-strike data into a format compatible with the Cartesian maps used in tracking and prediction. We believe that the resulting composite data sets can be useful in characterizing storm growth/decay. This work was done in anticipation of future availability of such data.

4. October 1987 — March 1988

a. Algorithm Refinements

Terminal Application:— The decision to focus near-term tracking and prediction work on TDWR applications had the following effect on TP algorithm development. The output products from the NEXRAD storm series algorithms, which included a centroid tracker, would no longer be available. Therefore, it was necessary to redefine the SEM algorithm so that it would compute products (i.e., storm centroids) that were previously requested from the storm series algorithms. *In addition, note that the correlation tracker now becomes the sole tracker.*

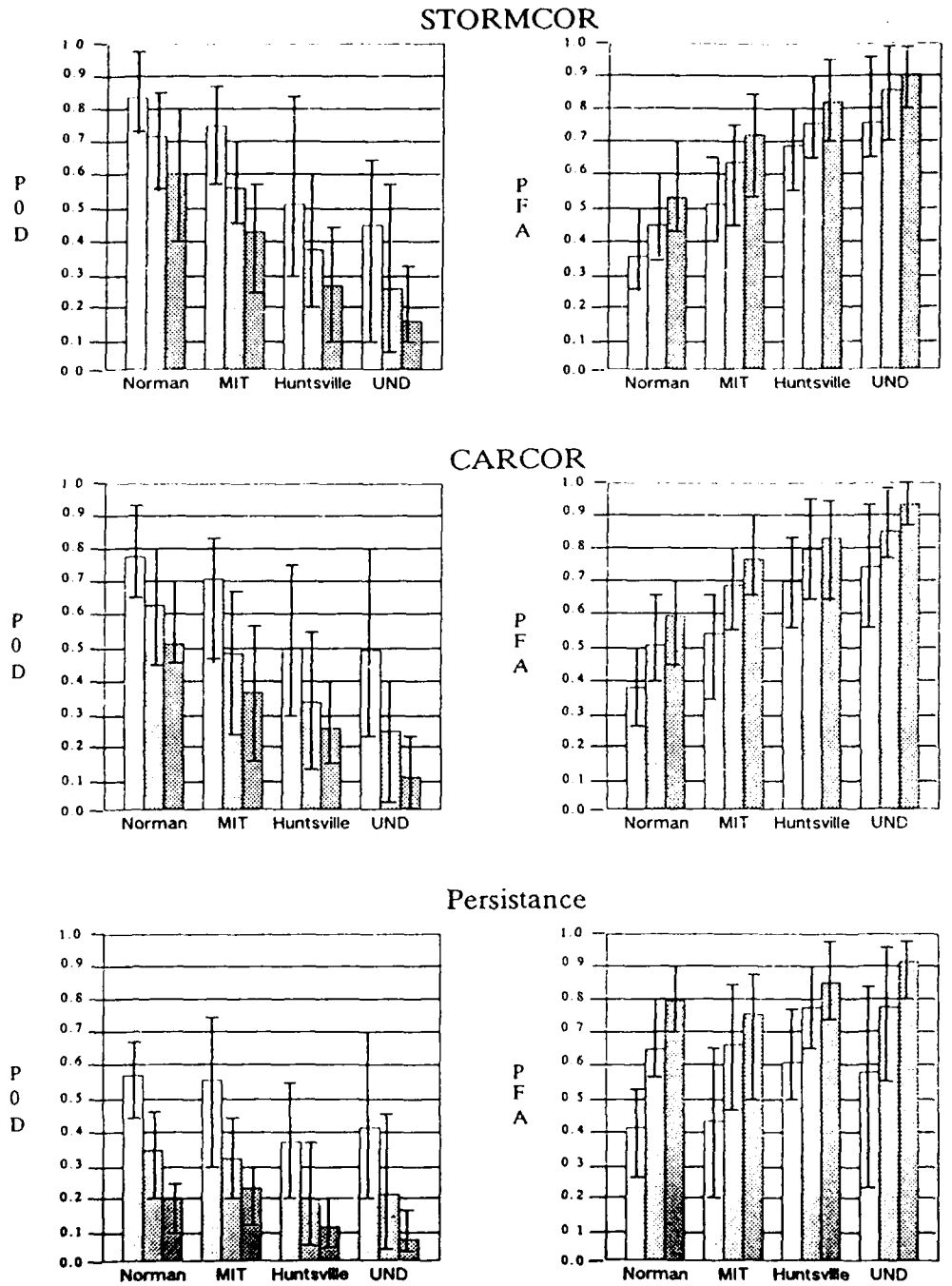

Figure IV-27. POD and PFA scores of STORMCOR, CARCOR, and persistence.

Improving Wind-Field Estimates:— Map extrapolation uses only the most recent *sample* of the wind field. These velocity estimates are not robust in the sense that wind-field estimates can be seen to change abruptly from one volume scan to the next. Errors in their values can significantly affect tracker performance.

A median-like filter for nonscalar quantities was developed as a means to reduce the number of *outlier* velocity estimates in the wind field. Preliminary observations of this manipulation were encouraging, and its evaluation will be included in the TDWR tracker performance evaluation (described below).

b. I/O Product Definition and Real-Time Implementation

Input Product Definition:— The TP algorithms were originally intended to operate on Cartesian maps of layered reflectivity products. Most of our evaluations are based on this assumption. However, the algorithms are flexible enough to work using any Cartesian map product.

The current design for the terminal application radar does not provide a layered reflectivity product. Therefore, we are examining the performance of the TP algorithms using the precipitation product (a single-tilt, Cartesian-coordinate sampling scaled to the National Weather Service precipitation levels) as input.

The terminal application evaluation of TP will necessarily include a comparison of performance using precipitation products vs layer reflectivity products.

Output Product Definition:— The current plan for TP output product is a graphical presentation similar to that illustrated in Figure IV-28. There, binary storm contours are presented along with a track vector indicating the storm's predicted amount and direction of motion. The length of the track vector indicates the amount of movement that will occur for the requested time interval (15 min in this example). We will also make available binary storm contours of the extrapolated storms, i.e., the silhouettes actually translated by the track vectors (SEM output). Later, operational evaluations may be used to eliminate one or the other of these presentations.

Real-Time Implementation:— We decided to prepare CARCOR for inclusion in the summer 1988 TDWR demonstration. It is in a more advanced state of development than STORMCOR and its performance capabilities are better understood.

Real-time implementation required restructuring of the algorithm and one major change in algorithm definition. We decided to remove the SEM *High-Resolution Extrapolation* feature after closer examination of its function.

High-resolution translation substitutes translation of storms on a Cartesian map with the following sequence of operations. An $n \times n$ Cartesian map is partitioned to give a finer resolution $pn \times pn$ Cartesian representation, where p typically equals 2 or 4. Storm translation is done on the high-resolution representation. The high-resolution picture is then mapped back to the coarser grid using a spatial averaging threshold. (Of the $p \times p$ high-resolution pixels that overlap one pixel of the original map, THRESH % (or greater) must be ON in order to turn the original

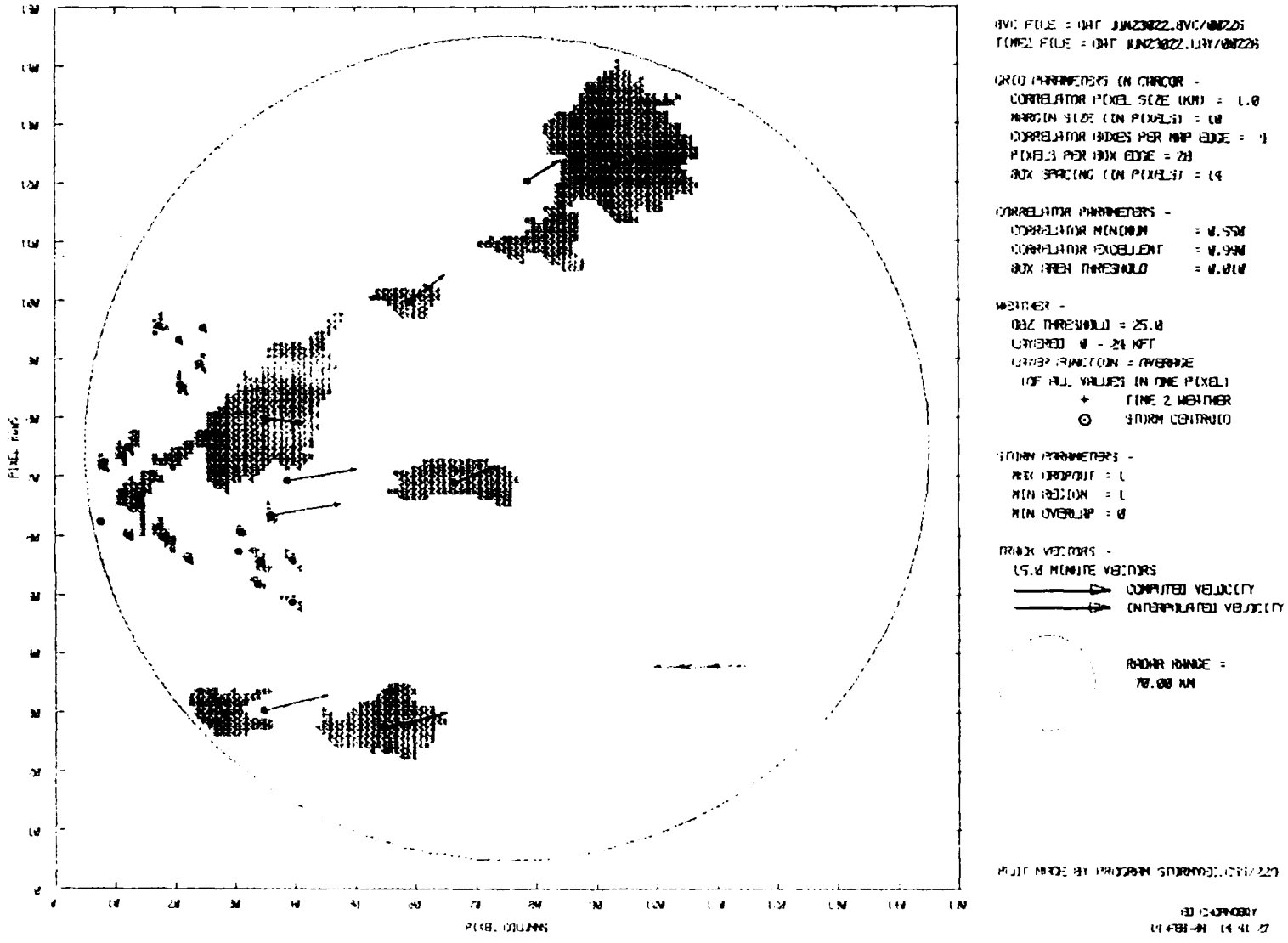

Figure IV-28. CARCOR track vectors, storm regions, and centroids.

109733-43

map pixel ON.) If THRESH is less than or equal to (greater than or equal to) 0.5, then the number of ON pixels in the translated map will be greater (less) than or equal to the number of ON pixels in the original map.

This feature required a large amount of computer memory and provided little tangible improvement in performance in the terminal environment where the coarse grid resolution is 1 km. The decision to remove the feature was based on the analysis of data obtained from two operational days at the Denver FL-2 test bed.

Timing estimates for the real-time algorithm will be obtained in April 1988.

c. Acquisition and Processing of Weather Data

Preliminary CARCOR Evaluation Using TDWR Scan Data:— Data from the FL-2 Denver test bed will be used to evaluate cross-correlation tracking and prediction performance in the terminal environment. The long task of layering data was begun during this period.

A preliminary evaluation of CARCOR using data obtained from five operational days of the Denver test bed has been completed. The results are summarized in Table IV-8, where average POD and PFA statistics are presented for 15-min predictions (a) using CARCOR/SEM and (b) for the persistence prediction. Average values, standard deviations, and range values are presented for three different scoring criteria. The value NFRAMES indicates the number of volume scans (predictions) that were scored for that day. The value NPATHS indicates the number of *flight paths* used in the scoring by the flight-paths method.

These results indicate that CARCOR can consistently improve predictive capabilities when compared with persistence. In general, there is also a decrease in PFA values (but, note the JUN09 summary). These results were taken as being encouraging, and a full evaluation is in progress.

d. Growth/Decay

Some preliminary work examining adaptive thresholding for the correlation tracker was done. The initial intent was to compensate for small growth/decay effects that alter storm silhouettes and thereby affect tracking performance. A nonmeteorological model was developed, but it did not provide the desired results. Continuation of this effort has been given a low priority, with a meteorologically oriented model the desired goal.

5. Goals

a. Short-Term Objectives

A cross-correlation tracker, cycling with the real-time system, is nearly available. Our first attempts at cycling the algorithm on the 3260 computer have revealed that the tracker currently has difficulty meeting a 5-min update time. We note that this timing estimate was made on a machine without an APU, and that the test-bed system will provide a speedup by a factor of 4.

TABLE IV-8

Summary of Preliminary Evaluation of CARCOR Using Data from Five Operational Days of the Denver Test Bed

T15xx1 arc summary statistics

DATE	NFRAMES	CRITERION	$\overline{POD}$ (σ_{POD})	RANGE	$\overline{PFA}$ (σ_{PFA})	RANGE	$\overline{NPATHS}$
JUN09	25	AREA	0.486 (0.153)	0.188-0.704	0.493 (0.142)	0.355-0.856	0.
		STRATEGIC	0.934 (0.123)	0.443-0.961	0.134 (0.057)	0.044-0.278	1000.
		TACTICAL	0.780 (0.116)	0.435-0.938	0.182 (0.082)	0.044-0.387	501.
JUN23	30	AREA	0.610 (0.115)	0.246-0.817	0.425 (0.074)	0.278-0.580	0.
		STRATEGIC	0.905 (0.056)	0.743-0.987	0.096 (0.039)	0.011-0.189	1000.
		TACTICAL	0.869 (0.080)	0.637-0.985	0.121 (0.069)	0.011-0.279	462.
JUL08	27	AREA	0.568 (0.104)	0.295-0.698	0.422 (0.104)	0.268-0.704	0.
		STRATEGIC	0.913 (0.058)	0.745-0.975	0.082 (0.039)	0.027-0.163	1000.
		TACTICAL	0.834 (0.105)	0.598-0.982	0.105 (0.075)	0.009-0.382	464.
AUG25	32	AREA	0.568 (0.089)	0.386-0.715	0.459 (0.066)	0.335-0.601	0.
		STRATEGIC	0.938 (0.038)	0.810-0.994	0.073 (0.028)	0.019-0.150	1000.
		TACTICAL	0.896 (0.073)	0.698-0.992	0.124 (0.072)	0.028-0.352	486.
JUN10	47	AREA	0.624 (0.145)	0.192-0.816	0.374 (0.127)	0.182-0.795	0.
		STRATEGIC	0.879 (0.056)	0.758-0.953	0.129 (0.047)	0.039-0.240	1000.
		TACTICAL	0.766 (0.103)	0.543-0.973	0.225 (0.123)	0.073-0.568	493.

(a)

T15xx1 arc summary statistics

DATE	NFRAMES	CRITERION	$\overline{POD}$ (σ_{POD})	RANGE	$\overline{PFA}$ (σ_{PFA})	RANGE	$\overline{NPATHS}$
JUN09	25	AREA	0.461 (0.155)	0.092-0.672	0.477 (0.145)	0.292-0.838	0.
		STRATEGIC	0.814 (0.125)	0.429-0.976	0.123 (0.052)	0.040-0.246	1000.
		TACTICAL	0.712 (0.243)	0.024-0.945	0.208 (0.168)	0.049-0.667	485.
JUN23	30	AREA	0.522 (0.096)	0.300-0.699	0.456 (0.074)	0.290-0.565	0.
		STRATEGIC	0.896 (0.047)	0.752-0.962	0.082 (0.043)	0.023-0.194	1000.
		TACTICAL	0.829 (0.091)	0.570-0.958	0.112 (0.061)	0.018-0.254	473.
JUL08	27	AREA	0.526 (0.093)	0.323-0.665	0.419 (0.090)	0.289-0.632	0.
		STRATEGIC	0.910 (0.052)	0.752-0.969	0.053 (0.034)	0.009-0.156	1000.
		TACTICAL	0.856 (0.074)	0.687-0.968	0.089 (0.073)	0.020-0.346	504.
AUG25	32	AREA	0.489 (0.076)	0.334-0.612	0.484 (0.057)	0.374-0.629	0.
		STRATEGIC	0.925 (0.035)	0.817-0.979	0.063 (0.026)	0.025-0.167	1000.
		TACTICAL	0.861 (0.074)	0.623-0.972	0.113 (0.044)	0.041-0.219	502.
JUN10	47	AREA	0.549 (0.148)	0.211-0.803	0.404 (0.147)	0.127-0.716	0.
		STRATEGIC	0.852 (0.052)	0.735-0.945	0.122 (0.046)	0.038-0.245	1000.
		TACTICAL	0.770 (0.124)	0.453-0.954	0.198 (0.085)	0.068-0.403	478.

(b)

Nevertheless, it is prudent to explore methods for improving algorithm timing. We are introducing a binary search method for locating the correlation surface peak. Conservatively, this should provide a speedup by a factor of 2.

The final requirement for the real-time algorithm is the inclusion of an internal monitoring mode providing verification of correct TP algorithm operation. The output of this mode will be a graphic presentation of algorithm status which can also serve as an adjunct to the normal TP output products.

The collection of single (1°) tilt data is necessary for performance evaluation, assuming a precipitation product input. These data, plus the layered data already collected, will be used to characterize the algorithm parameter settings that are optimal for terminal operations. A report summarizing all findings will also be initiated during this period.

b. Long-Term Objectives

Stabilization of the wind-field estimates, across time scans and spatially, is viewed as a necessary long-term goal. Our intentions are to introduce a linear model for the velocity vector field and use linear filtering methods to smooth the estimates spatially and temporally. An important consideration here will be the proper handling of missing velocity values.

Doppler-velocity data will be explored for potential use in growth/decay compensation. In particular, we will begin with an empirical study examining cases of known failure by the TP algorithms that are attributable to growth/decay effects.

M. ADVANCED SIGNAL-PROCESSING CONCEPTS: CLUTTER FILTERING AND MULTIRATE SCHEMES FOR VELOCITY DE-ALIASING

1. Introduction

It is well known that multirate pulse trains, i.e., radar pulse trains containing multiple intersample spacings, can be used to reduce the effects of velocity ambiguities that exist in pulsed Doppler radar estimation. Our interest is in applying this technique to the TDWR, a NEXRAD-like radar designed to operate at short ranges and low elevation angles. Interference from clutter is therefore significant and introduces the need for clutter filters which will, we hope, have minimal degrading effects (in particular, estimate bias) on the three product estimates used in subsequent processing, i.e., Doppler spectral power, spectral mean, and standard deviation. However, the use of multirate sampling schemes complicates the design of such filters, which provides the motivation for this research effort. Initial work on the problem and some issues facing the TDWR design in particular are detailed in a Lincoln Laboratory Project Report.[15]

This summary covers a 12-month period, and the presentation is subdivided into 6-month intervals. During the first interval, definition of the problem and an outline of the proposed work was completed. During the second interval, the actual design and evaluation process was begun.

2. March — October 1987

a. Preliminary Design Strategies

Many publications have appeared detailing the means by which velocity estimates, with an unambiguous range equivalent to that obtained with uniform sampling at an interval T, can be obtained with data obtained from a sampling scheme using two intervals, $T_1 = c_1T$ and $T_2 = c_2T$, where c_1 and c_2 are relatively prime integers. Our intentions are to examine the degrading effects of clutter and, in particular, develop a suitable means for combining successful clutter suppression with a double-PRT method that extends the maximum unambiguous velocity limit. Our initial study will compare two alternative sampling methods which use a double-PRT scheme.

In the first method, *batch PRT* (a sequence of uniformly spaced pulses with interpulse interval T_1) is presented first and then followed by a second sequence of uniformly spaced pulses with interpulse interval T_2. This data set can be viewed as two separate data sequences, and, as such, each is filtered separately for clutter returns. Clutter filters for these sequences are easily developed using standard techniques. However, since the total number of points is limited by the dwell time and each sequence is therefore limited to half of that total, this may place a significant limitation on the achievable transition bandwidth — a significant constraint for weather radars. Perhaps equally important is the loss of usable data due to filter edge effects which can have a severe effect on the quality (i.e., estimator variance) of the computed product estimates. Preliminary computations indicate that it may not be possible to achieve the NEXRAD requirement of 50-dB clutter suppression for an S-band radar. We will translate the problem to C-band, where we believe that a suitable design can be achieved.

The second sampling method, *alternating PRT*, uses return samples that are obtained by sampling with two alternating interpulse intervals. This data set is processed as a single sequence, and therefore does not necessarily require data editing to eliminate filter edge effects. However, this data set presents a challenging design problem since the data are not uniformly sampled. Simple examples (assuming a pulse pair estimator) show that a FIR filter introduces a bias to the velocity product estimate. For real coefficient FIR filters, the best that can be achieved is a "linear phase bias," and that will occur when the filter coefficients are allowed to be time-varying. In particular, the filter must consist of two alternating sets of filter coefficients and both sets must satisfy either an *odd* or *even* symmetry constraint. The challenge is to design the double set of filter coefficients under constraints that will result in minimal (or a correctable) bias in the velocity product estimate. In addition, the filter should not have severe effects on the remaining two product estimates. This time-varying FIR design forms the basis for our initial investigations, but it is by no means the only way to achieve the filtering objective. For example, methods combining linear interpolators with conventional clutter filters may also, in the long term, be explored.

b. General Outline of Goals

The characteristics of alternating coefficient filters are not well understood, and it is necessary to determine the feasibility of their design. It is not our intention to approach this as a

general problem, but on a case-by-case basis only. Three preliminary design strategies for an alternating FIR structure are proposed for evaluation. The first is based on a modification of the *windowing* method, the second focuses on an optimal Chebyshev design, and the third selects coefficients to maximize the signal-to-clutter power ratio for given clutter model structures. Our short-term goal will be to concentrate on design using the windowing method, since this represents the simplest design. In particular, we will determine if suitable time-varying filters can be developed that satisfy the *linear phase bias* constraint mentioned above. This is nearly certain considering the nature of the *frequency-sampling* design and the form of the constraints stated above. At this point it will be possible to compare the clutter filtering capabilities for the batch method vs those for the alternating method. This comparison will be done for a C-band radar in the context of TDWR NEXRAD. The point of focus will rest on the 50-dB clutter suppression requirement for NEXRAD radars. There will be a twofold assessment of the criterion: comparisons will be based on average power transfer functions (average, since the alternating filter is time-varying) and by simulation using simulated clutter signals as the sole filter input. If the alternating filter does not compare favorably with the batch method, then it will be necessary to evaluate the potential for success using an alternate design method. In particular, a design maximizing the signal-to-clutter power ratio will decide if the 50-dB clutter requirement can be achieved by an alternating PRT filter. This design is proposed contingent on the results of the windowing design. If a window-based design can provide competitive clutter suppression, then the next step would be to compare the bias and velocity errors that are obtained using the two methods. The criteria and algorithms for such an evaluation have not yet been determined. This concludes the short-term goal proposal: an acceptance or rejection of alternating PRT filters using the 50-dB clutter suppression requirement only. The subsequent analysis of velocity errors and possible consideration of alternate designs (e.g., Chebyshev approximation) are considered longer-term objectives, with priority given to the examination of velocity errors.

3. October 1987 — March 1988

Staggered (Time-Varying) Filter Design:— Our initial efforts attempt to control velocity bias, introduced by staggered pulse-train filters, by constraining it to be linear with frequency. Two algorithms for the design of staggered time-varying filters were developed: a method based on the selection of frequencies, and a *maximally* flat method.

Since FIR filters for batch processing are easier to design and evaluate, they will be used as the *benchmark* by which to evaluate the performance of the staggered time-varying filters. During this reporting period, software development for the design of such filters has begun.

Simple comparison based on frequency-domain characteristics may not be sufficient for proper analysis of these filters. Our evaluations will include a characterization based on operational characteristics as follows. Two clutter models, continuous and discrete, characteristic of weather clutter returns will be used to measure filter effectiveness with respect to the TDWR clutter suppression requirements. The software to generate clutter models and perform the analysis is under current development.

4. Future Goals

The first goal for the near term will be the completion of software development necessary for filter design and analysis. The second goal will be to formulate the batch-processing problem for C-band performance and to propose designs that meet the clutter suppression requirements for TDWR. Lastly, the project will move to a comparison of performance between batch processing and staggered PRT processing.

On a longer term, it will be necessary to examine and characterize the velocity bias and estimation errors introduced by the filtering operation. If no design can be found to satisfy the clutter power suppression requirement of 50 dB, it will become necessary to re-examine the filter design problem relaxing the linear phase bias constraint.

V. USE OF NEXRAD/TDWR IN ATC SYSTEM

A. FEDERAL METEOROLOGICAL HANDBOOK SUPPORT

The eleventh volume of the Federal Meteorological Handbook (FMH-11) was prepared to provide operational guidelines for the operation of the NEXRAD system. The task was delegated to five working groups, each of which has the responsibility for certain portions of FMH-11. The groups were made up of representatives of the agencies developing NEXRAD, as well as advisors from the NEXRAD Interim Operational Test Facility (IOTF) and from institutions like Lincoln Laboratory. A representative from Lincoln Laboratory served on Working Group E (WGE) which has been tasked to write the sections of FMH-11 specifying operational modes, scanning strategies, product mixes, product shedding priorities, and mode selection/deselection criteria.

Lincoln Laboratory provided technical support to the FMH-11 working group in the area of scan strategy. During this reporting period, we received a draft of the FMH-11 and held a coordinating meeting in late December 1986. However, Lincoln personnel were unable to attend that meeting due to the termination of Center Weather Processing funding which had supported Lincoln Laboratory participation.

There were several deficiencies in the nominal NEXRAD precipitation/severe-weather scan strategy, namely:

(1) Algorithms which depend on volumetric information (e.g., hail index, severe-weather probability, cross section) and the FAA high-altitude and super high-altitude composition reflectivity and turbulence would exhibit suboptimal performance due to gaps in coverage.

(2) *Banding* in echo tops and in the FAA high- and super high-layer products.

(3) Small-scale phenomena such as storm initiation might be detected too slowly.

(4) A cone of silence above 18.5°.

(5) Low-level outflow phenomena (e.g., microbursts, downbursts) may not be detected.

Rectifying the deficiencies cited above will involve augmentation of the NEXRAD system's computational capability and software.

B. RADAR WORKING GROUP SUPPORT

The Center Weather Processor program office has set up a Radar Working Group (RWG) to discuss issues such as (1) characteristics of the NEXRAD products for use in the CWP, (2) mosaicking of the results of various NEXRAD systems within a CWP, and (3) requirements for the CWP product display type (e.g., raster vs contour) and spatial resolution.

Lincoln personnel have participated in the RWG for several years, focusing principally on NEXRAD product characteristics and display formats. The RWG met in Washington, DC on 9 March 1987 to discuss a variety of NEXRAD issues. Based on experience with the NEXRAD algorithm, it appeared that some degree of CWSU interpretation would be needed for turbulence data. However, it was not certain whether the current CWSU meteorologists would have the time and opportunity to provide reliable turbulence information routinely in a weather-impacted situation, especially extensive line storms. Since the CWP products from NEXRAD have only very coarse vertical resolutions, their ability to depict the vertical structure of turbulence within line storms remains an unresolved issue.

The echo-tops algorithm and product are also of concern. Fairly coarse resolution (e.g., 12,000, 20,000, 25,000 and 40,000 ft altitude) may be sufficient for Air Route Traffic Control Center (ARTCC) use. However, the Mode S transmission of the echo-tops product, via the Weather Communications Processor, might necessitate higher resolution data. Additionally, the granularity in the NEXRAD vertical coverage and the lack of tests for meteorological validity of the echo-tops data in the current product will further limit its utility.

Problems will arise in mosaicking the storm extrapolation maps produced by various radars, particularly where a storm passes over the mosaic boundary between two radars during the prediction period (e.g., 30 min). That would cause significant problems for boundary-based mosaicking since the storm may not yet be in track by the sensor whose sector is being entered.

The problem can be alleviated by several means:

(1) Data adaptive mosaicking of the storm extrapolation maps.

(2) Choosing boundaries so that both sensors at the boundary have coverage beyond the mosaic boundary so that they can track a storm before it crosses a boundary.

(3) Modifying the storm tracking/prediction outputs so that the storm extrapolation maps would be produced in the CWP rather than the NEXRAD sensors.

We are uncertain at this time how the issues described above will be resolved given the uncertainties in the near-term NEXRAD computational capability and the lack of CWP funding for such studies.

C. WEATHER IMAGE DATA COMPRESSION

1. Introduction

Initially, hazardous weather warnings provided by the NEXRAD and TDWR weather radars are to be supplied to pilots as verbal warnings from controllers band on alphanumeric (ribbon) displays or supervisor observations of geographical situation displays. While these messages will alert pilots to the existence of hazardous phenomenon, they will provide neither detailed information concerning spatial extent of the hazard nor overall situation information for choosing the

best escape path. To provide pilots with that additional useful information to avoid hazardous weather, the Federal Aviation Administration (FAA) is actively developing the capability to provide real-time graphic information of these events by use of the Mode Select (Mode S) data link. Through the use of the data link's extended length message (ELM) format, there will be the ability to supply weather information in graphic form — the same information the controllers have — in a timely and understandable manner.

The maps will be shown on a cockpit display. The resolution and graphics of the displays will be specifically tailored to the situation the aircraft is in when the data are transmitted. Display differences would chiefly be in the en-route or terminal portion of a flight.

While it could be advantageous to provide as much weather information over the channel as possible, the bandwidth of the data link is limited. The transmission of weather data has been restricted (restricted both technically and administratively) to a data block no greater than 4 ELMs (each of approximately 1400 bits). The inherent information within the maps and bandwidth of the channel can be made compatible only through the use of compression.

2. Current Work

The work this reporting period has focused on the following:

(a) Investigating two-dimensional coding schemes which could potentially compress images to 1 ELM.

(b) Testing of various compression techniques against a much larger set of images.

(c) Developing a program to assess certain human-factors issues such as tolerable image simplification and orientation in an operationally relevant context.

Work in each of these areas is summarized below and reported more completely in an ATC project report scheduled for publication in 1988.

3. Weather Images for Compression Assessment

With no analytical model for a weather map, the effectiveness of a particular compression scheme can be measured only through experimentation. The experiment format chosen consisted of six compression schemes (divided into one-dimensional schemes) and 106 maps (divided into en-route and terminal areas). All compression schemes were run against all maps to enable a conclusive decision to be made regarding their effectiveness.

The images represented a wide variety of weather conditions, taken at a number of Doppler weather radar test sites. An effort was made to select maps representative of NEXRAD and TDWR product types. All maps are represented on a 64×64 pixel grid* with the product levels

* The map resolution was suggested by FAA personnel as an operationally useful resolution which was compatible with general aviation low-cost displays.

quantized to three or four levels. The maps are representative of those to be transmitted in the terminal area (primarily for use in maneuvering in the terminal area) consisting of a 1-km layer with a resolution of 1×1 km per pixel. The en-route maps (for use in strategic or tactical weather avoidance) consist of three layers: lower than 15,000 ft, 15,000 to 30,000 ft, and above 30,000 ft at a resolution of 4×4 km per pixel.

The product types chosen for this study are listed in Table V-1.

TABLE V-1

Selected Product Types

Reflectivity at Three NWS Levels	
Level 1, light precipitation boundary	<15 dBz
Level 2, moderate rain	>15, <30 dBz
Level 3, heavy rain	>30 dBz
Reflectivity at Four NWS Levels	
Level 4, extremely heavy rains (possible hail)	>45 dBz
Turbulence at Three MacCready Levels	
Level 1, light	$0 < \epsilon^{1/3} < 1.5$
Level 2, moderate	$1.5 < \epsilon^{1/3} < 3.5$
Level 3, heavy	$\epsilon^{1/3} > 3.5$
Echo Tops at Three Levels	
Level 1, low tops	$H < 15$ kft
Level 2, intermediate tops	15 kft $< H <$ 30 kft
Level 3, high tops	$H > 30$ kft

See Figure V-1 for an example of a terminal reflectivity map, and Figure V-2 for an en-route map. See Figure V-3 for an echo-top example.

The radar data used were obtained in Cambridge, MA; Memphis, TN; Huntsville, AL; Denver, CO; and Norman, OK. The weather types represented included microbursts, line storms, and thunderstorms with heavy rain.

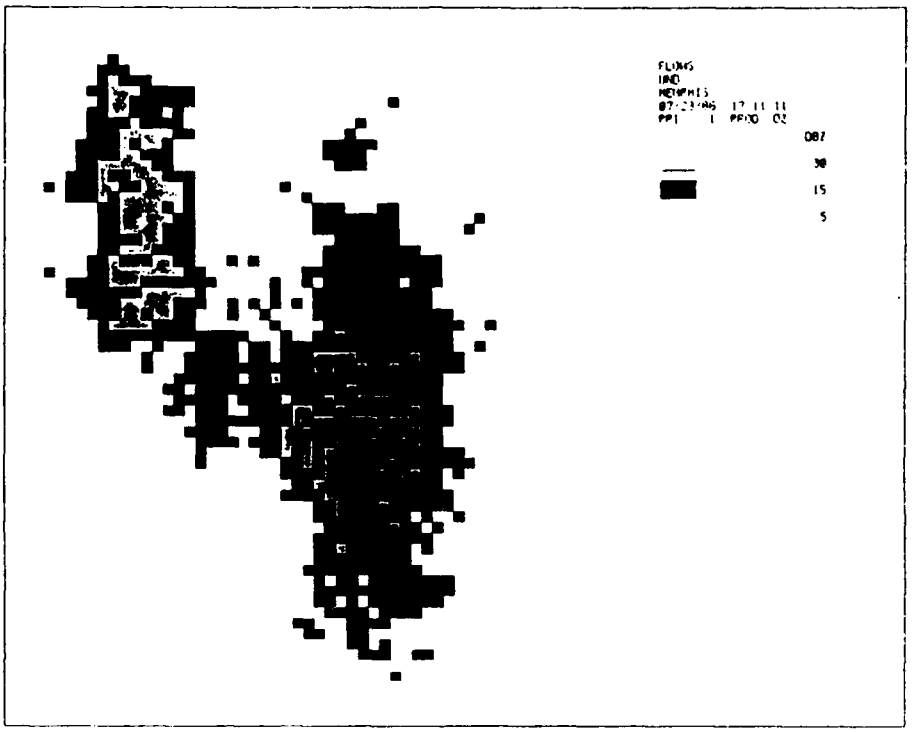

109733-46

Figure V-1. Terminal map.

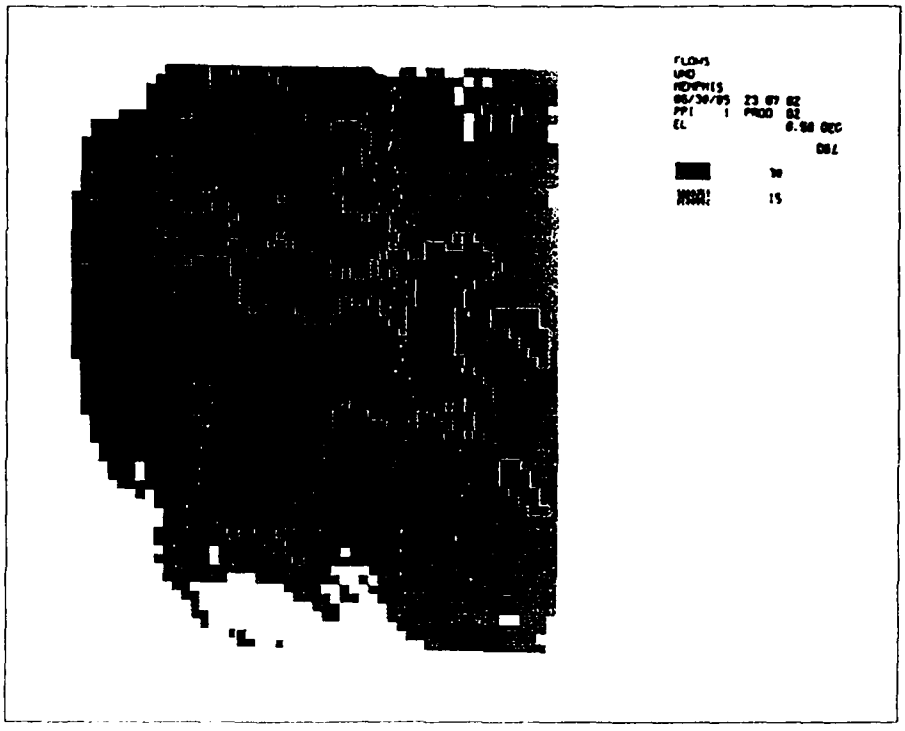

109733-47

Figure V-2. En-route map.

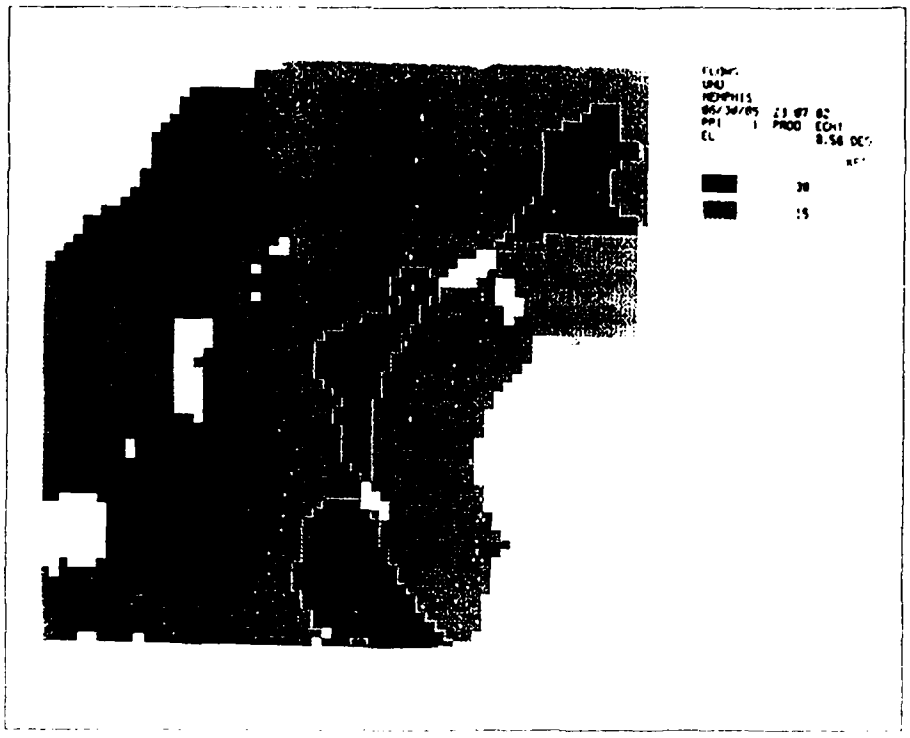

109733-48

Figure V-3. Echo tops.

4. One-Dimensional Codes

The original requirement of compression was to reduce the weather maps to below 4 ELMs (5000 bits) and to have the reconstructed image be a pixel-by-pixel replica of the original map. These requirements led to an investigation of one-dimensional compression schemes. We have considered one-dimensional compression schemes which act upon the image as a sequence of serial characteristics. The algorithms tested were all reversible (i.e., no information loss). The specific coding algorithms tested are as follows.

a. Select Coding

In an attempt to provide the advantages of run-length coding while overcoming the inefficiencies of encoding short run lengths, select coding was implemented. Select coding is a variation of run-length coding where very short runs (specifically for this study, those shorter than 3 pixels) are not encoded. For these cases, pixel values are transmitted unaltered.

To increase efficiency there is a special provision for the encoding of very long run lengths. It allows optimization of the code through the selection of the number of bits used to represent the run count and is approximately equal to $\log_2$ times average run length.

b. Huffman Coding

While select coding can enhance the effectiveness of run-length coding, theory tells us that when successive run lengths are independent, the most efficient codes should be entropy codes. They are those codes whose word lengths are based on the frequency of occurrence of a symbol. The most efficient · f these is Huffman coding.

In its truest form, Huffman coding consists of deriving a unique code table for each source to be encoded. To decode the transmission, the table must also be transmitted. The small size of each image makes the overhead associated with the table transmission unacceptable. To overcome this problem, the encoding (decoding) table is precalculated (and stored) from a composite of experimental cases.

c. Variable-to-Block Coding

Weather images having a large number of scattered cells within the image have a difficult-to-run length code. The cells tend to be located such that they break up long run lengths of identical consecutive pixels. With variable-to-block coding we will be able to take advantage of the patterns created by scattered cells.

Variable-to-block codes are those whose output is constrained to be of a fixed length. Like run-length coding, the length of source code contained in the fixed output code block is dependent on the redundancy of the source. Yet, unlike run-length coding, the redundancy is not restricted to consecutive identical pixels.

The two specific codes considered in the studies were Lempel-Ziv and Welch codes. Both techniques adapt the source process as a part of the encoding procedure.

d. One-Dimensional Results

The results of the one-dimensional compression routines were:

(1) Typical encoding results for the terminal maps with raster scanning are shown in Table V-2. Of the 46 cases studied, Huffman run-length coding offered the greatest degree of compression in 43 cases, with variable-to-block proving superior in the other three.

(2) By altering the method of scanning an image from a raster pattern (simple right-to-left reading) to a space-filling curve (visiting every pixel in a quadrant before progressing to the next), further compression can be realized. Using the Hilbert scanning pattern, an improvement in 45 of the 46 cases was realized.

e. En-Route Maps

Typical encoding results for the en-route maps with raster scanning are shown in Table V-3. Huffman run-length coding offered the greatest degree of compression in all cases. In all but two cases, Hilbert scanning offered some improvement.

TABLE V-2

Encoded Map Size (in ELMs) for Terminal Map Data Set

Coding Technique	Map Type		
	Reflectivity (3 Level)	Turbulence (3 Level)	Echo Tops (4 Level)
Run Length	4.2*	4.9*	1.9
Select	2.6*	3.0*	1.8
Huffman	2.0	2.4*	1.3
Lempel-Ziv	3.4*	3.9*	1.7
Welch	2.3	2.7*	1.4

* Worst-case map exceeded 4 ELMs.

TABLE V-3

Encoded Map Size (in ELMs) for En-Route Data Sets

Coding Technique	Map Type		
	Reflectivity 2(3 Level)	Turbulence (3 Level)	Echo Tops (3 Level)
Run Length	4.2*	5.0*	1.9
Select	2.6*	3.0*	1.8
Huffman	2.0	2.4*	1.3
Lempel-Ziv	3.5*	2.7*	1.7
Welch	2.3	3.9*	1.4

* Worst-case map exceeded 4 ELMs.

f. One-Dimensional Conclusions

The following conclusions were drawn from the preliminary testing.

(1) The 4-ELM limit is attainable for reflectivity and echo-tops images with one-dimensional coding techniques, albeit some degree of source information is required to meet the 4-ELM objective.

(2) Huffman coding of the run lengths provided the best overall results.

(3) If the computational power is available, all images should be scanned with the Hilbert scanning (or an appropriate space-filling curve) pattern.

(4) Run-length coding could not, on the average, achieve a compressed image less than 4 ELMs.

(5) Alphanumerics should be transmitted separately from the weather image.

5. Two-Dimensional Codes

If the weather maps can be compressed to under a single ELM, eliminating the need to transmit multiple linked ELMs, this service becomes far more attractive from the viewpoint of the Mode S data link. On the average, the one-dimensional schemes can reduce a map to 2.26 ELMs. To provide for the higher degrees of compression, more efficient (two-dimensional) schemes were implemented.

By removing the process of converting the image from a two- to a one-dimensional source and operating on the two-dimensional source, algorithms can be developed that will greatly increase compression. While the Hilbert scanning strategy has taken advantage of, to a small measure, the two-dimensional nature of the image, we have developed and tested algorithms which more nearly consider the structural properties of weather images. In all cases, median filtering with a 3×3 filter was used as a preprocessing step. The specific coding algorithms tested and a brief description of their operation are presented below.

a. Vector Coding

Vector coding maps a block of J image samples into one of a finite set of representative vectors and then transmits a code word that identifies the vector. To increase compression and keep the processing simple, not all possible J sample blocks are assigned unique code words; instead, code words are assigned to a subset of possible blocks and a minimum mean-squared error (MSE) criteria are used for the assignment of the code words to remaining blocks. It is easy to see the direct trade-off that can be made between compression and distortion. Figure V-4 is a representation of images that have been coded with complete (17 code words) and minimal (3 code words) code book sets per 2×2 pixel.

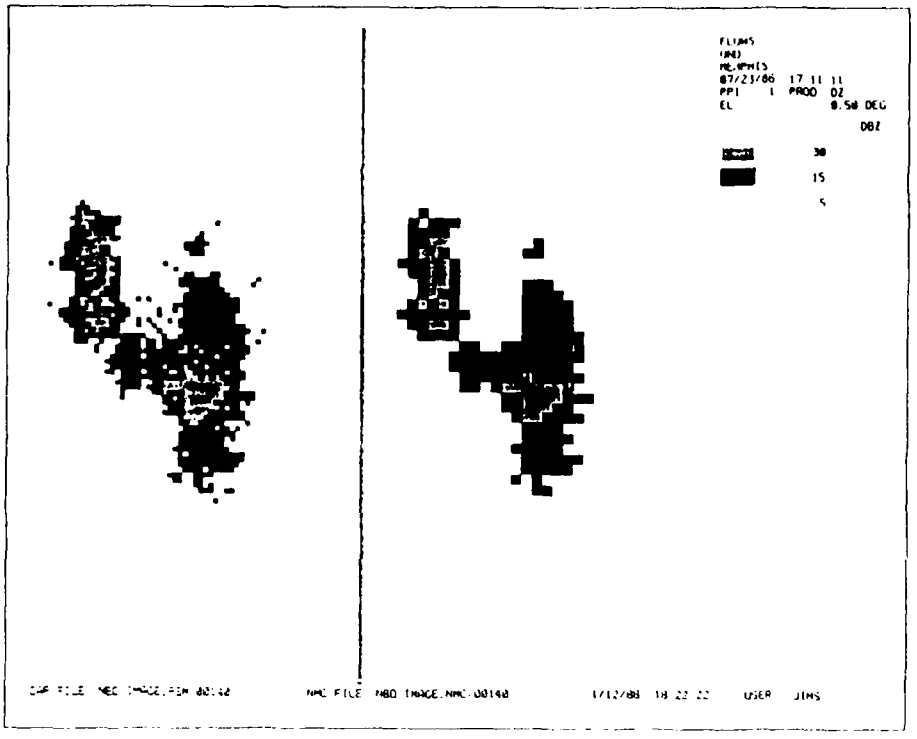

109733-49

Figure V-4. Vector coding.

b. Contour Coding of Spatially Smoothed Images

Within a weather map there generally will exist a number of assorted weather regions. The information contained in those regions consists of their intensity level, size, and location within the map. By converting each separate weather region into one-dimensional sequences of contour points (each point consisting of an x and y location), and by then processing those sequences, compression may be realized.

Contouring can become an effective means of compression by first smoothing the image and then the contour stream. By reducing the original information content of the map by filtering (median filtering for this study) and reducing the number of points used to represent the region contours, sizable compression can be realized. Figure V-5 is an example of compression fidelity trade-off involved with this type of coding.

c. Representation by Simple Shapes

The final method of compression, and perhaps the most promising, is shape representation. With this method, an area of weather is represented by simple shapes and then encoded as the set of descriptors of these shapes. Reconstruction is then a simple task of displaying, according to their descriptors, the representative shapes.

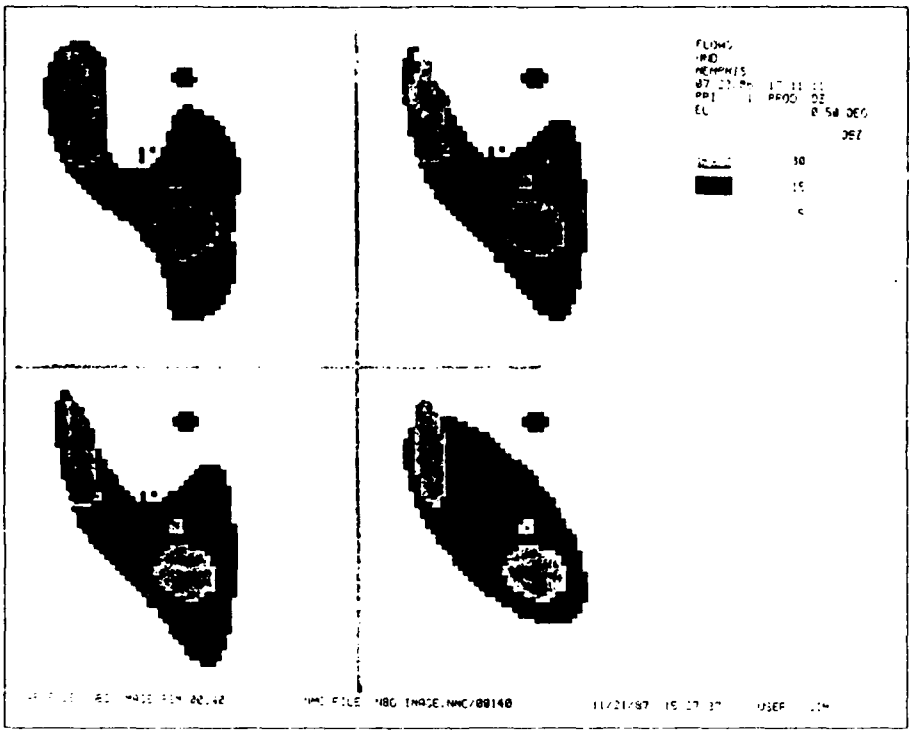

109733-50

Figure V-5. Effects of smoothing.

The shape chosen for representation was the ellipse. The versatility of this form (by varying parameters, it can represent anything from a line to a circle) makes it ideal for approximating weather shapes.

The method presently used to fit shapes (ellipses) is one of *feedback fitting*. With this method an ellipse is fitted to a weather area, and then the fitted ellipse is subtracted from the connected region to yield a residual region. Fitting is performed on the residual regions and the fitted ellipses are subtracted from these regions; the procedure will continue until the remaining undescribed area is below a set threshold. Figure V-6 demonstrates the ellipses fitted to a weather image, and Figure V-7 shows the resulting decoded image.

The drawback with the present method of shape fitting is twofold. The present algorithm is slow and CPU intensive; also, the representations of the image produced by this coding algorithm tend to be overfilled representations of the original. The overfilling is due to the starting procedure for the algorithm. The first ellipse is fitted from the centroid of the connected region. If the region is not very elliptical in shape, the ellipse created will greatly overestimate this region. Overestimation is not only visually displeasing, it also makes the coding procedure less effective. On the positive side, this is present only on the encoding (on-ground) side; the decoding (on-board) operations are fast and easy to implement.

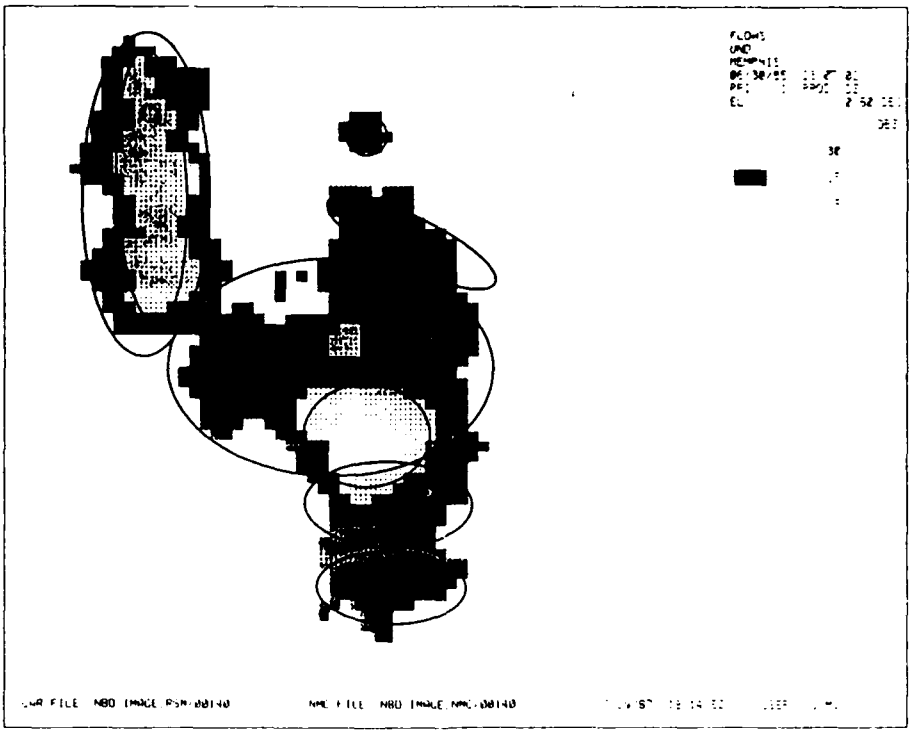

109733-61

Figure V-6. Fitted ellipses.

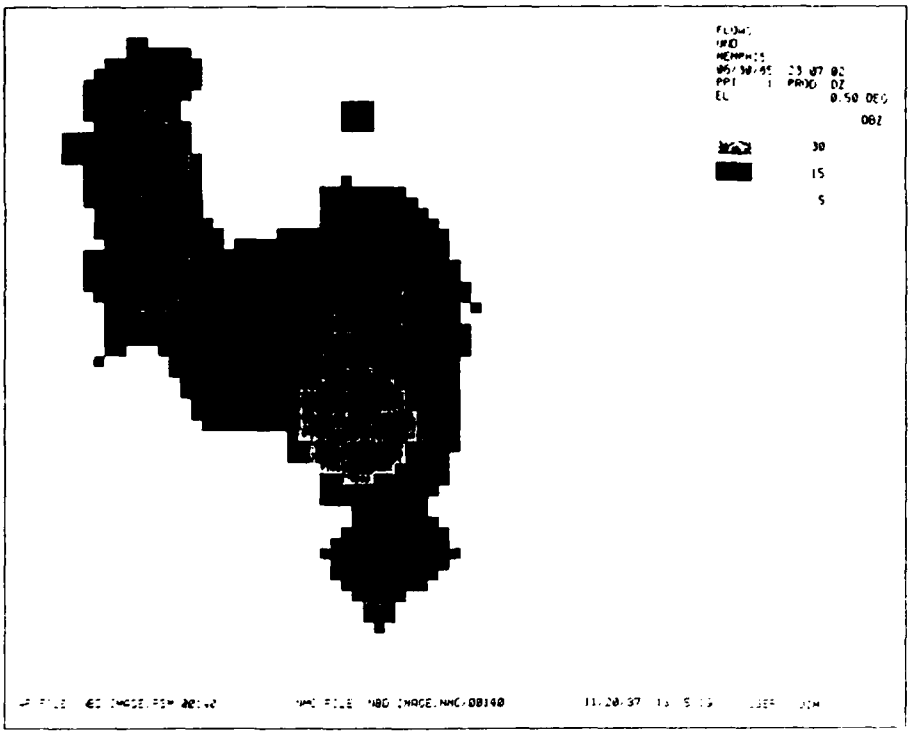

109733-62

Figure V-7. Decoded image resulting from Figure V-6.

A method for increasing the efficiency of shape fitting would be to fit ellipses to shapes that already resembled ellipses. That would require pre-segmenting a connected region of weather into a set of *ellipse-like* regions. The present algorithm forms segments on the basis of convex angles. Assuming regular polygons (those with no angles greater than 180°) are shapes that are well suited to be fit by ellipses, the weather regions are subdivided at convex angles. The convex angles are matched on a minimum MSE criteria. After the image has been subdivided, ellipses are fitted to the subdivisions. The segmentation approach has worked well on a very limited set of images, but needs further experimentation to determine its reliability in full automated operation.

d. Two-Dimensional Results

Table V-4 shows representative numerical results for the two-dimensional techniques which appear to be most promising from the viewpoint of data fidelity.

An advantage of the approaches with fidelity parameters (most especially the contour and shape fitting codes) is that the results are not specifically tied to the information content of the weather image. Parameters in the algorithms can be adjusted to reduce each image to a pre-determined bit level.

TABLE V-4

Encoded Map Size (in ELMs) for Terminal Map Data Set

Coding Technique	Map Type		
	Reflectivity (3 Level)	Turbulence (3 Level)	Echo Tops (4 Level)
MF*/Run Length	2.8†	2.9†	1.7
MF*/Select	2.1	2.2	1.5
MF*/Huffman	1.4	1.6	1.0
MF*/Lempel-Ziv	2.4†	2.6†	1.4
MF*/Welch	1.9	2.1	1.4
MF*/Uniform Contour Resampling	Average = 1.8 Worst case = 3.5		
MF*/Ellipse Fitting	Average = 0.8 Worst case = 1.6		

* MF = 9-point median filtering applied to images before encoding.

† Worst-case map exceeded 4 ELMs.

Shape fitting appears to be the most promising approach, since the average number of bits present in a compressed map was typically below 1 ELM. If this could be achieved for all the maps, the possibility exists of a much more effective use of the Mode S data link.

e. Two-Dimensional Conclusions

The results of all the two-dimensional codes were encouraging. As was expected when the study was initiated, they were able to provide a substantial increase in compression over the linear codes. However, data-fidelity requirements must be clarified.

6. Future Work

The initial study of the compression of weather graphics for the Mode S data link is missing some critical elements. The nature of the two-dimensional codes (reproducing approximate representations of an image) makes the final image quality criteria a key factor in the code design. If the compression effects can be quantified and measured, a compression routine and bit limits can be determined. There is also the issue of how to best utilize the additional compression. To bring Mode S weather graphics services to their full fruition, we have recommended the following:

(a) The continued development of coding techniques, with an emphasis on the approaches (e.g., approximation of storm contours by ellipses) which offer dramatic reductions in the data link requirements.

(b) Off-line analysis of image fidelity criteria, based on use of the images to support pilot decision-making.

(c) On-ground testing of products in a flight simulator.

(d) An in-flight demonstration of product delivery and utility assessment using data from the FAA Doppler weather test bed.

REFERENCES

1. J.T. DiStefano, "Study of Microburst Detection Performance During 1985 in Memphis, TN," Project Report ATC-142, Lincoln Laboratory, MIT (5 August 1987).

2. F.V. Brock, G.H. Saum, and S.R. Semmer, J. Atmos. Oceanic Technol. 3, 573 (1986).

3. M.W. Merritt, "Automated Detection of Microburst Windshear for Terminal Doppler Weather Radar," *Digital Image Processing and Visual Communications Technologies in Meteorology*, Proc. SPIE **846**, 61-68 (1987).

4. S.D. Campbell and S.H. Olson, J. Atmos. Oceanic Tech. **4**, 5 (1987).

5. R.D. Roberts and J.W. Wilson, "Nowcasting Microburst Events using Single Doppler Radar Data," preprints, 23rd Conf. on Radar Meteorology, AMS, Boston, MA, 1986, pp. 14-17.

6. M. Isaminger, "Huntsville Microburst Precursors," Lincoln Laboratory, MIT (1987), private communication.

7. J. McCarthy and J. Wilson, "The Classify, Locate and Avoid Wind Shear (CLAWS) Project at Denver's Stapleton International Airport: Operational Testing of Terminal Weather Hazard Warnings with Emphasis on Microburst Wind Shear," preprints, 2nd Intl. Conf. on Aviation Weather Systems, AMS, Boston, MA, 1986, pp. 247-256.

8. D.R. Mann, "TDWR Clutter Residue Map Generation and Usage," Project Report ATC-148, Lincoln Laboratory, MIT (29 January 1988).

9. U.S. Department of Transportation, Federal Aviation Administration, Specification, Terminal Doppler Weather Radar, FAA-E-2806a (December 21, 1987).

10. M.E. Weber, "Ground Clutter Processing for Wind Measurements with Airport Surveillance Radars," Project Report ATC-143, Lincoln Laboratory, MIT (4 November 1987).

11. H. Uyeda and D.S. Zrnic', J. Atmos. Oceanic Technol. 3, 36 (1985).

12. S.C. Crocker, "TDWR PRF Selection Criteria," Project Report ATC-147, Lincoln Laboratory, MIT (15 March 1988).

13. B.G. Laird, "On Ambiguity Resolution by Random Phase Processing," 20th American Meteorological Society Conference on Radar Meteorology, Boston, MA, 1981, pp. 167-172.

14. J.C. Brasunas, "A Comparison of Storm Tracking and Extrapolation Algorithms," Project Report ATC-124, Lincoln Laboratory, MIT (31 July 1984).

15. M. Goldburg, "Clutter Rejection for Doppler Radars with Multirate Sampling Schemes," Project Report ATC-149, Lincoln Laboratory, MIT (to be published).

GLOSSARY

AC	Aircraft
ac	Alternating Current
A/D	Analog-to-Digital Converter
AEL	Algorithm Enunciation Language
AFGL	Air Force Geophysics Laboratory
AGC	Automatic Gain Control
AGL	Above Ground Level
AI	Artificial Intelligence
ALU	Arithmetic Logic Unit
ANG	Air National Guard
AN/MSC-46	A Satellite Tracking System
AP	Auxiliary Processor
APU	Auxiliary Processing Unit
ARTCC	Air Route Traffic Control Center
ASCII	American Standard Code for Information Interchange
ASR-8	A type of Airport Surveillance Radar
ASR-9	A type of Airport Surveillance Radar
ATC	Air Traffic Control
ATCRBS	Air Traffic Control Radar Beacon System
bpi	bits per inch
CAR	Cartesian
CARCOR	A Storm Tracking Algorithm
C-Band	5.60 to 5.65 GHz
CFT	Common Radar Data Tape Format
CIDF	Common Instrument Data Format
CLAWS	Classify, Locate, and Avoid Wind Shear
CMF	Common Mesonet Format
COHMEX	Cooperative Huntsville Meteorology Experiment
COHO	Coherent Oscillator
CPI	Coherent Processing Interval
CPU	Central Processing Unit
CST	Central Standard Time
CWP	Central Weather Processor
CWSU	Central Weather Processor Service Unit
DAA	Data Acquisition and Analysis Processor
dBz	A unit of weather reflectivity
dc	Direct Current
DCP	Data-Collection Platform

°/s	degrees per second
°/s^2	degrees per second per second
DIFAX	Digital Facsimile Circuit
DMA	Direct Memory Access
DOT	Department of Transportation
ELM	Extended Length Message
FA	False Alarm
FAA	Federal Aviation Administration
FAATC	FAA Technical Center
FAR	False-Alarm Rate
FIR	Finite Impulse Response
FL-2	An FAA-Lincoln Laboratory test-bed radar
FL-3	An FAA-Lincoln Laboratory test-bed radar
FLOWS	FAA-Lincoln Laboratory Operational Weather Studies
FMH-11	Federal Meteorological Handbook Volume 11
Fortran 77	A formula translation computer language
FTP	File Transfer Protocol
FY	Fiscal Year
GF	Gust Front
GMT	Greenwich Mean Time
I	In Phase
IF	Intermediate Frequency
I/O	Input/Output
IOTF	Interim Operational Test Facility
ips	inches per second
JAWS	Joint Airport Weather Studies
JSPO	Joint System Program Office
LASERFAX	Laser Facsimile Transmission System
LAWS	Low-Altitude Wind Shear
LL	Lincoln Laboratory
LLP	Lightning Location and Protection
LLWAS	Low-Level Wind Shear Alert System
MB	Microburst
mb	millibars of Hg
MBGRAF	A program used to analyze mesonet/LLWAS data
MESOPLOT	A program plotting mesonet/LLWAS products
MFLOP	Megaflop
MODEC	A computer program monitoring the position of aircraft
Mode S	Mode Select

MON	Monitor
MPM	Multiported Memory
MSE	Mean-Squared Error
MSFC	Marshall Space Flight Center
MUX	Multiplexer
NASA	National Aeronautics and Space Administration
NCAR	National Center for Atmospheric Research
NESDIS	National Environmental Satellite, Data, and Information Service
NETCHAR	Mesonet Storage and Retrieval Package
NETPAC	Network Characteristics Package
NEXRAD	Next Generation Weather Radar
NFRAMES	The number of volume scans scored for a particular day
NOAA	National Oceanographic and Atmospheric Administration
NPATHS	A value indicating the number of flight paths (used with CARCOR)
NSSL	National Severe Storms Laboratory
NTR	NEXRAD Technical Requirements
NWS	National Weather Service
OS/32	A computer operating system
OT&E	Operational Test and Evaluation
PAM	Portable Automated Mesonet
PC	Personal Computer
PDL	Program Documentation Language
PE	Processing Element
PFA	Probability of False Alarms
PID	Pulse Interference Detector
POD	Probability of Detection
POINT	A type of radar scan
PPI	Plan Position Indicator
PRF	Pulse Repetition Frequency
PROFS	Prototype Regional Observing and Forecasting Service
PRT	Pulse Repetition Time
Q	Quadrature Phase
RAM	Random Access Memory
RATFOR	Rational Fortran
RF	Radio Frequency
RFQ	Request for Quotation
RHI	Range Height Indicator
RRWDS	Radar Remote Weather Display System
RS-232	A computer interface port
RTS	Real-Time System
RWG	Radar Working Group

S-Band	2.70 to 2.90 GHz
SCCS	Unix Source Code Control System
SDC	Synchro/Digital Converter
score_tool	A program producing plots from ground truth and algorithm outputs
SEM	Storm Extrapolation Map
SP	Signal Processor
STC	Sensitivity Time Control
STORMCOR	A Storm Correlation Algorithm
TCP	Transmission Control Protocol
TCP/IP	TCP/Internet Protocol
TDWR	Terminal Doppler Weather Radar
TP	The Tracking and Prediction Algorithm
TRACON	Terminal Radar Approach Control
TRD	Technical Requirements Document
UND	University of North Dakota
Unix	*Generic* Operating System developed by Bell Laboratories
UT	Universal Time
UTC	Universal Time Coordinated (= GMT)
VME	VMEbus, an IEEE standard chassis backplane bus
WGE	Working Group E
WINDAVG	A program used to generate ground truth for wind-shift estimates
WSI	Weather Services International
WSR-57	A Weather Service Radar
WSR-74	A Weather Service Rdar
WX	Weather
WxShell	Weather Shell
YAPS	Yet Another Processing System